Control of the spontaneous emission rate of atoms trapped in spherical shell cavities

Francisco Nogueira Lima

Thesis advisor: Marcelo Leite Lyra

Evaluators:

Professor Marcelo Leite Lyra (IF-UFAL)

Professor Rodrigo de Paula Almeida Lima (IF-UFAL)

Professor Italo Marcos Nunes de Oliveira (IF-UFAL)

Professor Fernando Jorge Sampaio Moraes (DF-UFRPE)

Professor Nami Fux Svaiter (CBPF)

TESE DE DOUTORADO

"Control of the spontaneous emission rate of atoms trapped in spherical shell cavities"

por
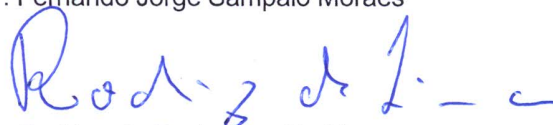
Francisco Nogueira Lima

A Banca Examinadora composta pelos professores Marcelo Leite Lyra (presidente da banca e orientador), do Instituto de Física da Universidade Federal de Alagoas, Fernando Jorge Sampaio Moraes, da Universidade Federal Rural de Pernambuco, Rodrigo de Paula Almeida Lima, do Instituto de Física da Universidade Federal de Alagoas, Italo Marcos Nunes de Oliveira, do Instituto de Física da Universidade Federal de Alagoas, e Nami Fux Svaiter, do Centro Brasileiro de Pesquisas Físicas consideram o candidato aprovado com grau "A".

Maceió, 21 de maio de 2019

Prof. Dr. Marcelo Leite Lyra

Prof. Dr. Fernando Jorge Sampaio Moraes

Prof. Dr. Rodrigo de Paula Almeida Lima

Prof. Dr. Italo Marcos Nunes de Oliveira

Prof. Dr. Nami Fux Svaiter

"Se não fosse imperador, desejaria ser professor. Não conheço missão maior e mais nobre que a de dirigir as inteligências jovens e preparar os homens do futuro".

D. Pedro II

Acknowledgments

- My family, especially my wife Luana Renata de Negreiros Nogueira and our lovely baby Jhean de Negreiros Nogueira. To my beautiful family, mother, grandmother, brothers, etc., as well as to God.

- My thesis advisor Professor Marcelo Leite Lyra for the great environment of research and extraordinary knowledge, always with academic humility, tranquility, patience, etc. Thanks for the excellent contributions and advisement. He is an incredible person and great mentor.

- Thanks to Professor Rodrigo Lima (IF-UFAL) for the essential contributions to this work, my best regards to him.

- My friends from IFPI and partners of doctor's degree, Alexandro das Chagas, Antônio Carlos, Herbert Sousa, José Francisco e José Rodrigues, for the good academic environment over all these years.

- My special friend J. Moreira from IFPI-Campus São Raimundo Nonato for the fundamental advisement towards writing this work. And my friend Gesivaldo Silva from IFMA for motivational conversations.

- To Professor José Pimentel from UFPI for the fundamental basis in Physics during the years as an undergraduate, that will keep for the rest of my life.

Abstract

Within a first-order time-dependent perturbation approach, we compute the spontaneous decay rate of a two-level system placed in the vicinity of a perfectly reflecting spherical surface (exterior and interior) as well as the spontaneous emission rate of a two-level system trapped between two perfectly reflecting concentric spheres. We consider a model system in which the emitter is represented by a two-level monopole coupled to a Hermitian massless scalar field. Using the method of images, we determine the appropriate Wightman's function evaluated in the world line of the atom. For the atom trapped between the radii of the concentric spheres, Wightman's function of the atom incorporates contributions from an infinite set of variable image charges, satisfying Dirichlet boundary conditions. We provide analytical expressions for the decay rate to investigate the radiation process of the atomic system near a single sphere and trapped between the concentric spheres. We provide a detailed analysis on the dependence of the decay rate on a sphere radius, atom's location, and emitted radiation frequency. What is more, on the case of spherical shells, we analyze the decay rate on different relationships between the radii of spheres and the radiation energy emitted. As it turns, we reveal regimes of strong suppression of the spontaneous emission rate, and development of irregular oscillations as function of quantum emitted energy.

Resumo

Dentro de uma teoria de perturbação dependente do tempo de primeira ordem calculamos a taxa de emissão espontânea de um sistema de dois níveis posicionado na vizinhança de uma superfície esférica perfeitamente refletora (exterior e interior), bem como a taxa de emissão espontânea de um sistema de dois níveis aprisionado entre duas esferas concêntricas perfeitamente refletoras. Consideramos um modelo do sistema no qual o emissor é representado por um monopolo de dois níveis acoplado a um campo escalar Hermitiano sem massa. Usando o método das imagens determinamos a função apropriada de Wightman avaliada na linha de universo do átomo. Para o átomo preso entre os raios das esferas concêntricas, a função de Wightman do átomo incorpora contribuições de um conjunto infinito de cargas imagens variáveis, satisfazendo as condições de contorno de Dirichlet. Fornecemos expressões analíticas para a taxa de decaimento, afim de investigar o processo de radiação do sistema atômico próximo de uma única esfera e preso entre as esferas concêntricas. Apresentamos uma análise detalhada da dependência da taxa de decaimento com o raio de esfera, localização do átomo e frequência da radiação emitida. Além disso, no caso de cascas esféricas analisamos a taxa de decaimento para diferentes relações entre os raios das esferas e a energia de radiação emitida. Por fim, revelamos regimes de forte supressão da taxa de emissão espontânea e o desenvolvimento de oscilações irregulares como função da energia quântica emitida.

Contents

1

Introduction

Spontaneous and stimulated emission processes are responsible for almost all the light that reaches our eyes: sun, light from a lamp, screen of a computer or smartphone, etc. The physical idea of spontaneous emission was introduced by Einstein in 1917 [1]: if a light source (atoms, molecules, nanocrystals, etc.) is in an excited energy state with energy E_2, it may decay spontaneously (without any external stimulus) to the lower energy state E_1, releasing the energy difference between the two states, in the form of a photon. The photon will have frequency ν and energy $h\nu$, given by the Planck equation $E_2 - E_1 = h\nu$, where h is the Planck constant (or commonly written as $E_2 - E_1 = \hbar\omega$, where $\hbar$ is the reduced Planck constant). The phase of the photon in spontaneous emission and the direction in which the photon propagates are random. The same does not apply to a stimulated emission, that is, the process in which an incident photon of specific frequency can interact with an excited atomic electron, or other excited molecular state, bringing it to a lower energy level. In this case the released energy is transferred to the electromagnetic field, creating a new photon with a phase, frequency, polarization and direction of travel identical to the photons of the incident wave. A diagram of energy levels, which illustrates the process can be seen in Fig. 1.1.

Spontaneous emission cannot be explained using the classical electromagnetic theory and is considered as a fundamentally quantum process. A physical expla-
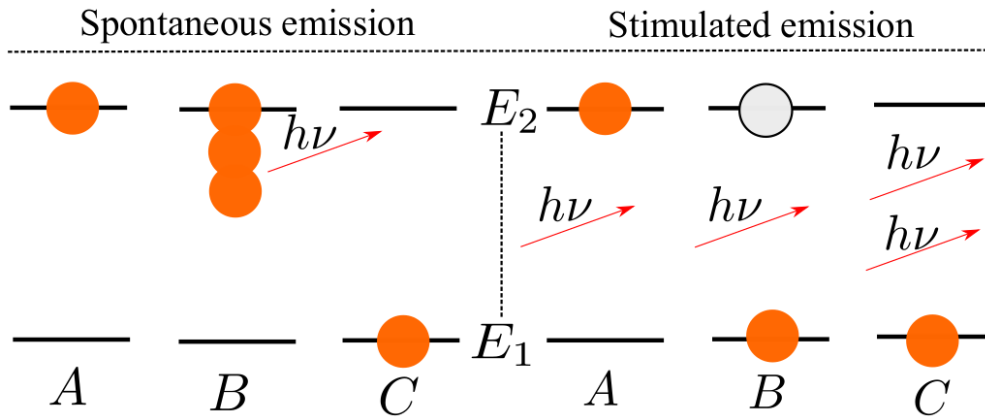
Figure 1.1: The spontaneous emission is illustrated on the left: A - atom in the excited state (energy E_2); B - emission of a photon ($h\nu$); C - atom in the ground state (energy $E_1 < E_2$). And the stimulated emission, on the right: A - before emission, with the atom in the excited state (energy E_2), and an incident photon; B - during emission of a photon ($h\nu$); C - After emission, with atom in the ground state (energy $E_1 < E_2$), and two emissions of a photon.

nation for spontaneous emission generally invokes the vacuum modes of the electromagnetic field [2]. After the development of the Jaynes-Cummings model [3], describing a two-level atomic system interacting with a quantized field mode within an optical cavity, it is possible to predict non-intuitively that the rate of spontaneous emission could be controlled depending on the boundary conditions of the surrounding vacuum field. Those experiments later originated the Cavity Quantum Electrodynamics (CQED), whereby it is possible to study the effects of mirrors and cavities on radiative corrections.

Spontaneous emission is not just an intrinsic property of excited systems, but is strongly dependent on the spectral content of zero-point fluctuations of the electromagnetic vacuum, and completely influenced by the presence of boundaries. Since the seminal work of Purcell [4], it is known that the environment has a profound influence on the decay rate of excited systems. In particular, when an excited system is close to interfaces, the imposed boundary conditions modify the density of possible electromagnetic modes. As a result, the decay rate changes due to the system's

coupling with the modified vacuum modes. When free atoms are positioned inside a cavity, the spontaneous emission rate is different from the value in free space [5,6].

The control of spontaneous emission processes is fundamental for the appropriate performance of optoelectronic devices, such as lighting screens, lasers, optical amplifiers and solar cells. The possibility of adjusting or controlling the spontaneous emission of radiation by excited systems has been interpreted as an important advancement for the development of a new class of quantum optical devices, such as nanospectrometers, nanolasers as well as electroluminescent and photonic band-gap structures [7–11].

The possibility of enhancement or suppression of the radiative emission rate of emitters positioned near conducting walls, wedges, spheres and cylinders, or trapped in microcavities such as parallel walls, spheres and ellipsoids has been extensively explored in recent years [5,12–36]. Recently, the spontaneous decay rate of quantum entangled atoms near interfaces has been a subject of increasing interest due to the possibility of generating and controlling quantum entangled radiation fields [37–40].

The first experimental work on inhibited spontaneous emission was performed by Drexhage, Kuhn and Schaefer (see Ref. [41]). In that work, the fluorescence of a thin dye film close to a mirror is investigated. They observed a reduction in the fluorescence decay of up to 25% resulting from the stationary-wave standard close to the mirror. Drexhage's experiment already provided a conclusive evidence that spontaneous emission rate depends essentially on the local optical environment. What is more, similar experiments were conducted by de Martini et al [42]. The experiment consists of the first achievement in optics of the resonant coupling of atoms with a single mode of the radiation field. Gabrielse and Dehmelt [43] also observed the inhibited spontaneous emission in 1985. Experiments with a single electron stored in a Penning trap demonstrate that cyclotron orbits had lifetimes up to 10 times larger than when calculated in free space. The electrodes of the trap form a cavity, which separates the cyclotron motion from the vacuum radiation field leading to a longer lifetime. Experiments with Rydberg atoms on inhibition of

spontaneous emission was also performed by Hulet et al [16] and by Jhe et al [44]. Hulet et al observed in their experiments that spontaneous radiation by an atom in a Rydberg state has been inhibited by the use of parallel conducting planes. In that work they observed that spontaneous emission is abruptly "turned off" at the cutoff frequency of the waveguidelike structure. The natural lifetime is measured to be increased by a factor of at least 20. Jhe et al observed that the radiative decay of Cs atoms excited into the $5D_{5/2}$ level and passing between two metallic mirrors spaced by a $1.1\mu m$ gap depends on its angular momentum. Furthermore, the spontaneous emission at a wavelength of $3.49\mu m$ is suppressed for the substates with maximum angular momentum normal to the mirrors, which survives without significant decay during approximately 13 natural lifetimes.

It has been observed by Goy et al [15] that the spontaneous-emission lifetime of Rydberg atoms is shortened by a large ratio when these atoms are crossing a high-Q superconducting cavity tuned to resonance with a millimeter-wave transition between adjacent Rydberg states. The experiment is performed with Rydberg atoms of Na excited in the 23s state in a niobium superconducting cavity resonant at 340 GHz. The cooling of the cavity had the advantage of totally suppressing the black-body field. The latter effect is completely absent if optical transitions are observed. In 1991 suppression and enhancement of spontaneous emission in semiconductor microcavities were demonstrated in experiments by Yamamoto et al (see a list of the above experiments in Ref. [45]).

It is incontrovertible that the spontaneous decay rate is drastically modified when the excited system is positioned close to interfaces. An interesting experimental result is shown in Fig. 1.2 [46, 47], where the spontaneous emission rate of a monolayer of Eu^{3+} ions positioned above a planar silver mirror is investigated as a function of the Eu^{3+} ion-metal separation. We can observe two different physical processes governing the behavior of excited molecules above metallic interfaces: for separations greater than about 10 spacer layers, the lifetime oscillates as a function of ion-metal separation and afterwards, as the ion-metal separation increases, the
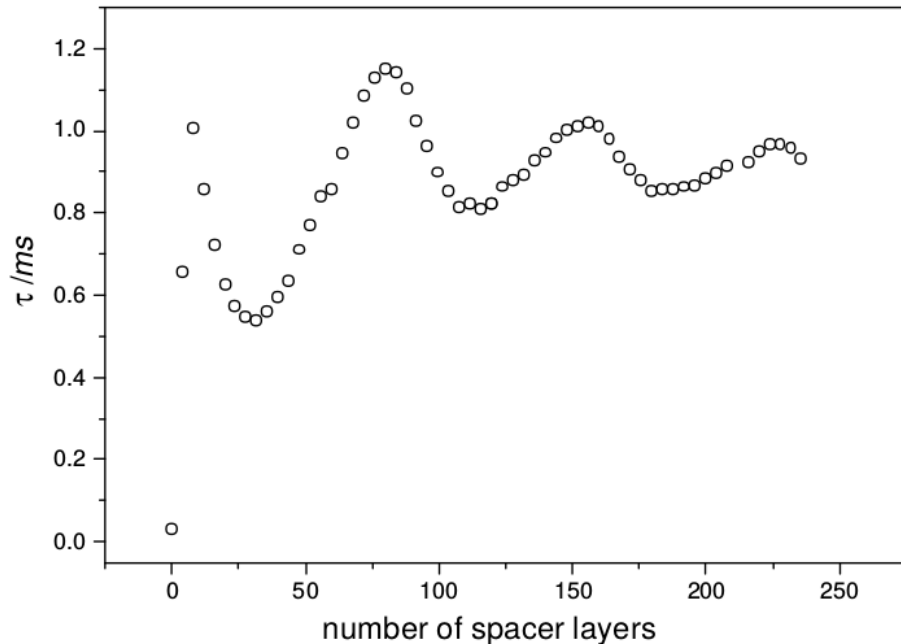
Figure 1.2: Experimental measure of the excited state lifetime of the Eu^{3+} complex in front of a silver mirror as a function of the ion-metal separation. The thickness of a single spacer layer is $2.6nm$. Figure taken from Ref. [46].

amplitude of the oscillations decreases. These features result from the interference between the direct emission from the dipole and that reflected from the mirror.

The result presented in Ref. [46] is similar to the one of Drexhage [41]. Yet, it makes it possible to deduce, as latter investigated in this work about spherical symmetries, how non-planar interfaces can modify the spontaneous decay rate of an excited system. Recently, it has been shown that the spontaneous emission can be either enhanced or suppressed using invisibility cloaks or gradient index lenses, with modification of the local density of optical states [48]. When the excited system is close to the interfaces, the boundary conditions modify the density of possible electromagnetic modes. Currently, the spontaneous decay rate of quantum entangled atoms close to interfaces has been a subject of growing interest of the scientific community [37–40].

Field-theoretical approaches have provided important insights on the influence of

boundary walls on the radiative process of detectors stimulated by the fluctuations of the quantum vacuum. Using a simple theoretical model in which the atom is represented by a two-level monopole coupled to a massless scalar field and the time-dependent perturbation theory within a first-order approach it is possible to obtain an analytical expression for the asymptotic decay rate as well as the method of images to calculate the appropriate Wightman's function evaluated in the world line of the atom. This function is associated with the boundary conditions. Although this approximation does not include polarization effects, such a model captures the essential ingredients needed to understand the influence of the field's mode changes induced by the presence of bounding surfaces on the atom's spontaneous emission, as demonstrated by Ford et al [19] that, in order to focus on the specific contribution of the modified field fluctuations, theoretically investigated the radiative properties of a two-level system in the presence of mirrors using the formalism and method described in the next chapter.

Experiments performed with spherical SiO_2 colloids with two different diameters doped with Erbium at different concentrations have shown a large difference in the spontaneous emission rate for both colloid sizes [22]. However, two factor influences on the spontaneous decay process, and thus are usually superposed: the modification of the field quantum fluctuations and polarization effects [24, 30, 32]. Other experiments performed with CdSe-CdS core-shell structures show that the involved dimensions for different samples has significant relevance in the decay process [49], and studies on the amplification of the spontaneous emission of such synthesized structures [50] also show such an effect.

In the present work, motivated by the above experiments, we extend exactly the same formalism and method used by Ford et al [19] to investigate the spontaneous decay rate of a two-level system close to a sphere with a perfectly reflecting surface (see Fig. 3.1), i.e., within a first-order time-dependent perturbation approach and method of images it is possible to calculate the appropriate Wightman's function, and an analytical expression for the decay rate of spontaneous emission. Both exte-

rior and interior problems are studied. Similarly, we studied the spontaneous decay rate of a two-level system trapped between perfectly reflecting concentric spheres (as shown in Fig. 4.1). Recently, the Casimir effect between two spherical shells was investigated [51]. For the atom trapped between the radii of the concentric spheres, Wightman's function of the atom incorporates contributions from an infinite set of variable image charges, satisfying Dirichlet boundary conditions. This approach has been previously used with success in the description of photodetection processes [52–55], in the investigation of the influence of parallel mirrors and strings on the radiation process [19, 56] and in recent studies of entanglement effects on radiative processes [38, 57–62].

This work is organized as follows. In the next chapter, we present the main aspects of the first-order perturbation theory, and that of the method of images applied to an excited monopole coupled to a Hermitian massless scalar field. We also present the theoretical basis of how a two-level detector interacting with a scalar field in the vacuum state (the formalism used in Ref. [55]) can be described as well as the calculation of the spontaneous decay rate performed by Ford et al to investigate the behavior of excited systems placed in the presence of mirrors: decay rate near one mirror and decay rate in the presence of two mirrors. The next two chapters are intended to compute the decay rate for the case, in which the two-level system is placed in the vicinity of a sphere with a perfectly reflecting surface, and in addition to calculating the decay rate of the atomic system placed between two concentric spheres with radii a and b. We provide a detailed analysis on the dependence of the decay rate on the atom's position, the radius of the sphere as well as on the frequency of the emitted radiation; and for the case of the spherical shell we analyze the decay rate on different relationships between the radii of the spheres and the emitted radiation energy. In the last chapter we summarize our most important findings and present some perspectives for future works. Throughout this text, we use units of $\hbar = c = 1$.

2

Formalism and method

In this chapter we present the main aspects of the first-order perturbation theory, and the method of images applied to an excited monopole coupled to Hermitian massless scalar field. We also present the theoretical basis of how it can describe a two-level detector interacting with a scalar field in the vacuum state (the formalism used in Ref. [55]) as well as the calculation of the spontaneous decay rate performed by Ford et al to investigate the behavior of excited systems placed in the presence of mirrors: decay rate near one mirror and decay rate in the presence of two mirrors.

2.1 A review on perturbation theory

Let us start with a brief review on perturbation theory and method of images, coming from quantum mechanics and electromagnetism courses.

2.1.1 Time-independent perturbation theory (non-degenerate case)

Let us suppose we solve the time-independent Schrodinger equation, and we find the complete set of eigenfunctions Ψ_n and energy eigenvalues E_n, as described in

Eq. 2.1

$$H^0 \Psi_n^0 = E^0 \Psi_n^0 \quad \Rightarrow \quad \left\{ \; \Psi_n^0, E_n^0 \quad \text{(eigenfunctions and energy eigenvalues)} \right. \quad (2.1)$$

where $\langle \Psi_n^0 | \Psi_m^0 \rangle = \delta_{mn}$, with $\delta_{mn} = 1$ for $m = n$ and $\delta_{mn} = 0$ for $m \neq n$.

Let us assume we apply a small perturbation on the potential in the Schrodinger equation. Now we are interested the solution of the Schrodinger equation of the perturbed system given by Eq. 2.2.

$$H \Psi_n = E \Psi_n \quad \Rightarrow \quad \left\{ \; \Psi_n, E_n \quad \text{(new eigenfunctions and energy eigenvalues)} \right. \quad (2.2)$$

Note that in Eq. 2.1 we use the index 0 in Ψ_n to denote the solutions of the non-perturbed system.

We need to find the new eigenfunctions Ψ_n and new energy eigenvalues E_n of the perturbed system. But the perturbed potential introduces certain problems in Schrodinger equation to be solved using the same rules previously used to solve the non-pertubed Schrodinger equation, as we learn in elementary courses of quantum mechanics. In addition, it is necessary to use a systematic procedure to obtain approximate solutions of Eq. 2.2. The procedure is also known as perturbation theory. This method allows of solving the Schrodinger equation of the pertubed system from the exact solutions of the non-perturbed system.

Let us start by writing the Hamiltonian H of the perturbed system as follows

$$H = H^0 + \lambda H', \quad (2.3)$$

where H^0 is the non-perturbed Hamiltonian, H' is a perturbation and λ is a small coefficient. Writing the eigenfunctions and energy eigenvalues of the Hamiltonian

H given by Eq. 2.3, we have that, respectively

$$\Psi_n = \Psi_n^0 + \lambda\Psi_n^1 + \lambda^2\Psi_n^2 + ... \tag{2.4}$$

$$E_n = E_n^0 + \lambda E_n^1 + \lambda^2 E_n^2 + ... \tag{2.5}$$

By substituting the eigenfunctions and energy eigenvalues above for Eq.2.3, and after some algebraic manipulations as well as grouping of terms, it is possible to obtain Eq. 2.5.

$$H^0\Psi_n^0 + \lambda(H'\Psi_n^0 + H^0\Psi_n^1) + \lambda^2(H' + \Psi_n^1 + H^0\Psi_n^2) + ...$$
$$= E_n^0\Psi_n^0 + \lambda(E_n^1\Psi_n^0 + E_n^0\Psi_n^1) + \lambda^2(E_n^1\Psi_n^1 + E_n^0\Psi_n^2 + E_n^2\Psi_n^0) + ... \tag{2.5}$$

What is more, we can group the terms according to the order of λ coefficients likewise and obtain the set of equations below, that provides the corrections in the eigenfunctions and energy eigenvalues introduced by the pertubation. Eqs. 2.6, 2.7 and 2.8 are used to calculate, respectively the " zero-order", first-order and second-order corrections. The other corrections can be obtained the same way.

$$H^0\Psi_n^0 = E_n^0\Psi_n^0 \tag{2.6}$$

$$H'\Psi_n^0 + H^0\Psi_n^1 = E_n^1\Psi_n^0 + E_n^0\Psi_n^1 \tag{2.7}$$

$$H'\Psi_n^1 + H^0\Psi_n^2 = E_n^1\Psi_n^1 + E_n^0\Psi_n^2 + E_n^2\Psi_n^0 \tag{2.8}$$

Notice that in expression 2.6 we have the Schrodinger equation of the non-perturbed system.

Let us calculate it using Eq. 2.7, the first-order corrections in eigenfunction and energy eigenvalues denoted by Ψ_n^1 and E_n^1. To do this, we use bra-ket notation

multiplying all terms of expression 2.7 by the corresponding bra $\langle\Psi_n^0|$.

$$\langle\Psi_n^0|H^{'}|\Psi_n^0\rangle + \langle\Psi_n^0|H^0|\Psi_n^1\rangle = \langle\Psi_n^0|E_n^1|\Psi_n^0\rangle + \langle\Psi_n^0|E_n^0|\Psi_n^1\rangle \qquad (2.9)$$

$$\Rightarrow \boxed{E_n^1 = \langle\Psi_n^0|H^{'}|\Psi_n^0\rangle}, \qquad (2.10)$$

that represents the first-order correction in the energy eigenvalues. This is simply the expected value of the perturbation Hamiltonian while the system is in the unperturbed state. Rewriting the Eq. 2.7 as follows, we can compute the first-order correction in eigenfunction Ψ_n^1.

$$(H^0 - E_n^0)\Psi_n^1 = -(H^{'} - E_n^1)\Psi_n^0 \qquad (2.11)$$

We know that the eigenfunctions Ψ_n^0 of the non-perturbed system are a complete set. Then, we can express any function $f(x)$ as linear combination of eigenfunctions from non-perturbed system, given by $f(x) = \sum_n c_n\Psi_n^0$. Here, we can apply this consideration to write Ψ_n^1.

$$\Psi_n^1 = \sum_{m\neq n} c_m^{(n)}\Psi_m^0 \qquad (2.12)$$

Our problem comes down to finding the coefficients $c_m^{(n)}$, where index n just denotes that we are interested in the coefficients of Ψ_n^1. Substituting Eq. 2.12 into Eq. 2.11

$$(H^0 - E_n^0)\sum_{m\neq n} c_m^{(n)}\Psi_m^0 = -(H^{'} - E_n^1)\Psi_n^0, \qquad (2.13)$$

that can be rewritten as

$$\sum_{m\neq n}(E_m^0 - E_n^0)c_m^{(n)}\Psi_m^0 = -(H^{'} - E_n^1)\Psi_n^0. \qquad (2.14)$$

To calculate the coefficients $c_m^{(n)}$ it is convenient to return to the bra-ket notation

and multiply the expression given by Eq. 2.14 by bra $\langle \Psi_l^0 |$

$$\sum_{m \neq n} (E_m^0 - E_n^0) c_m^{(n)} \langle \Psi_l^0 | \Psi_m^0 \rangle = -\langle \Psi_l^0 | H' | \Psi_n^0 \rangle + \langle \Psi_l^0 | E_n^1 | \Psi_n^0 \rangle. \tag{2.15}$$

If $l = n$, the left side of equation vanishes

$$0 = -\langle \Psi_n^0 | H' | \Psi_n^0 \rangle + E_n^1 \Rightarrow E_n^1 = \langle \Psi_n^0 | H' | \Psi_n^0 \rangle, \tag{2.16}$$

which is equivalent to the expected value of the perturbation Hamiltonian while the system is in the unperturbed state, already obtained above. This result does not help us find the second-order correction in the eigenfunction. But if $l \neq n$ then:

$$(E_l^0 - E_n^0) c_l^{(n)} = -\langle \Psi_l^0 | H' | \Psi_n^0 \rangle. \tag{2.17}$$

Now, changing index l by m we get the sought coefficient $c_m^{(n)}$

$$c_m^{(n)} = \frac{\langle \Psi_m^0 | H' | \Psi_n^0 \rangle}{(E_n^0 - E_m^0)}. \tag{2.18}$$

The first-order correction in eigenfunction can be written as

$$\boxed{\Psi_n^1 = \sum_{m \neq n} \frac{\langle \Psi_m^0 | H' | \Psi_n^0 \rangle}{(E_n^0 - E_m^0)} \Psi_m^0}. \tag{2.19}$$

When two unperturbed states have the same energy, they are named degenerate states. Note that this expression does not apply to degenerate cases, which is studied in the next subsection. It is important to stress that the energy given by $E_n \approx E_n^0 + E_n^1$, with corrections up to the first-order from perturbative system is very close to the exact energy. But this does not happen in the eigenfunctions. Here, we conclude the systematic procedures of the first-order perturbation theory.

Take now the expression given by Eq. 2.8 to obtain the second-order corrections in the energy eigenvalues. Let us start multiplying the mentioned equation by bra

$\langle\Psi_n^0|$, as follows

$$\langle\Psi_n^0|H'|\Psi_n^1\rangle + \langle\Psi_n^0|H^0|\Psi_n^2\rangle = \langle\Psi_n^0|E_n^1|\Psi_n^1\rangle + \langle\Psi_n^0|E_n^0|\Psi_n^2\rangle + \langle\Psi_n^0|E_n^2|\Psi_n^0\rangle. \quad (2.20)$$

After some elementary algebraic procedures it is possible to cancel some terms and obtain

$$E_n^2 = \sum_{m\neq n} c_m^{(n)}\langle\Psi_n^0|H'|\Psi_m^0\rangle, \quad \text{where} \quad c_m^{(n)} = \frac{\langle\Psi_m^0|H'|\Psi_n^0\rangle}{(E_n^0 - E_m^0)}. \quad (2.21)$$

As it turns, the second-order correction can be written as

$$E_n^2 = \sum_{m\neq n} = \frac{|\langle\Psi_n^0|H'|\Psi_m^0\rangle|^2}{(E_n^0 - E_m^0)}. \quad (2.22)$$

This is a fundamental result of second-order perturbation theory.

The procedures already described above are repeated to obtain the other corrections. The complex algebraic manipulations to the calculating the other corrections should not add additional contents to the results we need in this work. In particular, we are interested in understanding the process of spontaneous emission, which should occur through time-dependent perturbation theory, subject of the next subsections. But before, let us pass to degenerate case.

2.1.2   Time-independent perturbation theory (degenerate case)

We have presented a calculation methodology to obtain the corrections in the energy eigenvalues and eigenfunctions valid for non-degenerate cases. But what happens when two eigenstates Ψ_a^0 e Ψ_b^0 from Hamiltonian H^0 has the same energy $E_a^0 = E_b^0$? Note that $\langle\Psi_a^0|\Psi_b^0\rangle = 0$. The expressions of the corrections obtained in the previous subsection cannot be used because they are divergent (See Eqs. 2.19 and 2.22). For cases in which the eigenstates share the same energy, we use the degenerate perturbation theory.

Let us begin understanding the theory by presenting the case of double degeneracy. Afterwars we analyze the degeneracy of higher orders. Applying the Schrodinger equation to the two states of same energy E^0:

$$H^0\Psi_a^0 = E^0\Psi_a^0 \quad \text{and} \quad H^0\Psi_b^0 = E^0\Psi_b^0. \tag{2.23}$$

We can create a new state Ψ^0 given by linear combination of Ψ_a^0 and Ψ_b^0, with α and β auxiliary coefficients to keep the normalization of the states indexed by a and b, as written below

$$\Psi^0 = \alpha\Psi_a^0 + \beta\Psi_b^0. \tag{2.24}$$

This new eigenstate Ψ^0 given by Eq. 2.24 is also eigenfunction from H^0, as it is later demonstrated.

$$H^0\Psi^0 = \alpha H^0\Psi_a^0 + \beta H^0\Psi_b^0 \tag{2.25}$$

$$= \alpha E^0\Psi_a^0 + \beta E^0\Psi_b^0 \tag{2.26}$$

$$= E^0(\alpha\Psi_a^0 + \beta\Psi_b^0) \tag{2.27}$$

$$\Rightarrow \boxed{H^0\Psi^0 = E^0\Psi^0} \quad \text{(showing that Ψ^0 is eigenfunction from H^0.)} \tag{2.28}$$

The Hamiltonian H of the perturbed system is given by $H = H^0 + \lambda H'$, where H' is a perturbation introduced in the system. When we apply this perturbation, the degeneracy rises as λ increases between 0 and 1. In order to solve Schrodinger's equation $H\Psi = E\Psi$ of the perturbed system let us invoke the same considerations already described in subsection 2.1.2, where the corrections on energy eigenvalues and eigenfunctions are given by:

$$E = E^0 + \lambda E^1 + \lambda^2 E^2 + ... \quad \text{and} \quad \Psi = \Psi^0 + \lambda\Psi^1 + \lambda^2\Psi^2 + ... \tag{2.29}$$

Similar to the calculations of the previous subsection, i. e., by substituting Eqs.

2.29 in Schrodinger's equation and comparing the terms according to the λ order, we obtain the first-order equation

$$H^0\Psi^1 + H^{'}\Psi^0 = E^0\Psi^1 + E^1\Psi^0, \tag{2.30}$$

which, multiplied by the correspondent bra $\langle\Psi_a^0|$, can be rewritten

$$\langle\Psi_a^0|H^0|\Psi^1\rangle + \langle\Psi_a^0|H^{'}|\Psi^0\rangle = E^0\langle\Psi_a^0|\Psi^1\rangle + E^1\langle\Psi_a^0|\Psi^0\rangle. \tag{2.31}$$

By replacing the Eqs. 2.23 and 2.24 for Eq. 2.31 and after some simple algebraic procedures, we obtain

$$\alpha\langle\Psi_a^0|H^{'}|\Psi_a^0\rangle + \beta\langle\Psi_a^0|H^{'}|\Psi_b^0\rangle = E^{'}\alpha. \tag{2.32}$$

This expression is commonly written as

$$\alpha W_{aa} + \beta W_{ab} = E^1\alpha, \tag{2.33}$$

where a generic $W_{ij} = \langle\Psi_i^0|H^{'}|\Psi_j^0\rangle$, being matrix elements of $H^{'}$.

If we had multiplied the Eq. 2.30 by the bra $\langle\Psi_b^0|$ instead of bra $\langle\Psi_a^0|$, we would have obtained the following equation

$$\alpha W_{ba} + \beta W_{bb} = E^1\beta. \tag{2.34}$$

We can group Eqs. 2.33 and 2.34 in matricial notation

$$\begin{pmatrix} W_{aa} & W_{ab} \\ W_{ba} & W_{bb} \end{pmatrix} \begin{pmatrix} \alpha \\ \beta \end{pmatrix} = E^1 \begin{pmatrix} \alpha \\ \beta \end{pmatrix} \tag{2.35}$$

Notice that the terms of the matrix above $W_{ij} = \langle\Psi_i^0|H^{'}|\Psi_j^0\rangle$ are the matrix elements of perturbation $H^{'}$ related to the states Ψ_a^0 and Ψ_b^0. This matrix representation is

well known in linear algebra, where E^1 represents the eigenvalues of the matrix with elements $W_{ij} = \langle \Psi_i^0 | H' | \Psi_j^0 \rangle$, and $\begin{pmatrix} \alpha \\ \beta \end{pmatrix}$ represents the eigenfunctions. But here, it is sufficient to solve the system given by Eqs. 2.33 and 2.34. After some simplifications, we have

$$W_{ab}W_{ba} + (E^1 - W_{aa})(W_{bb} - E^1) = 0. \tag{2.36}$$

This expression is a quadratic equation and has two roots denoted $E_\pm^1$ given by

$$E_\pm^1 = \frac{1}{2}\left[(W_{aa} + W_{bb}) \pm \sqrt{(W_{aa} - W_{bb})^2 + 4|W_{ab}|^2}\right], \tag{2.37}$$

which is a fundamental result of the perturbation theory for the degenerate case, representing the corrections of first-order in the energy eigenvalues.

An interesting particular case occurs when $\alpha = 0$. For this value $E^1 = W_{bb}$. In addition, if $\alpha = 0$ then $\beta = 1$ by the normalization condition. See that in Eq. 2.33, under these conditions, $W_{ab} = W_{ba} = 0$. On the other hand, it is possible to conclude that $E_-^1 = W_{bb}$ and $E_+^1 = W_{aa}$. But if we remember

$$E_+^1 = W_{aa} = \langle \Psi_a^0 | H' | \Psi_a^0 \rangle \quad \text{and} \quad E_-^1 = W_{bb} = \langle \Psi_b^0 | H' | \Psi_b^0 \rangle. \tag{2.38}$$

Note also that when $\alpha = 0$ then $\Psi_+^0 = \Psi_a^0$ and $\Psi_-^0 = \Psi_b^0$. Now, consider the following theorem that helps to find the linear combinations that are really of physical interest, as occurred for $\alpha = 0$ and $\beta = 1$ and, therefore, $W_{ab} = W_{ba} = 0$.

Theorem: Let A be a Hermitian operator. Consider $[A, H^0] = 0$ and $[A, H'] = 0$ and Ψ_a^0, Ψ_b^0 are degenerate eigenstates of H^0 and also non-degenerate eigenstates of A, being ν and μ (with $\nu \neq \mu$) energy eigenvalues of Ψ_a^0 and Ψ_b^0, respectively. Then, $W_{ab} = 0$.

Proof:

$$[A, H^{'}] = 0 \tag{2.39}$$

$$\langle \Psi_a^0 | [A, H^{'}] | \Psi_b^0 \rangle = 0 \tag{2.40}$$

$$\langle \Psi_a^0 | AH^{'} - H^{'}A | \Psi_b^0 \rangle = 0 \tag{2.41}$$

$$\langle \Psi_a^0 | AH^{'} | \Psi_b^0 \rangle - \langle \Psi_a^0 | H^{'}A | \Psi_b^0 \rangle = 0 \tag{2.42}$$

$$\nu \langle \Psi_a^0 | H^{'} | \Psi_b^0 \rangle - \mu \langle \Psi_a^0 | H^0 | \Psi_b^0 \rangle = 0 \tag{2.43}$$

$$(\nu - \mu) \langle \Psi_a^0 | H^{'} | \Psi_b^0 \rangle = 0 \tag{2.44}$$

$$\text{as} \quad \nu \neq \mu \quad \text{then} \quad W_{ab} = 0 \tag{2.45}$$

When $W_{ab} = 0$, Ψ_a^0 and Ψ_b^0 are the eigenstates of physical interest that are eigenstates of Eq. 2.35.

We have studied so far the second-order perturbation theory. To analyse the higher-order perturbation theory, it is necessary to generalize the matricial equation given by to expression 2.35 and construct the characteristic equation using the matrix elements $W_{ij} = \langle \Psi_i^0 | H^{'} | \Psi_j^0 \rangle$. In this case, it is possible to obtain the first-order correction in the energy E^1.

2.1.3 Time-dependent perturbation theory

We have seen so far the so-called quantum statistics, where the potential depends just on the position

$$V(\vec{r}, t) = V(\vec{r}). \tag{2.46}$$

Hence, wave function $\Psi(\vec{r}, t)$ in time-dependent Schrodinger equation could be separated by the product of two parties: the first part is dependent just on position $\psi(\vec{r})$ and the second part is dependent just on time $\phi(t)$.

$$H\Psi(\vec{r}, t) = i\hbar \frac{\partial \Psi(\vec{r}, t)}{\partial t} \tag{2.47}$$

$$\Psi(\vec{r}, t) = \psi(\vec{r})\phi(t), \quad \text{where} \quad \phi(t) \approx e^{-\frac{it}{\hbar}}, \tag{2.48}$$

and $\psi(\vec{r})$ leads the independent-time Schrodinger equation $H\psi = E\psi$. Note that $|\Psi|^2 = |\psi(\vec{r})|^2$. This is the relevant physical quantity. Observe that all expected probabilities and values are constant over time due to this expression $|\Psi|^2 = |\psi(\vec{r})|^2$. Sometimes we even have states that we call stationary states ψ_i. These states also sometimes are not dependent on the time. But remember more elementary courses which state that although a linear combination of these stationary states could depend on time, and expected values of the energies and probabilities remain constant in time.

Here, we are interested in investigating a change of state of E_i energy to the E_j energy. Then, it is necessary that the system makes a transition between the mentioned states. This transition is also named "quantum jump". The transition phenomena cannot be explained using the formalism studied in the last subsections. In order to fully understand that, a time-dependent potential ($V(\vec{r}, t)$) must be inserted into the system, which means approaching a field in Physics known as

quantum dynamics.

There are few real solvable problems in quantum dynamics, but the solved problems are physically valuable. Fortunately, if the time-dependent part of the Hamiltonian $(H^{'}(t))$ is much smaller than the independent part of time (H^0), the time-dependent part can be treated as a perturbation $(H^{'}(t) \ll H^0)$. Based on those considerations we develop the time-dependent perturbation theory to study an important physical phenomena: the emission and absorption of radiation by atoms.

Let us start with two-level system

$$H^0\Psi_a = E_a\Psi_a \quad \text{and} \quad H^0\Psi_b = E_b\Psi_b, \quad \text{with} \quad \langle\Psi_i|\Psi_j\rangle = \delta_{ij} \quad (i,j = a,b). \quad (2.49)$$

Any state can be expressed as a linear combination of these two states (ψ_a and ψ_b), including the state described in Eq. 2.50

$$\Psi(0) = c_a\psi_a + c_b\psi_b. \quad (2.50)$$

If there is no perturbation, Eq. 2.50 evolves as we already know, with its characteristic exponential factor and the time-dependent wave function is given by

$$\Psi(t) = c_a\psi_a e^{-i\frac{E_a t}{\hbar}} + c_b\psi_b e^{-i\frac{E_b t}{\hbar}}. \quad (2.51)$$

Physically, the coefficients $|c_a|^2$ are the probability of the system to be in the ψ_a state, and $|c_b|^2$ the probability of the system to be in the ψ_b state. The square modulus of coefficients c_a and c_b are also associated with the measuring of energies E_a and E_b, respectively. Notice that $|c_a|^2 + |c_b|^2 = 1$.

But what occurs in the perturbation system? Now we introduce a perturbation $H^{'}(t)$ in the complete Hamiltonian $H = H^0 + H^{'}$. In this case, the total Hamiltonian H depends on time, and Eq. 2.51 must be generalized by introducing the temporal

dependence in the coefficients. The time-dependent wave function can be written as

$$\Psi(t) = c_a(t)\psi_a e^{-i\frac{E_a t}{\hbar}} + c_b(t)\psi_b e^{-i\frac{E_b t}{\hbar}}. \tag{2.52}$$

We need to investigate the new time-dependent coefficients. See a simple example for a specific time $t = t_1$ and the system in the $\Psi(t_1) = \Psi_a$. Well, then we have that $c_a(t_1) = 1$ and $c_b(t_1) = 0$. At a later time $t = t_2$ we find that $c_a(t_2) = 0$ and $c_b(t_2) = 1$. Then, in such conditions we know that the particle is in $\Psi(t_2) = \Psi_b$. We say that the system had a transition from Ψ_a state to Ψ_b state. That is better visualized by following relations:

$$\begin{cases} t = t_1 \\ \Psi(t_1) = \Psi_a \\ c_a(t_1) = 1; \quad c_b(t_1) = 0 \end{cases} \Rightarrow \begin{cases} t = t_2 \\ \Psi(t_2) = \Psi_b \\ c_a(t_2) = 0; \quad c_b(t_2) = 1. \end{cases} \tag{2.53}$$

To solve the problem let us to calculate $c_a(t)$ and $c_b(t)$, with condition that $\Psi(t)$ satisfies the time-dependent Schrodinger equation.

$$H = H^0 + H^{'}(t) \tag{2.54}$$

$$H\Psi = i\hbar\frac{\partial\Psi}{\partial t} \tag{2.55}$$

$$H\Psi = i\hbar\frac{\partial\Psi}{\partial t} \tag{2.56}$$

Let us substitute the Eqs. 2.52 and 2.54 for equation 2.56

$$(H^0 + H^{'}(t))(c_a(t)\psi_a e^{-i\frac{E_a t}{\hbar}} + c_b(t)\psi_b e^{-i\frac{E_b t}{\hbar}}) \tag{2.57}$$

$$= i\hbar\frac{\partial\Psi}{\partial t}(c_a(t)\psi_a e^{-i\frac{E_a t}{\hbar}} + c_b(t)\psi_b e^{-i\frac{E_b t}{\hbar}}) \tag{2.58}$$

$$c_a(t)[H^0\psi_a]e^{-i\frac{E_a t}{\hbar}} + c_b(t)[H^0\psi_b]e^{-i\frac{E_b t}{\hbar}} + c_a(t)[H^{'}(t)\psi_a]e^{-i\frac{E_a t}{\hbar}} \tag{2.59}$$

$$+c_b(t)[H^{'}(t)\psi_b]e^{-i\frac{E_b t}{\hbar}} = i\hbar[\dot{c}_a(t)\psi_a e^{-i\frac{E_a t}{\hbar}} + \dot{c}_b(t)\psi_b e^{-i\frac{E_b t}{\hbar}} \tag{2.60}$$

$$+c_a(t)\psi_a(\frac{-iE_a}{\hbar})e^{-i\frac{E_a t}{\hbar}} + c_b(t)\psi_b(\frac{-iE_b}{\hbar})e^{-i\frac{E_b t}{\hbar}}] \tag{2.61}$$

Assuming that $H^0\psi_a = E_a\psi_a$ and $H^0\psi_b = E_b\psi_b$ in the expression above, and after some algebraic simplifications that imply in cancellation of similar terms

$$c_a(t)[H^{'}(t)\psi_a]e^{-i\frac{E_a t}{\hbar}} + c_b(t)[H^{'}(t)\psi_b]e^{-i\frac{E_b t}{\hbar}} \tag{2.62}$$

$$= i\hbar\dot{c}_a(t)\psi_a e^{-i\frac{E_a t}{\hbar}} + i\hbar\dot{c}_b(t)\psi_b e^{-i\frac{E_b t}{\hbar}}. \tag{2.63}$$

Multiplying all terms of this equation by the bra $\langle\psi_a|$

$$c_a(t)\langle\psi_a|H^{'}(t)|\psi_a\rangle e^{-i\frac{E_a t}{\hbar}} + c_b(t)\langle\psi_a|H^{'}(t)|\psi_b\rangle e^{-i\frac{E_b t}{\hbar}} = i\hbar\dot{c}_a(t)e^{-i\frac{E_a t}{\hbar}}. \tag{2.64}$$

Introducing the notation $H^{'}_{i,j} = \langle\psi_i|H^{'}(t)|\psi_j\rangle$ (with $j, j = a, b$), we can rewrite this expression as follows

$$\dot{c}_a(t) = -\frac{i}{\hbar}[c_a(t)H^{'}_{aa} + c_b(t)H^{'}_{ab}e^{\frac{-i[E_b - E_a]t}{\hbar}}]. \tag{2.65}$$

Similarly, we could have multiplied Eq. 2.63 by $\langle\psi_b|$ and obtained

$$\dot{c}_b(t) = -\frac{i}{\hbar}[c_a(t)H^{'}_{ba}e^{\frac{+i[E_b - E_a]t}{\hbar}} + c_b(t)H^{'}_{bb}]. \tag{2.66}$$

Notice that using the Eqs. 2.65 and 2.66 we can find $\dot{c}_a(t)$ and $\dot{c}_a(t)$. These equations are completely equivalent to the time-dependent Schrodinger equation and can be written in a matricial notation given by

$$\begin{pmatrix} \dot{c}_a(t) \\ \dot{c}_b(t) \end{pmatrix} = \frac{-i}{\hbar} \begin{pmatrix} H^{'}_{aa} & H^{'}_{ab}e^{\frac{-i[E_b - E_a]t}{\hbar}} \\ H^{'}_{ba}e^{\frac{+i[E_b - E_a]t}{\hbar}} & H^{'}_{bb} \end{pmatrix} \begin{pmatrix} c_a(t) \\ c_b(t) \end{pmatrix}. \tag{2.67}$$

Usually $H'_{aa} = H'_{bb} = 0$ and the terms of the matrix equation take a simpler form

$$\dot{c}_a(t) = -\frac{i}{\hbar} H'_{ab} e^{\frac{-i[E_b - E_a]t}{\hbar}} c_b(t). \qquad (2.68)$$

$$\dot{c}_b(t) = -\frac{i}{\hbar} H'_{ba} e^{\frac{+i[E_b - E_a]t}{\hbar}} c_a(t). \qquad (2.69)$$

Let us denote $\omega_0 = \frac{E_b - E_a}{\hbar}$ and note that $\omega_0 > 0$ when $E_b - E_a > 0$. Eqs. 2.68 and 2.69 can be rewritten as follows

$$\dot{c}_a(t) = -\frac{i}{\hbar} H'_{ab} e^{-i\omega_0 t} c_b(t). \qquad (2.70)$$

$$\dot{c}_b(t) = -\frac{i}{\hbar} H'_{ba} e^{+i\omega_0 t} c_a(t). \qquad (2.71)$$

So far, all presented procedures are exact and we make no suppositions on perturbation $H'(t)$. For a small pertubation H', we can solve the Eqs. 2.70 and 2.71 using a process of successive approximations named time-dependent perturbation theory. To apply this process let us suppose that the system is in a state where $c_a(0) = 1$ and $c_b(0) = 0$. It is important to emphasize that without the perturbation, the system would keep itself forever in such a condition. For this case, we are describing the zero-order, i.e, without perturbation.

Zero-order:

$$c_a^{(0)}(t) = 1 \quad \text{and} \quad c_b^{(0)}(t) = 0. \qquad (2.72)$$

Higher-orders:

$$\frac{d}{dt} c_a^{(n+1)}(t) = -\frac{i}{\hbar} H'_{ab} e^{-i\omega_0 t} c_b^{(n)}(t). \qquad (2.73)$$

$$\frac{d}{dt}c_b^{(n+1)}(t) = -\frac{i}{\hbar}H_{ba}'e^{+i\omega_0 t}c_a^{(n)}(t).$$ (2.74)

Having coefficients of n-order we can obtain the $(n+1)$-order coefficients. This way let us calculate the corrections.

First-order $(n = 1)$:

$$\frac{d}{dt}c_a^{(1)}(t) = -\frac{i}{\hbar}H_{ab}'e^{-i\omega_0 t}0 \Rightarrow \boxed{c_a^{(1)}(t) = 1} \quad \text{(a constant)}.$$ (2.75)

$$\frac{d}{dt}c_b^{(1)}(t) = -\frac{i}{\hbar}H_{ba}'e^{+i\omega_0 t}1.$$ (2.76)

$$\Rightarrow \boxed{c_b^{(1)}(t) = -\frac{i}{\hbar}\int_0^t H_{ba}'(t')e^{i\omega_0 t'}\,dt'}.$$ (2.77)

This result represents the first-order correction. Let us calculate the second-order correction.

Second-order $(n = 2)$:

$$\frac{d}{dt}c_a^{(2)}(t) = -\frac{i}{\hbar}H_{ab}'e^{-i\omega_0 t}c_b^{(1)}(t)$$ (2.78)

$$= -\frac{i}{\hbar}H_{ab}'e^{-i\omega_0 t}(-\frac{i}{\hbar})\int_0^t H_{ba}'(t')e^{i\omega_0 t'}\,dt'$$ (2.79)

$$\Rightarrow \frac{d}{dt}c_a^{(2)}(t) = \frac{-1}{\hbar^2}H_{ab}'e^{-i\omega_0 t}\left[\int_0^t H_{ba}'(t')e^{i\omega_0 t'}\,dt'\right]$$ (2.80)

$$\Rightarrow \boxed{c_a^{(2)}(t) = \frac{-1}{\hbar^2}\int_0^t H_{ab}'e^{-i\omega_0 t'}\left[\int_0^{t'} H_{ba}'(t'')e^{i\omega_0 t''}\,dt''\right]dt'}$$ (2.81)

Let us calculate the $c_b^{(2)}(t)$

$$\frac{d}{dt}c_b^{(2)}(t) = -\frac{i}{\hbar}H_{ba}'e^{+i\omega_0 t}c_a^{(1)}(t).$$ (2.82)

But $c_a^{(1)}(t) = 1$. Let us therefore continue

$$\Rightarrow \boxed{c_b^{(2)}(t) = -\frac{i}{\hbar} \int_0^t H_{ba}' e^{+i\omega_0 t'} dt' = c_b^{(1)}(t)}. \tag{2.83}$$

The used methodology can be extended to calculate the other corrections.

2.1.4 Time-dependent perturbation theory - emission and absorption

Let us apply the time-dependent perturbation theory to study the emission and absorption of radiation. But first let us study a type of perturbation that can help us characterize the emission and absorption processes of radiation, named sinusoidal perturbations. This type of perturbation can be written as

$$H'(\vec{r}, t) = V(\vec{r}) \cos(\omega t). \tag{2.84}$$

Now, to calculate the corrections we need to obtain the element H_{ba}', as described in previous subsection.

$$H_{ba}' = \langle \psi_b | H' | \psi_a \rangle = \langle \psi_b | V(\vec{r}) \cos(\omega t) | \psi_a \rangle \tag{2.85}$$

$$\Rightarrow H_{ba}' = \langle \psi_b | V(\vec{r}) | \psi_a \rangle \cos(\omega t) = V_{ba} \cos(\omega t) \quad (\text{with } V_{ba} \equiv \langle \psi_b | V(\vec{r}) | \psi_a \rangle) \tag{2.86}$$

Using time-dependent perturbation theory, the first-order corrections can be obtained as follows:

$$c_b(t) \approx -\frac{i}{\hbar} \int_0^t H_{ba}'(t') e^{i\omega_0 t'} dt' \tag{2.87}$$

$$c_b(t) \approx -\frac{iV_{ba}}{\hbar} \int_0^t \cos(\omega t') e^{i\omega_0 t'} dt' \tag{2.88}$$

$$\frac{e^{i\omega t'} + e^{-i\omega t'}}{2} = \cos(\omega t') \quad \text{(remembering of this identity)} \tag{2.89}$$

$$\Rightarrow c_b(t) \approx -\frac{iV_{ba}}{2\hbar} \int_0^t [e^{i(\omega_0+\omega)t'} + e^{-i(\omega_0-\omega)t'}]dt' \tag{2.90}$$

Solving the above integral

$$c_b(t) \approx -\frac{iV_{ba}}{2\hbar} \left[\frac{e^{i(\omega_0+\omega)t'}}{i(\omega_0-\omega)} + \frac{e^{i(\omega_0-\omega)t'}}{i(\omega_0-\omega)} \right]_0^t \tag{2.91}$$

$$\Rightarrow c_b(t) \approx -\frac{iV_{ba}}{2\hbar} \left[\frac{e^{i(\omega_0+\omega)t}-1}{i(\omega_0+\omega)} + \frac{e^{i(\omega_0-\omega)t}-1}{i(\omega_0-\omega)} \right] \tag{2.92}$$

$$\Rightarrow c_b(t) \approx -\frac{V_{ba}}{2\hbar} \left[\frac{e^{i(\omega_0+\omega)t}-1}{(\omega_0+\omega)} + \frac{e^{i(\omega_0-\omega)t}-1}{(\omega_0-\omega)} \right] \tag{2.93}$$

If $\omega \rightarrow \omega_0 \Rightarrow \omega_0 + \omega \gg \omega_0 - \omega$. Notice that the first term of the sum between brackets in Eq. 2.93 is negligible compared to the second term. In such a condition the Eq. 2.93 can be simplifield

$$c_b(t) \approx -\frac{V_{ba}}{2\hbar} \left[\frac{e^{i(\omega_0-\omega)t}-1}{(\omega_0-\omega)} \right] \tag{2.94}$$

$$\Rightarrow c_b(t) \approx -\frac{V_{ba}}{2\hbar} e^{i(\omega_0-\omega)t/2} \left[\frac{e^{i(\omega_0-\omega)t/2} - e^{-i(\omega_0-\omega)t/2}}{(\omega_0-\omega)} \right] \tag{2.95}$$

$$\frac{e^{i(\omega_0-\omega)t/2} - e^{-i(\omega_0-\omega)t/2}}{2i} = \sin(\omega_0-\omega)t/2 \quad \text{(remembering of this identity)} \tag{2.96}$$

$$\Rightarrow \boxed{c_b(t) \approx -\frac{V_{ba}}{\hbar} \frac{\sin(\omega_0-\omega)t/2}{\omega_0-\omega} e^{i(\omega_0-\omega)t/2}} \tag{2.97}$$

But the physical interest is in the calculation of the transition probability from a to b, given by $P_{a\rightarrow b}(t) = |c_b(t)|^2$.

$$P_{a\rightarrow b}(t) = |c_b(t)|^2 \approx \frac{|V_{ba}|^2}{|\hbar|^2} \frac{\sin^2(\omega_0-\omega)t/2}{(\omega_0-\omega)^2} \tag{2.98}$$

See that the maximum probability value is $P_{max}(t) = |\frac{|V_{ba}|}{\hbar(\omega_0 - \omega)}|^2$, and the expression of the probability oscillates between 0 and 1. Notice that $|\frac{|V_{ba}|}{\hbar(\omega_0 - \omega)}|^2 \ll 1$, in reason of the hypothesis of small perturbation. Equation 2.98 is plotted in Fig. 2.1.
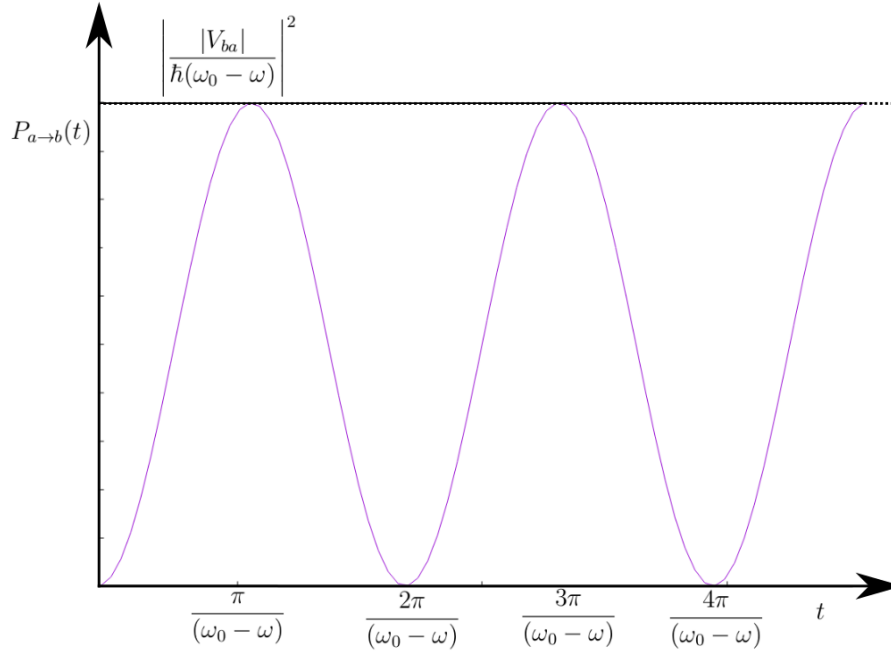

Figure 2.1: Transition probability as time function. $|\frac{|V_{ba}|}{\hbar(\omega_0 - \omega)}|^2 \ll 1$ is the maximum value of probability.

The Fig. 2.1 shows the transition probability of the system between the ψ_a and ψ_b states.

Here, it is already possible to understand the phenomenon of absorption, stimulated emission, and spontaneous emission of radiation. Consider an atomic system in a lower energy state ψ_a being irradiated by monochromatic light. Then, the transition probability to a higher energy state ψ_b, can be calculated using the Eq. 2.98, already deduced above. The incident monochromatic light can be treated as a perturbation, and we know from elementary courses of electrodynamics, as well as quantum mechanics courses, that perturbation can be written as $V_{ba} = -pE_0$ (where $p \rightarrow$ dipole moment and $E_0 \rightarrow$ monochromatic electric field). See references [63,64]

for a broader study. For this system the transition probability is given by

$$P_{a\to b}(t) = |c_b(t)|^2 \approx \left(\frac{pE_0}{\hbar}\right)^2 \frac{\sin^2(\omega_0 - \omega)t/2}{(\omega_0 - \omega)^2}. \tag{2.99}$$

To make the transition, the system absorbed the energy of the field $E_b - E_a = \hbar\omega$. We say that the system "absorbed" a photon. Notice that $P_{ba}(t) = P_{ab}(t)$. This is a curious fact known as stimulated emission, in which an incident photon of specific frequency can interact with an excited atomic electron, or other excited molecular state, bringing it to a lower energy level. In this case the released energy is transferred to the electromagnetic field, creating a new photon with a phase, frequency, polarization, and direction of travel identical to the photons of the incident wave, as discussed in chapter 1 (See Fig. 1.1).

The physical system may, however, spontaneously decay from a higher energy state to a lower energy state in a process called spontaneous emission. Spontaneous emission cannot be explained using the classical electromagnetic theory and is considered as a fundamentally quantum process. A physical explanation for spontaneous emission generally invokes the zero-point energy of the electromagnetic field [2], as also discussed in chapter 1. There are some methods for calculating the spontaneous emission rate, such as through the Einstein's coefficients as well as the selection rules that are also useful for calculating the spontaneous emission rate (See references [63, 64] for a complete study).

Time-dependent perturbation theory (Dyson's series)

Only a few class of problems are exactly solved using the formalism to obtain the first-order, second-order corrections and so on, discussed in subsection 2.1.3 for a two-level system. We need to be satisfied with the approximate perturbative expansion given by Eq. 2.100,

$$c_n(t) = c_n^{(0)} + c_n^{(1)} + c_n^{(2)} + ..., \tag{2.100}$$

where $c_n^{(1)}, c_n^{(2)}, ...$ are mentioned corrections.

Similar to the result provided by the Eq. 2.72, to obtain the all corrections given by the right-side of the Eq. 2.100 in a more general case, we must consider $c_n^{(0)} = \delta_{nl}$ (independent of t), as already deducted for a two-level system. To obtain the other corrections $(c_n^{(1)}, c_n^{(2)}, ...)$ is enough successive substitutions in a broader matricial equation then the Eq. 2.67. This is the development methodology of the time-dependent perturbation theory attributed to Dirac.

Another methodology, very powerful, applicable to more general and advanced problems, such as relativistic quantum field theory and many-body theory, it is to work with evolution operator $U_I(t, t_0)$ instead of $c_n(t)$ in the interaction picture (see Ref. [64]).

Let us define the time-evolution operator in the interaction picture

$$|\alpha, t_0; t\rangle_I = U_I(t, t_0)|\alpha, t_0; t_0\rangle_I. \tag{2.101}$$

The Schrodinger differential equation for the state ket in the interaction picture can be written as

$$i\hbar \frac{d}{dt} U_I(t, t_0) = V_I(t) U_I(t, t_0). \tag{2.102}$$

Under the initial condition given by the below equation

$$U_I(t, t_0)|_{t=t_0} = 1, \tag{2.103}$$

the differential equation given by expression 2.102 is analogous to the integral equation

$$U_I(t, t_0) = 1 - \frac{i}{\hbar} \int_{t_0}^{t} V_I(t') U_I(t', t_0) dt'. \tag{2.104}$$

By iteration, it is possible to obtain an approximate solution to the Eq. 2.104

$$U_I(t, t_0) = 1 - \frac{i}{\hbar} \int_{t_0}^{t} V_I(t') \left[1 - \frac{i}{\hbar} \int_{t_0}^{t'} V_I(t'') U_I(t'', t_0) dt'' \right] dt', \qquad (2.105)$$

And so on, as follows

$$U_I(t, t_0) = 1 - \frac{i}{\hbar} \int_{t_0}^{t} V_I(t') + \left(\frac{-i}{\hbar} \right)^2 \int_{t_0}^{t} dt' \int_{t_0}^{t'} dt'' V_I(t') V_I(t'') \qquad (2.106)$$

$$+ ... + \left(\frac{-i}{\hbar} \right)^n \int_{t_0}^{t} dt' \int_{t_0}^{t'} dt'' ... \int_{t_0}^{t^{(n-1)}} dt^{(n)} V_I(t') V_I(t'') ... V_I(t^{(n)}) + ... \qquad (2.107)$$

It is important to stress that after Freeman J. Dyson applied with success the method described to covariant quantum electrodynamics (QED), the series above passed to be nominated Dyson series.

Knowing $U_I(t, t_0)$ we can determine the evolution of a state ket at the any t, since the initial state $t = 0$

$$|i, t_0 = 0; t\rangle_I = U_I |i\rangle \qquad (2.108)$$

$$= \sum_n |n\rangle \langle n| U_I(t, 0) |i\rangle, \qquad (2.109)$$

where $\langle n| U_I(t, 0) |i\rangle$ is associated to the $c_n(t)$, as we will see follow. The conection between the evolution operator $U(t, t_0)$ in Schrodinger picture with $U_I(t, t_0)$ in interaction picture can be obtained:

$$|\alpha, t_0; t\rangle_I = e^{\frac{iH_0 t}{\hbar}} |\alpha, t_0; t\rangle_S \qquad (2.110)$$

$$= e^{\frac{iH_0 t}{\hbar}} U(t, t_0) |\alpha, t_0; t\rangle_S \qquad (2.111)$$

$$= e^{\frac{iH_0 t}{\hbar}} U(t, t_0) e^{\frac{-iH_0 t_0}{\hbar}} |\alpha, t_0; t_0\rangle_t \qquad (2.112)$$

$$U_I(t, t_0) = e^{\frac{iH_0 t}{\hbar}} U(t, t_0) e^{\frac{-iH_0 t_0}{\hbar}}. \qquad (2.113)$$

Thus we have

$$\langle n|U_I(t, t_0)|i\rangle = e^{\frac{t(E_n t - E_i t_0)}{\hbar}} \langle n|U(t, t_0)|i\rangle, \tag{2.114}$$

And now we can compute the transition probability looking to the matrix element between energy eigenstates of H_0. The transition probability is defined as the square of the modulus $\langle n|U(t, t_0)|i\rangle$.

$$|\langle n|U_I(t, t_0)|i\rangle|^2 = |\langle n|U(t, t_0)|i\rangle|^2. \tag{2.115}$$

Consider the system in a physical situation which $t = t_0$. Now, applying the interaction picture, we have

$$|i, t_0; t_0\rangle_s = e^{\frac{-iE_t t_0}{\hbar}}|i\rangle, \tag{2.116}$$

So in the interaction picture we obtain a simple equation.

$$|i, t_0; t_0\rangle_I = |i\rangle \tag{2.117}$$

Let us write the state ket at a later time

$$|i, t_0; t\rangle_I = U_I(t, t_0)|i\rangle. \tag{2.118}$$

Notice that, if we compare Eq. 2.118 with the expansion given by equation

$$|i, t_0; t\rangle_I = \sum_n c_n(t)|n\rangle, \tag{2.119}$$

we observe an interesting result

$$c_n(t) = \langle n|U_I(t, t_0)|i\rangle. \tag{2.120}$$

This result shown by Eq. 2.120, if we compare with pertubation expansion for $U_I(t, t_0)$ substituted in Eq. 2.120, provides

$$c_n^{(0)}(t) = \delta_{nl} \quad \text{independent of t} \tag{2.121}$$

$$c_n^{(1)}(t) = \frac{-i}{\hbar} \int_{t_0}^{t} \langle n|V_I(t^{'})|i\rangle dt^{'} = \frac{-i}{\hbar} \int_{t_0}^{t} e^{l\omega_{nl}t^{'}} V_{nl}(t^{'}) dt^{'} \tag{2.122}$$

$$c_n^{(2)}(t) = \left(\frac{-i}{\hbar}\right)^2 \sum_n \int_{t_0}^{t} dt^{'} \int_{t_0}^{t^{'}} dt^{''} e^{l\omega_{nl}t^{'}} V_{nm} e^{l\omega_{ml}t^{''}} V_{ml}(t^{''}) \tag{2.123}$$

Remembering that

$$e^{\frac{l(E_n - E_t)t}{\hbar}} = e^{l\omega_{nl}t}. \tag{2.124}$$

The transition probability for $|i\rangle \rightarrow |n\rangle$ (with $n \neq i$) is given by

$$P(i \rightarrow n) = |c_n^{(1)}(t) + c_n^{(2)}(t) + ...|^2. \tag{2.125}$$

The fundamentals of the perturbation theory presented so far, in particular, the formalism of the first-order time-dependent perturbation approach, will be useful in the next chapters.

2.2   The method of images

From electrodynamics courses, we know the uniqueness theorem for Poission's ($\nabla^2 V = \rho/\epsilon_0$) or Laplace's equations ($\nabla^2 V = 0$). In particular, whatever the method whereby the solution of Laplace's equation is obtained, the solution is that, and no other. Frequently, it is not easy to obtain an analytic solution to either of these equations. Even when it is possible to do so, it may require a solid mathematical basis.

Fortunately, we can conjecture the real physical situation with another situation, constructed in an intuitive way, but which satisfies the same boundary conditions of the real problem. Then, we can apply the uniqueness theorem of Laplace's equation to solve the intuitive problem. This method is named as method of images, and it is used to calculate the potential function an arbitrary position of the space caused by the q charge in the presence of a spherical surface, as we show follow.

In both cases, real and intuitive situation, the solution V (potential function) of the Laplace's equation must satisfies the Dirichlet boundary condition, i. e., $V = 0$ at all points at the surface or other type of envoled limits. Using the method of images considering the function $G(\vec{r})$ analogous to the electric field to characterize the modulus of the total electric field caused by the set of real and image charges shown in Fig. 2.2. As we know $G(\vec{r})$ is composed by the sum of the electric field of
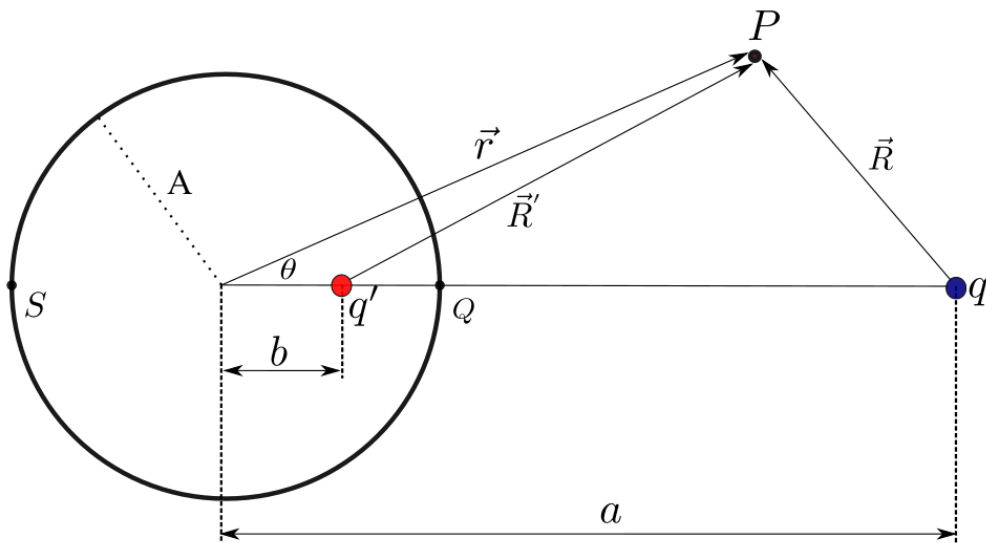

Figure 2.2: Schematic view for a real charge and its image (exterior problem).

the real charge and its respective image q', satisfying Dirichlet conditions.

$$G(\vec{r}) = \frac{q}{R^2} + \frac{q'}{R'^2},$$

(2.126)

where R and R' are obtained of the law of cosines

$$R^2 = r^2 + a^2 - 2ra\cos\theta \tag{2.127}$$

$$R'^2 = r^2 + b^2 - 2rb\cos\theta. \tag{2.128}$$

Notice that R and R' are indicated in Fig. 2.2 and denote the position of point P in relation to the real charge and image charge, respectively. In addition, the other parameters are: $a \to$ charge's position, $b \to$ images's position and $A \to$ radius of the sphere.

The function $G(\vec{r})$ can be written as

$$G(\vec{r}) = \frac{q}{r^2 + a^2 - 2ra\cos\theta} + \frac{q'}{r^2 + b^2 - 2rb\cos\theta}. \tag{2.129}$$

In order to obtain the position b and the value of the image charge q', we can consider the Dirichlet boundary condition, because if G vanishes at all points on the spherical surface, G is null in the Q and S points $(G(Q) = G(S) = 0)$. Applying this condition it is possible to obtain b and q' as described below.

$$\frac{q}{(a-A)^2} + \frac{q'}{(A-b)^2} = 0 \tag{2.130}$$

$$\frac{q}{(a+A)^2} + \frac{q'}{(A+b)^2} = 0 \tag{2.131}$$

$$q(A-b)^2 + q'(a-A)^2 = 0 \tag{2.132}$$

$$q(A+b)^2 + q'(a+A)^2 = 0 \tag{2.133}$$

$$q^{'} = -q\frac{(A-b)^2}{(a-A)^2} \tag{2.134}$$

$$q(A+b)^2 - q\frac{(A-b)^2}{(a-A)^2}(a+A)^2 = 0 \tag{2.135}$$

$$\cancel{q}(A+b)^2 + (a-A)^2 - \cancel{q}(A-b)^2(a+A)^2 = 0 \tag{2.136}$$

$$(A+b)(a-A) - (A-b)(a+A) = 0 \tag{2.137}$$

$$Aa - A^2 + ba - bA - (Aa + A^2 - ba - bA) = 0 \tag{2.138}$$

$$\cancel{Aa} - A^2 + ba - \cancel{bA} - \cancel{Aa} - A^2 + ba + \cancel{bA} = 0 \tag{2.139}$$

$$-\cancel{2}A^2 + \cancel{2}ba = 0 \tag{2.140}$$

As it turns

$$\boxed{b = \frac{A^2}{a}}, \tag{2.141}$$

which represents the searched position of the image charge. Substituting Eq. 2.141 in Eq. 2.134

$$q^{'} = q\frac{(A-\frac{A^2}{a})^2}{(a-A)^2} = -q\frac{(\frac{Aa-A^2}{a})^2}{(a-A)^2} \tag{2.142}$$

$$q^{'} = -q\frac{[A(a-A)]^2}{(a-A)^2} = -qA^2\frac{\cancel{(a-A)^2}}{a^2}\frac{1}{\cancel{(a-A)^2}}, \tag{2.143}$$

Thus, we have the value of the image charge $q^{'}$ and its sign is opposite to the atom

$$\boxed{q^{'} = -q\frac{A^2}{a^2}}. \tag{2.144}$$

The interior problem, when the atom is positioned in the interior region of the sphere is shown in Fig. 2.3. In this case, the opposite image charge emerges in the exterior region. Now, the parameters a is the images's position, ρ is the charges's position and A is the radius of the sphere. Here, the charge and its images remains
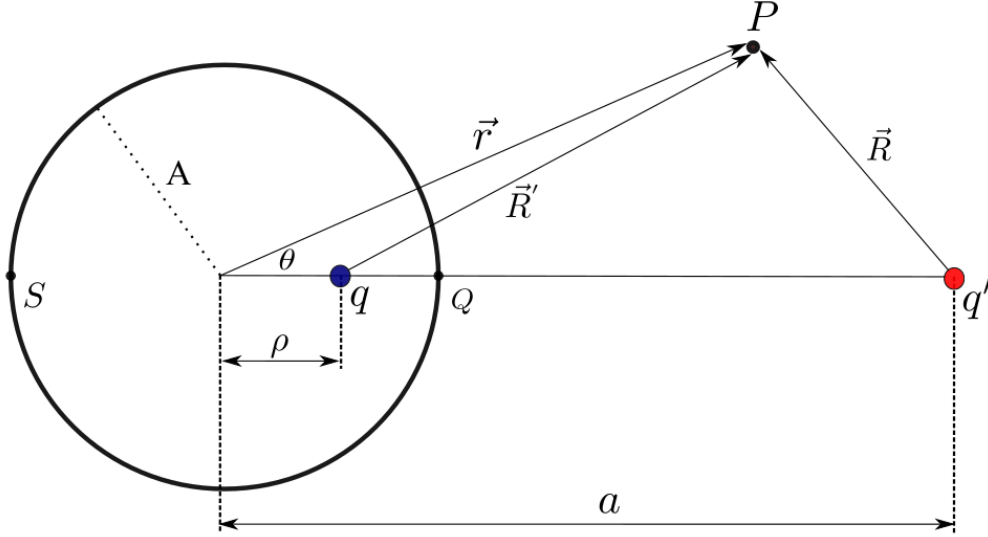
Figure 2.3: Schematic view for a real charge and its image (interior problem).

denoted by the q and q', respectively. The $G(\vec{r})$ can be written as

$$G(\vec{r}) = \frac{q}{R^2} + \frac{q'}{R'^2}. \tag{2.145}$$

As $\vec{R} = \vec{r} - \vec{\rho}$ and $\vec{R'} = \vec{r} - \vec{a}$ the parameters that appear in Eq. 2.145 are calculated of the same way for the exterior problem (atom positioned in exterior region of the sphere).

$$G(\vec{r}) = \frac{q}{r^2 + \rho^2 - 2r\rho\cos\theta} + \frac{q'}{r^2 + a^2 - 2ra\cos\theta} \tag{2.146}$$

From the Dirichlet boundary conditions, in particular, of $G(Q) = G(S) = 0$, we have

$$\frac{q}{(A - \rho)^2} + \frac{q'}{(a - A)^2} = 0 \tag{2.147}$$

$$\frac{q}{(A + \rho)^2} + \frac{q'}{(a + A)^2} = 0 \tag{2.148}$$

Therefore, solving the system of above equations

$$\boxed{a = \frac{A^2}{\rho}} \quad \text{and} \quad \boxed{q^{'} = q\frac{A^2}{\rho^2}}. \tag{2.149}$$

A very interesting fact in the values of the position and image charge given by the Eq. 2.149 is the similarity with the obtained values of the external problem. These parameters are such as we would have if we physically look to the Fig. 2.3 and imagining the Fig. 2.2, that is, by permute the positions of the atom and its image.

The results of this section is useful in the chapters 3 and 4 to calculate the spontaneous emission rate of a two-level system positioned in the vicinity of a perfectly reflecting spherical surface as well as for the same atomic system positioned between concentric spheres. In these chapters, the results of this subsection will be extended.

2.3 A theoretical model for understanding the spontaneous emission processes

Let us start by reviewing the standard theoretical description of the radioactive processes of atoms. Here, we consider the simplest model for the coupling between the atom and the field that captures the essential features associated with the spontaneous emission processes, where the atom is represented by a two-level monopole system, which is coupled to a Hermitian massless scalar field. The interaction Hamiltonian at time τ can be written as

$$H_{int}(\tau) = c_1 m(\tau)\phi(x(\tau)), \tag{2.150}$$

where c_1 is a small coupling constant, $m(\tau)$ is the monopole operator of the atom, and $\phi(x)$ is the scalar field operator at the atom's position. This model has been previously used to describe a detector of scalar fields excitations [52,53,55] as well as to study the spontaneous decay of quantum entangled atoms [38,57–61]. The general

formalism presented here is exactly the same formalism used in photo-detection theory [65].

The system's Hilbert space is taken as the direct product of the Hilbert space of the atom and the quantized field $H = H_A \otimes H_F$. The total Hamiltonian can be generally written as

$$H = H_A + H_F + H_{int}, \tag{2.151}$$

where H_A is the non-interacting atom's Hamiltonian, H_F is the Hamiltonian of the free field and H_{int} represents the coupling between the atom and the vacuum field. In order to investigate the spontaneous decay process, we consider the initial state of the system as being in the form $|\tau_i\rangle = |e\rangle \otimes |\phi_i\rangle$, where $|e\rangle$ is the excited state of the atom and $|\phi_i\rangle$ is the field in initial vacuum state. In the interaction picture, the evolution of the combined atom-field system is obtained by Schrodinger's equation

$$i\frac{\partial}{\partial\tau}|\tau\rangle = H_{int}|\tau\rangle, \tag{2.152}$$

And the time evolution of the combined atom-field state is governed by the evolution operator

$$U(\tau_f, \tau_i) = 1 - i \int_{\tau_i}^{\tau_f} H_{int}(\tau')U(\tau', \tau_i)d\tau'. \tag{2.153}$$

From equation 2.152, the state of the system at time τ can be formally written as $|\tau_f\rangle = U(\tau_f, \tau_i)|\tau_i\rangle$. In the regime of weak atom-field coupling, the interaction Hamiltonian can be taken as a small perturbation. Up to first-order in the perturbation expansion, the evolution operator assumes the simpler form

$$U(\tau_f, \tau_i) = 1 - i \int_{\tau_i}^{\tau_f} H_{int}(\tau)d\tau. \tag{2.154}$$

The probability amplitude for the transition from the initial state at τ_i into the final

state $|g\rangle \otimes |\phi_f\rangle$ is given by

$$\langle g\phi_f|U(\tau_f, \tau_i)|e\phi_i\rangle = -i \int_{\tau_i}^{\tau_f} \langle g\phi_f|H_{int}(\tau)|e\phi_i\rangle d\tau, \tag{2.155}$$

where $|\phi_f\rangle$ is an arbitrary state of the field and $|g\rangle$ is the atom's ground state.

Within this approach, the transition probability from the atom's excited state at τ_i into the ground state at τ_f is given by

$$P(E, \tau) = c_1^2 |\langle e|m(0)|g\rangle|^2 F(E, \tau_f), \tag{2.156}$$

where the term $c_1^2|\langle e|m(0)|g\rangle|^2$ is known as the atom's selectivity and $F(E, \tau_f)$ is the field's response function

$$F(E, \tau_f, \tau_i) = \int_{\tau_i}^{\tau_f} d\tau' \int_{\tau_i}^{\tau_f} d\tau'' e^{-iE(\tau'-\tau'')} \times \langle \Phi_i|\phi(x(\tau'))\phi(x(\tau''))|\Phi_i\rangle. \tag{2.157}$$

If we want to know in which state the atom will be at time $\tau = \tau_f$, let us suppose that the initial state of the field is the vacuum state, $|\Phi_i\rangle = |0\rangle$. In this case, in Eq. 2.157 we are using the positive Wightman function associated with the scalar field and evaluated on the world line of the atom, with the assumption that at $\tau = \tau_i = 0$ the atom in the excited state and the field in the vacuum state. Then Eq. 2.157 can be written as,

$$F(E, \tau) = \int_0^\tau d\tau \int_0^\tau d\tau' e^{-iE(\tau-\tau')} G^+(x(\tau), x(\tau')). \tag{2.158}$$

Here $E = E_e - E_g > 0$ represents the frequency $\omega = E$ (in units of $\hbar = 1$ of the emitted radiation). $G^+(x(\tau), x(\tau')) = \langle 0|\phi(x(\tau))\phi(x(\tau'))|0\rangle$ is the positive scalar field Wightman function in the vacuum field state $|0\rangle$. This function includes the vacuum fluctuation contributions and can provide the change in the probability of transition when we introduce boundaries into the excited system.

2.4 A two-level detector interacting with a scalar field in the vacuum state in empty space

Here, we are interested in measuring the activity of the scalar field in the vacuum state along the world line of a two-level system. Then Wightman's function that appears in Eq. 2.158 takes the general form [55]

$$G^+(x(t'), x(t'')) = -\frac{1}{(4\pi)^2} \frac{1}{(\Delta t)^2 - (\mathbf{x}' - \mathbf{x}'')^2}. \tag{2.159}$$

The Wightman function associated with an inertial detector that travels in the world line $x^\mu(\tau)$ is dependent only on time interval between the two points, and the Eq. 2.159 is simplifield to

$$G^+(x(\tau), x(\tau')) = -\frac{1}{(4\pi)^2} \frac{1}{(\Delta\tau - i\epsilon)^2}, \tag{2.160}$$

where $\Delta\tau = \tau_f - \tau_i$ and the ϵ was introduced to the correct specification of the singularities in Wightman function in the empty Minkowski space. Note that $(1 - v^2)^{1/2}$ is absorbed in $i\epsilon$. In such conditions, making the following change of variables $\zeta = \tau - \tau'$ and $\eta = \tau + \tau'$ we can use the expression discussed in previous section given by Eq. 2.158, but now written to any time interval, just replacing the null initial time by that at any instant of time τ_i, to obtain

$$F(E, \Delta\tau) = -\frac{1}{4\pi^2} \int_{-\Delta\tau}^{\Delta\tau} d\zeta (\Delta\tau - |\zeta|) e^{-iE\zeta} \frac{1}{(\zeta - i\epsilon)^2}. \tag{2.161}$$

Note that this last equation can be separated into two equations as follows

$$F(E, \Delta\tau) = F_I(E, \Delta\tau) + F_{II}(E, \Delta\tau), \tag{2.162}$$

where

$$F_I(E, \Delta\tau) = -\frac{1}{4\pi^2} \int_{-\Delta\tau}^{\Delta\tau} d\zeta \Delta\tau \frac{e^{-iE\zeta}}{(\zeta - i\epsilon)^2} \tag{2.163}$$

and

$$F_{II}(E, \Delta\tau) = \frac{1}{4\pi^2} \int_{-\Delta\tau}^{\Delta\tau} d\zeta \frac{|\zeta|e^{-iE\zeta}}{(\zeta - i\epsilon)^2}. \tag{2.164}$$

Using complex variable methods the integrals given by equations 2.163 and 2.164 can be solved taking the limit $\epsilon \to 0$ and using the Cauchy theorem, providing the equation

$$\int_{-\Delta\tau}^{\Delta\tau} d\zeta \frac{e^{-iE\zeta}}{(\zeta - i\epsilon)^2} = 2\pi i Res\left[\frac{e^{-iE\zeta}}{(\zeta - i\epsilon)^2}; i\epsilon\right]\Theta(-E) - \int_{R/[\tau_i, \tau_f]} d\zeta \frac{e^{-iE\zeta}}{(\zeta - i\epsilon)^2} \tag{2.165}$$

$$= 2\pi E\Theta(-E) - 2\int_{\Delta\tau}^{\infty} d\zeta \frac{\cos E\zeta}{\zeta^2}, \tag{2.166}$$

that we replace in Eq. 2.162, and after some manipulations, we obtain

$$F_I(E, \Delta\tau) = \frac{\Delta\tau}{2\pi}\left[-E\Theta(-E) + \frac{\cos E\Delta\tau}{\pi\Delta\tau} + \frac{|E|}{\pi}\left(Si|E|\Delta\tau - \frac{\pi}{2}\right)\right], \tag{2.167}$$

where $Si(z)$ is the sine integral function defined by

$$Si(z) = \int_0^z \frac{\sin t}{t} dt. \tag{2.168}$$

Equation $F_{II}(E, \Delta\tau)$ is then

$$F_{II}(E, \Delta\tau) = \frac{1}{2\pi^2}(-\gamma + Ci|E|\Delta\tau - ln|E|\epsilon), \tag{2.169}$$

where $Ci(z)$ is the cosine integral function defined by

$$Ci(z) = \gamma + \ln z + \int_0^z \frac{\cos t - 1}{t} dt. \tag{2.170}$$

Note that using equations 2.169 and 2.170 that $F_{II}(E, \Delta\tau)$ has two divergences: the first given by $\ln\Delta\tau$ as $\Delta\tau \to 0^+$; and the second by $\ln\epsilon$. The divergence that occurs in $\ln\Delta\tau$ was already expected, but $\ln\epsilon$ divergence does not make any sense and needs to be removed through a renormalization procedure. Let us define the renormalized response function by $F_{ren}(E, \Delta\tau)$ as follows

$$F_{ren}(E, \Delta\tau) = F(E, \Delta\tau) - \frac{1}{(2\pi)^2}\ln\Delta\tau/\epsilon. \qquad (2.171)$$

Therefore

$$F_{ren}(E, \Delta\tau) = \frac{1}{2\pi^2}\left[|E|\Delta\tau\left(\pi\Theta(-E) + Si|E|\Delta\tau - \frac{\pi}{2}\right) + \cos E\Delta\tau \right.$$
$$\left. + \int_0^{\Delta\tau} d\zeta\frac{\cos(E\zeta) - 1}{\zeta}\right]. \qquad (2.171)$$

In Eq. 2.171, $\Theta(-E)$ is the spontaneous emission contribution and the other terms are emission and absorption terms induced by the vacuum fluctuations. But the renormalized expression still misbehaves: for $\Delta\tau < 1/|E|$, it assumes a nonzero value that vanishes quickly, and for $|E|\Delta\tau > 1$, it assumes negative values that are unmeaning for probabilities. This is due to the fact that we are dealing with a first-order approximation, and consequently, they are valid just for "small" values of $\Delta\tau$.

This problem can be superated defining the decay rate $R(E, \Delta\tau)$, when multiplied by the selectivity provides the probability of transition per unity of time:

$$R(E, \Delta\tau) = \frac{1}{\Delta\tau}F_{ren}(E, \Delta\tau) = \frac{|E|}{2\pi^2}\left(\pi\Theta(-E) + Si|E|\Delta\tau - \frac{\pi}{2}\right)$$
$$+ \frac{1}{2\pi^2\Delta\tau}\left(\cos E\Delta\tau + \int_0^{\Delta\tau} d\zeta\frac{\cos(E\zeta) - 1}{\zeta}\right). \qquad (2.171)$$

Then, in the limit $\Delta\tau \to \infty$, the decay rate is given by

$$\lim_{\Delta\tau\to\infty} R(E,\Delta\tau) = \frac{|E|}{2\pi}\Theta(-E). \qquad (2.172)$$

We can conclude that there is no spontaneous excitation after a long atom-field interaction time and that the spontaneous decay rate approaches to a constant proportional to the energy gap.

2.5 Spontaneous decay rate in the presence of mirrors

As already mentioned at the end of the section 2.3, the response function F written in terms of the Wightman function can provide us with the change in the probability of transition when we introduce boundary conditions into the system. Here, we wish to present a successful model used by Ford et al to measuring the change of the vacuum fluctuations, evaluated on the world line of the atom, due to the presence of perfectly reflecting mirrors. This same method, as discussed in the first chapter, can later be extended to compute the transitions in the presence of spherical surfaces, the core of this work, as seen in the next chapters. If we introduce an infinite perfectly reflecting plate at $z = 0$ into the system and suppose that the atom is at rest at a distance $\eta/2$ from the plate, the world line is given by $x^\mu(x) = (\tau, 0, 0, \eta/2)$.

The supposition of perfect reflection at the plate is similar to the supposition that we have a perfect conductor plate in the case of electromagnetic fields. Then, if the initial state of the system at $\tau = \tau_i$ is $|e\rangle \otimes |0\rangle$, to first order, for the system to evolve to $|g\rangle \otimes |\Phi_f\rangle$, where $|\Phi_f\rangle$ is an arbitrary final field configuration, in a finite time interval $\Delta\tau = \tau_f - \tau_i$, the probability of transition is proportional to the

response function and given by the equation below, as demonstrated in section 2.3,

$$F(E, \tau_f, \tau_i) = \int_{\tau_i}^{\tau_f} d\tau \int_{\tau_{\tau_i}}^{\tau_f} d\tau' e^{-iE(\tau - \tau')} G^+(x(\tau), x(\tau')), \qquad (2.173)$$

which contains in positive Wightman function satisfying Dirichlet boundary conditions on the mirror $G^+(x(\tau), x(\tau'))$ the physical effects introduced into the system by the presence of mirrors, i.e., capturing the empty space contribution (or empty Minkowski spacetime) as well as the correction due to the boundary.

2.5.1 Asymptotic decay rate near to one mirror

Let us introduce the variables $\zeta = \tau - \tau'$ and $\lambda = \tau + \tau'$, then we have the positive Wightman function given by

$$G^+(x, x') = -\frac{1}{4\pi^2} \frac{1}{(\zeta - i\epsilon)^2} + \frac{1}{4\pi^2} \frac{1}{(\zeta - i\epsilon)^2 - \eta^2}, \qquad (2.174)$$

that by construction is null at the mirror and has two terms, one associated with the two-level system, and the other with its image, as shown in Fig. 2.4. By substituting
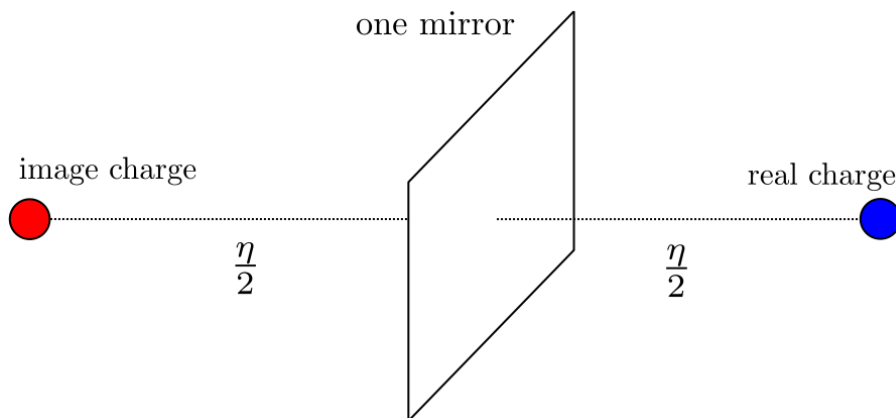

Figure 2.4: Schematic view of the real charge (blue bullet) and its image (red bullet) near to one mirror.

Eq. 2.174 for Eq. 2.173, we obtain

$$F(E, \Delta\tau, \eta) = F_M(E, \Delta\tau) + F_{\partial\Gamma}(E, \Delta\tau, \eta), \tag{2.175}$$

where

$$F_M(E, \Delta\tau) = -\frac{1}{4\pi^2} \int_{-\Delta\tau}^{\Delta\tau} d\zeta \frac{(\Delta\tau - |\zeta|)e^{-iE\zeta}}{(\zeta - i\epsilon)^2} \tag{2.176}$$

is the empty-space contribution, and the

$$F_{\partial\Gamma}(E, \Delta\tau, \eta) = -\frac{1}{4\pi^2} \int_{-\Delta\tau}^{\Delta\tau} d\zeta \frac{(\Delta\tau - |\zeta|)e^{-iE\zeta}}{(\zeta - i\epsilon)^2 - \eta^2} \tag{2.177}$$

is the correction due to the boundary conditions introduced into the system by the mirror. Similar to the mathematical procedures already considered in the section 2.4, here we introduce the infinitesimal parameter ϵ to correct specify the singularities of the Wightman function. In line with that we can define an instantaneous rate as

$$R = \frac{\partial F(E, \Delta\tau)}{\partial \Delta\tau}, \tag{2.178}$$

which provides the transition probability per unit proper time, normalized by the selectivity of the atom, given by

$$R(E, \Delta\tau, \eta) = R_M(E, \Delta\tau) + R_{\partial\Gamma}(E, \Delta\tau, \eta), \tag{2.179}$$

where

$$R_M(E, \Delta\tau) = -\frac{1}{4\pi^2} \int_{-\Delta\tau}^{\Delta\tau} d\zeta \frac{e^{-iE\zeta}}{(\zeta - i\epsilon)^2} \tag{2.180}$$

and

$$R_{\partial\Gamma}(E, \Delta\tau, \eta) = \frac{1}{4\pi^2} \int_{-\Delta\tau}^{\Delta\tau} d\zeta \frac{e^{-iE\zeta}}{(\zeta - i\epsilon)^2 - \eta^2}. \tag{2.181}$$

The integrals given by equations 2.180 and 2.181 can be solved using the complex variables method. Let us start with the first one, which provides the transition rate in empty Minkowski spacetime, using the known residue theorem. To do that, let us take the limit $\epsilon \to 0$ and we have

$$\int_{-\Delta\tau}^{\Delta\tau} d\zeta \frac{e^{-iE\zeta}}{(\zeta - i\epsilon)^2} = 2\pi E\Theta(-E) - 2\int_{\Delta\tau}^{\infty} d\zeta \frac{\cos E\zeta}{\zeta^2}. \qquad (2.182)$$

We can obtain it after some algebraic manipulations, by substituting Eq. 2.182 in Eq. 2.180, the empty-space rate

$$R_M(E, \Delta\tau) = \frac{1}{2\pi}\left\{ -E\Theta(-E) + \frac{\cos(E\Delta\tau)}{\pi\Delta\tau} + \frac{|E|}{\pi}\left(-\frac{\pi}{2} + Si(|E|\Delta\tau) \right) \right\} \qquad (2.183)$$

where $Si(z)$ is the sine integral function, and the equation 2.183 has the expected behavior for $|E|\Delta\tau \gg 1$: when $E < 0$ the spontaneous decay is given by $-E/2\pi$ and when $E > 0$ the spontaneous excitation is forbidden. For a small $\Delta\tau$ regime, both rates diverge as $1/\Delta\tau$. The short switching time that produces a great disturbance in the system may be associated with the observed divergence. But in our work we are more interested in the term given by Eq. 2.181. Then, in order to calculate the correction in the rate due to the mirror (the $R_{\partial\Gamma}$), let us divide the integration range into two intervals: $[-\Delta\tau, 0]$ and $[0, \Delta\tau]$. By changing the integration variable in the first integral, we obtain

$$R_{\partial\Gamma}(E, \Delta\tau, \eta) = \frac{1}{2\pi^2}Re\int_0^{\Delta\tau} d\zeta \frac{e^{-iE\zeta}}{(\zeta - i\epsilon)^2 - \eta^2} = \frac{1}{2\pi}Re\int_0^{\Delta\tau} d\zeta f(E, \eta, \zeta, \epsilon) \qquad (2.184)$$

where the function f is analytic, except at the points $\{\eta + i\epsilon, -\eta + i\epsilon\}$. The limit $\epsilon \to 0$ can be taken directly for $0 \le \Delta\tau \le \eta$. Into this interval, $R_{\partial\Gamma}(E, \Delta\tau, \eta)$ is continuous on $\Delta\tau$ and given by

$$R_{\partial\Gamma}(E, \Delta\tau, \eta) = \frac{1}{2\pi^2}\int_0^{\Delta\tau} d\zeta \frac{cosE\zeta}{(\zeta^2 - \eta^2)}. \qquad (2.185)$$

We can observe for $\Delta\tau < \eta$ interval, $R_{\partial\Gamma}(E, \Delta, \eta) \neq 0$. Apparently this is an acausal effect, because the emitted photon does not have time to travel to the mirror and be reflected back to the atom. However, we can think this happens because the presence of the mirror modifies the quantized field to which the atom is coupled. It is important to note the atom is not interacting directly with the plate as much as it is interacting with the modified vacuum fluctuations in the vicinity of the atom. In this sense, it is better to consider the atom as coupled to these vacuum fluctuations than to interacting directly with its image.

For $\Delta\tau > \eta$ interval the contribution of the plate to spontaneous emission rate can also be calculated as follows

$$R_{\partial\Gamma}(E, \Delta\tau, \eta) = \frac{1}{2\pi}\Theta(-E)\frac{\sin\eta E}{\eta} + \frac{1}{2\pi^2}\int_{\Delta\tau}^{\infty} d\zeta \frac{\cos E\zeta}{\zeta^2 - \eta^2}. \tag{2.186}$$

The total asymptotic decay rate of spontaneous radiation is thus obtained by substituting Eqs. 2.183 and 2.186 for Eq. 2.179 as well as by taking the limit $\tau \to \infty$, which results in

$$\lim_{\Delta\tau\to\infty} R(E, \Delta\tau, \eta) = \frac{-E}{2\pi}\Theta(-E)(1 - \frac{\sin\eta E}{\eta E}). \tag{2.187}$$

This asymptotic decay rate plotted as a function of $E\eta$ was extracted from [19] and it is shown and discussed in the next subsection. This important theoretical result reproduces qualitatively the experiments presented in literature very well, as exposed in the next subsection.

2.5.2   Asymptotic decay rate in the presence of two mirrors

In this section, the main goal is to obtain Wightman's positive function of a two-level monopol positioned between two perfectly reflecting parallel plates, using the same method described in previous section to check the influence of one plate on the rate of spontaneous emission. The methodology is broadly discussed in Ref. [19,55].

Let us consider the atom positioned between the two mirrors at $z = 0$ and $z = l$ (the exact atom's position at the $x = y = 0$, and $z = \eta/2$), as shown in Fig 2.5. Using the method of images to calculate the positive Wightman function evaluated
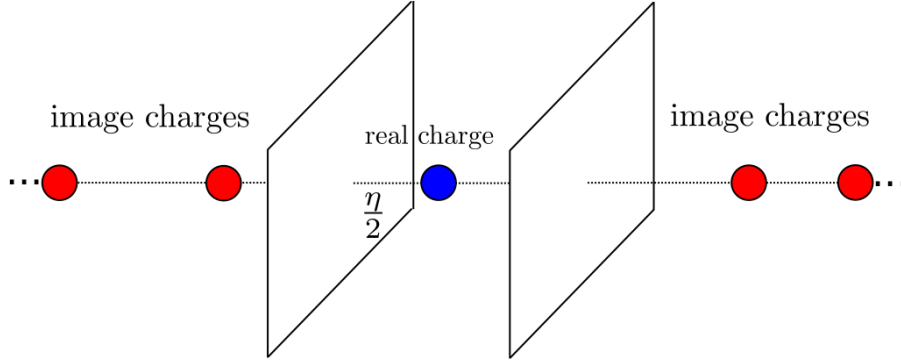

Figure 2.5: Schematic view of the real charge (blue bullet) and its infinite images (red bullets) in the presence of two mirrors.

on the world line of the atom makes it possible to obtain

$$G^+(x, x') = -\frac{1}{4\pi^2} \sum_{k=-\infty}^{\infty} \frac{1}{(\zeta - i\epsilon)^2 - (2kl)^2} \qquad (2.188)$$

$$+\frac{1}{4\pi^2} \sum_{k=-\infty}^{\infty} \frac{1}{(\zeta - i\epsilon)^2 - (\eta - 2kl)^2}. \qquad (2.189)$$

Now, by substituting Eq. 2.189 for Eq. 2.173, and reproducing the same mathematical procedures of the previous sections, the spontaneous emission rate can be calculated exactly, being given by

$$\lim_{\Delta\tau \to \infty} R(E, \Delta\tau, \eta, l) = \frac{-E\Theta(-E)}{2\pi} \sum_{k=-\infty}^{\infty} \left[\frac{\sin 2kEl}{2kEl} - \frac{\sin E(\eta - 2kl)}{E(\eta - 2kl)} \right]. \qquad (2.190)$$

This rate is a discontinuous function of El, which is due to the discreteness of the wave number in the direction normal to the mirrors, as it is discussed in Fig. 2.6 b) for the excited atomic system positioned at the center of cavity given by the mirrors. If we take the average in Eq. 2.190 over $0 \le \frac{1}{2}\eta \le l$ interval, the consequent series

can be exactly computed using the identity

$$\sum_{k=-\infty}^{\infty} \int_0^a f(x+ka)dx = \int_{-\infty}^{\infty} f(x)dx, \tag{2.191}$$

which after a straightforward calculation, we can obtain

$$\lim_{\Delta\tau\to\infty} \langle R(E,l,\Delta\tau) \rangle = \frac{|E|}{2\pi}\left(1+\frac{y}{n+y}\right), \tag{2.192}$$

where $El = \pi(n+y)$, $n = 0,1,2,...,0 < y < 1$, and $\langle\rangle$ means for an average over atom's position. When El/π is an integer we can label it as a resonant cavity. The mean rate has a discontinuous jump and reaches a value equal to the rate of transition in the free space. In non-resonant cavities, the mean rate is inhibited and consequently the mean lifetime of the excited state is enhanced (See Ref. [19]).

As stated in the introduction, the theoretical model addressed in this chapter contains the essencial ingredients to understanding and investigating spontaneous decay processes of the excited systems placed in vicinity of boundary surfaces.

In Fig. 2.6 some results for the asymptotic decay rate of spontaneous emission obtained by Ford et al are presented.

In Fig. 2.6 a) shows the asymptotic rate for the excited atomic system in the presence of a perfectly conducting plate as a function of $E\eta$ (See Eq. 2.187), where the field vanishes at the mirror due to Dirichlet boundary conditions, and the rate vanishes at $\eta = 0$. See there are regions where the rate of transition is suppressed, and regions where it is enhanced, as usually presented in literature [41, 46, 47]. In Fig. 2.6 b), the asymptotic rate of spontaneous emission is shown, this time for the system trapped at the center of the cavity (between the two parallel plates), as a function of the cavity size (See Eq. 2.190). In particular, when a two-level system is trapped between parallel walls, the spontaneous decay process can be substantially suppressed when the distance between the walls is much smaller than the wavelength of the emitted radiation. On the other hand, the decay rate can
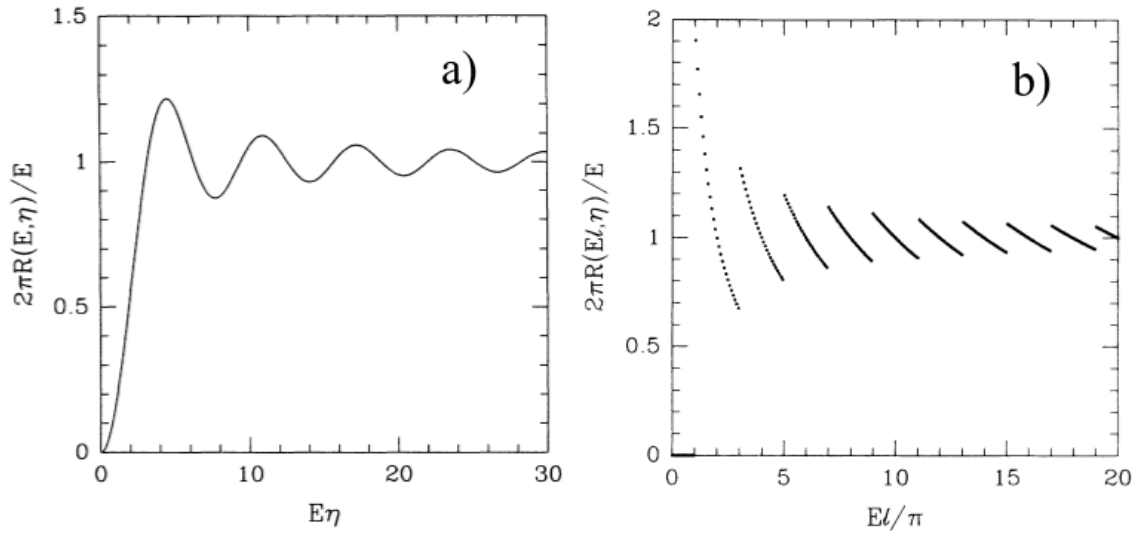
Figure 2.6: a) The asymptotic rate of spontaneous emission in the presence of a perfectly conducting plate as a function of the atom distance to the mirror. By construction see that for $E\eta \to 0$ the spontaneous emission vanishes, and when $E\eta \to \infty$ the free atom result is recovered. b) The asymptotic rate of spontaneous emission in the presence of two parallel plates as a function of the cavity size (emitter at the center). In both cases E is the absolute value of the transition energy. Figure taken from Ref. [19].

be strongly enhanced due to the emergence of resonant modes [19]. Enhanced and suppressed regions in the emission process shown in Fig. 2.6 b) are in agreement with typical experimental results presented in literature [16].

The model will be extended to the case in which the atomic system is near a spherical surface as well as when the system is trapped in spherical shell cavities, the core of this research and subject of the next two chapters.

3

Spontaneous decay rate in the vicinity of a reflecting sphere

To start with, let us recall the main result concerning the process of spontaneous emission by an excited two-level system interacting with the scalar field in the vaccum state, for the particular case in which the atom is at rest in the empty Minkowski space and Wigthman function is given by

$$G_M^+(x(\tau), x(\tau')) = -\frac{1}{4\pi^2} \frac{1}{(\zeta - i\epsilon)^2}, \tag{3.1}$$

where $\zeta = \tau - \tau'$ and the spontaneous emission process is usually characterized by the asymptotic decay rate defined as $R = \frac{\partial F(E, \Delta\tau)}{\partial \Delta\tau}|_{\Delta\tau \to \infty}$, with $\Delta\tau = \tau_f - \tau_i$, as discussed in the sections 2.4 and 2.5. In the case of an atom at rest in the empty space, it is shown that the rate in which it is given is by Eq. 2.180, where the integral is taken in the limit $\epsilon \to 0$ provide $R_M(E) = \frac{E}{2\pi}$. This expression shows that spontaneous decay rate in the empty space is proportional to the frequency of the emitted radiation.

The problem of a two-level monopole coupled to a scalar massless field in the vicinity of reflecting plates has been previously addressed [19], having shown that the decay rate is substantially suppressed when the atom is placed close to the walls

due to the imposed Dirichlet boundary conditions as well as the decay rate can be fully suppressed when the atom is placed between parallel walls when the distance between them is smaller than half of the radiation wavelength. Enhancement of the decay rate, as compared to the corresponding rate in the free space, has also been achieved when new field modes are supported by the cavity. The decay rate presents periodic modulations as a function of the cavity dimension or the atom's distance to the plates (see Ref. [19]). All these features are in agreement with experiments as well as with theoretical models of dipole atoms coupled with the vector quantized electromagnetic field [35, 66–68].

These findings support the conjecture that the simplified description based on a monopole two-level system coupled to a scalar field can indeed capture the essential mechanism behind the process of spontaneous emission near surface boundaries. We extend these theoretical approximations to the case of an atom placed in the vicinity of a perfectly reflecting spherical surface, as shown in Fig. 3.1. Let us start by placing
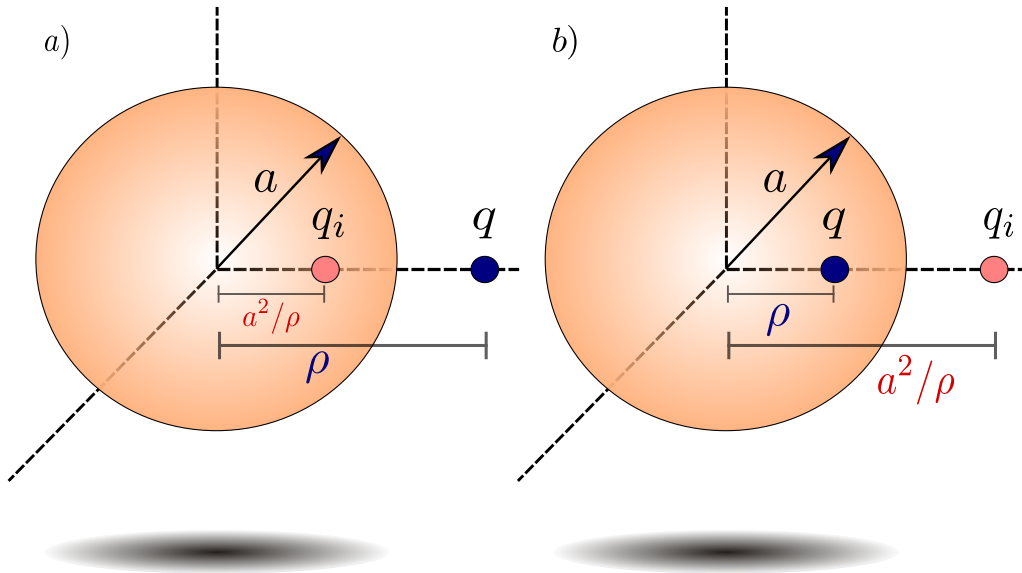

Figure 3.1: Schematic view of the two-level system (dark blue bullet) and its respective image (clear red bullet) in the vicinity of a perfectly reflecting sphere of radius a. The two-level system is placed at a distance ρ from the center of the sphere. a) Exterior problem; b) Interior problem.

the atom in the exterior region of a sphere of radius a. The Wigthman function can be obtained using the method of images. The atom induces the emergence of an image monopole in the interior region. The image's position and monopole charge are such that the field vanishes in the surface of the sphere, as imposed by the Dirichlet boundary conditions. Wightman's function can be written as

$$G^+(x(\tau), x'(\tau')) = -\frac{1}{4\pi^2}\frac{1}{(\zeta - i\epsilon)^2 + |x - x'|^2} \tag{3.2}$$

$$+\frac{1}{4\pi^2}\frac{1}{(\zeta - i\epsilon)^2 + |x - x_i'|^2/q_i}, \tag{3.3}$$

where x is an arbitrary position in the exterior region, x' is the atom's position, x_i' is the image's position and q_i is the modulus of the image's effective charge (its sign is opposite to the atom's monopole). When the atom is placed at a distance ρ from the center of the sphere $x' = (\rho, 0, 0)$, G^+ vanishes in all points x at the surface of the sphere, for any value of ζ, provided that $x_i' = (a^2/\rho, 0, 0)$ and $q_i = (a/\rho)^2$. In order to compute the spontaneous decay rate, Wightman's function on the world line of the atom at rest ($x = x'$) is needed. In this case, it assumes the simpler form

$$G^+(x(\tau), x(\tau')) = -\frac{1}{4\pi^2}\frac{1}{(\zeta - i\epsilon)^2}$$

$$+\frac{1}{4\pi^2}\frac{1}{(\zeta - i\epsilon)^2 + |\rho - a^2/\rho|^2/(a/\rho)^2}. \tag{3.3}$$

Notice that it reduces to Wightman's function in the empty space for $a \to 0$ and for $\rho \to \infty$, as expected. It vanishes at $\rho = a$ according to the imposed Dirichlet boundary condition.

The asymptotic decay rate can be directly calculated by replacing Wightman's function in Eq. 2.158, because the above function incorporates both contributions of the monopole and its image. The algebraic procedure is similar to the one used to compute the decay rate near infinite plates [19]. As a result the asymptotic decay

rate assumes the form

$$R(E, \rho, a) = \frac{E}{2\pi} \left(1 - \frac{\sin[(\rho^2/a - a)E]}{(\rho^2/a - a)E} \right). \tag{3.4}$$

Notice that when the distance of the atom to the sphere ρ is much larger than the radius a, the decay rate becomes the same as the one in the free space. The same limit is also achieved when the wavelength of the emitted radiation $\lambda \propto 1/E$ is much smaller then the distance of the atom to the sphere.

The case of the atom placed in the interior region of the sphere can also be solved using the method of images. The resulting expression for Wightman's function on the world line of the atom and the subsequent spontaneous decay rate are exactly the same ones obtained for the exterior problem with the restriction of $0 < \rho/a < 1$. It is interesting to stress that when the atom is placed at the center of the sphere, the decay rate becomes identical to that of a two-level system placed at a distance $a/2$ of a perfectly reflecting infinite plate [19].

There are three distinct length scales that influence the decay rate of the present two-level model system near a spherical surface, namely, the radius a of the sphere, the distance ρ of the atom to the center of the sphere, and the wavelength $\lambda \propto 1/E$ of the emitted radiation. As it happens, we provide a detailed analysis of the dependence of the spontaneous decay rate on these length scales for both exterior and interior problems.

In Fig. 3.2 we plot the relative decay rate (the spontaneous decay rate in the vicinity of the sphere $R(Ea, a/\rho)$ in units of the decay rate in the free space $R(E) = E/2\pi$) as a function of the inverse of the distance ρ of the two-level system to the center of the sphere normalized by the sphere's radius. Two representative values of Ea are shown. The spontaneous decay vanishes at the surface of the sphere by construction, as imposed by the Dirichlet boundary condition. As ρ increases (decreasing values of a/ρ), the decay rate converges to its free space value presenting oscillations with decaying amplitudes. At its maximum overshooting, the
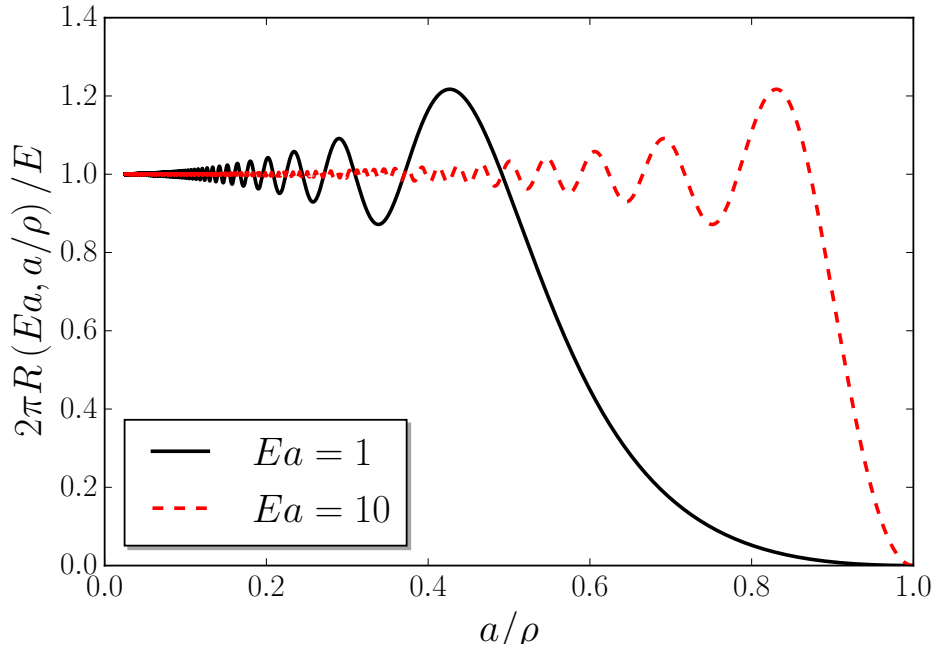
Figure 3.2: Relative decay rate $2\pi R/E$ as a function of a/ρ (exterior problem) for two representative values of Ea. It vanishes at the surface of the sphere by construction, converging to the free space value at large distances. In the regime of small energies, the distance of maximum overshooting scales as $E^{-1/2}$

spontaneous decay rate becomes approximately 21% larger than the one in the free space. This maximum relative decay rate is achieved at larger distances of the atom to the surface when the wavelength of the emitted radiation becomes larger (smaller energy), with the atom's position of maximum overshooting scaling as $E^{-1/2}$.

To illustrate more clearly the dependence of the decay rate on the energy of the emitted radiation, we plot in Fig. 3.3 the relative decay rate as a function of Ea for two fixed distances of the atom to the sphere's center. The decay rate converges to the free space value for very large energies, irrespective of the atom's distance to the sphere. In this regime, the wavelength of the emitted radiation becomes much smaller than the other length scales. The relative decay rate vanishes in the opposite
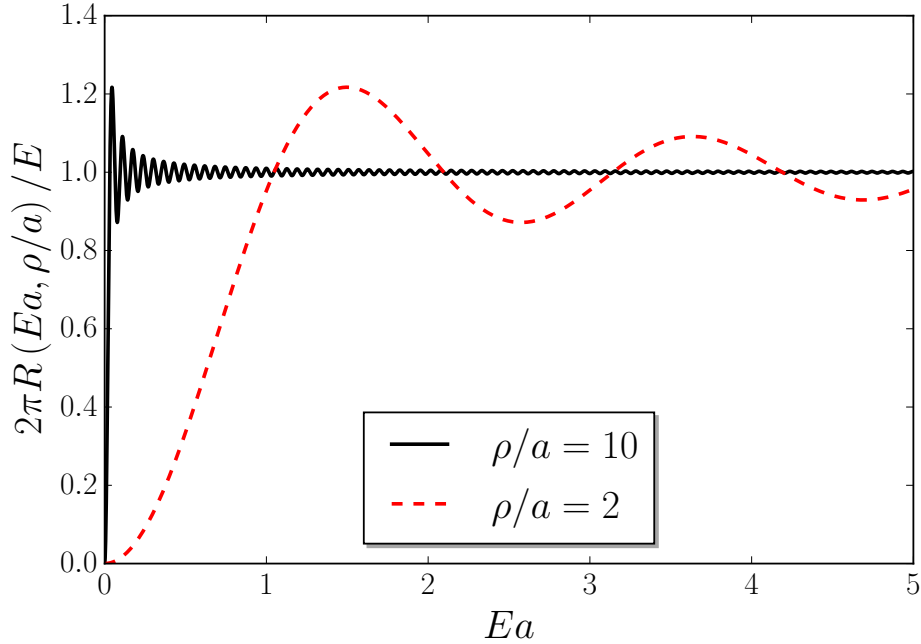
Figure 3.3: Relative decay rate (measured in units of the free space decay rate) as a function of Ea for two representative values of a/ρ (exterior problem). The crossover from the small to the high energy regime occurs through damped oscillations with the maximum overshooting energy scaling as $1/\rho^2$ at large distances.

regime of $Ea \to 0$. The crossover from the low to the high energy regime also occurs via damped oscillations, with the energy corresponding to the maximum relative decay rate scaling as $1/\rho^2$ when $\rho/a \gg 1$.

Let us now discuss the spontaneous decay process for the case of a two-level system trapped in the interior of the sphere. We start by plotting the relative decay rate as a function of Ea for distinct positions of the atom (see Fig. 3.4). When the atom is placed at the center of the sphere, we have already commented that the decay rate becomes exactly the same as that for a two-level monopole placed at a distance $a/2$ of an infinite reflecting plate [19]. When the atom is displaced towards the sphere surface, the wavelength of the decay rate oscillations increases, with the
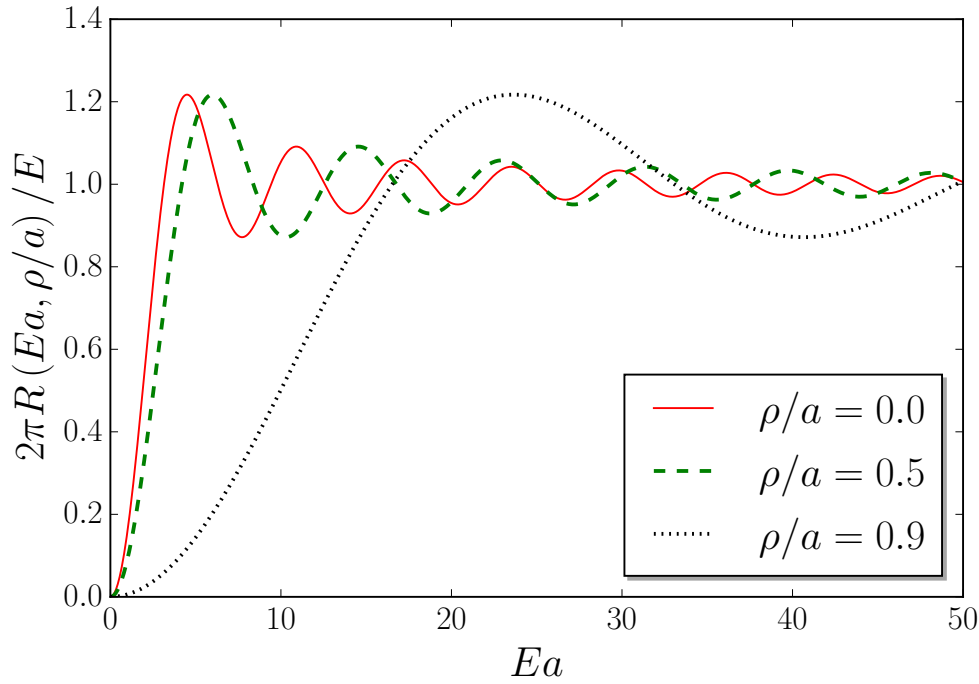
Figure 3.4: Relative decay rate as a function of Ea for three representative values of ρ/a (interior problem). The maximum overshooting scales as the inverse of the atom's distance to the surface $d = \rho - a$ when $\rho/a \to 1$.

energy of the first peak scaling with the distance of the atom to the surface $d = a - \rho$ proportionally to $1/d$ in the limit of $d \to 0$.

A series of interesting features can be extracted from the dependence of the decay rate on the atom's position for the interior problem (see Fig. 3.5). We depict typical curves by considering some relevant energy values. For $Ea < \pi$ the decay rate is always smaller than that in the free space, irrespective of the atom's position. For smaller energies, the relative decay rate if further suppressed. The maximum overshooting of the relative decay rate at the sphere's center occurs at $Ea \simeq 4.49$. For this energy, the relative decay rate decays monotonically to zero as the atom is displaced towards the sphere's surface. For larger energies, the relative decay rate
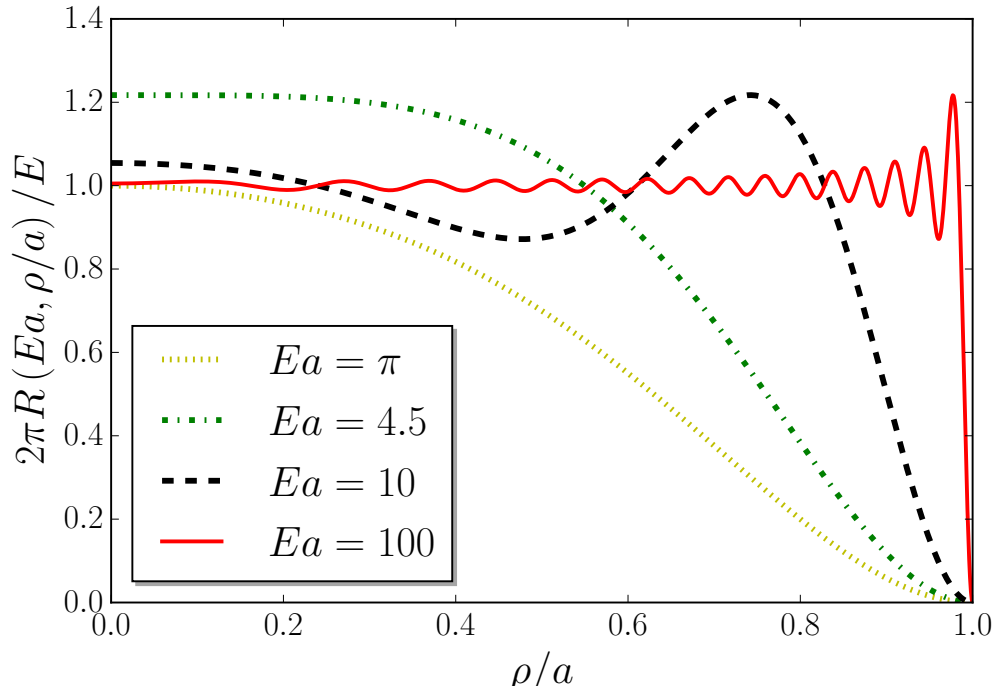
Figure 3.5: Relative decay rate $2\pi R/E$ as a function of ρ/a (interior problem) for some representative values of Ea. For $Ea < \pi$ the decay rate is smaller than the one in the free space, irrespective to the atom's position. The maximum overshooting occurs at the sphere's center for $Ea \simeq 4.49$. Oscillations are developed for larger energies.

develops damped oscillations.

We finish our analysis by reporting the decay rate averaged over the sphere's volume. The average decay rate is given by

$$\overline{R} = \frac{1}{4\pi a^3/3} \int_0^a 4\pi \rho^2 d\rho R(Ea, \rho/a). \tag{3.5}$$

This quantity accounts for the average decay rate of randomly quenched emitters uniformly distributed inside the sphere. The volume averaged spontaneous decay rate normalized by the free space decay is shown in Fig. 3.6 as a function of Ea. It

vanishes quadratically as $Ea \to 0$. Therefore, the average decay rate is substantially suppressed when the wavelength λ of the emitted radiation becomes larger than the size of the sphere. In the opposite regime of $a >> \lambda$, the average decay rate slowly converges to the free space value. The crossover between these two regimes takes place at $a/\lambda \sim 1$.
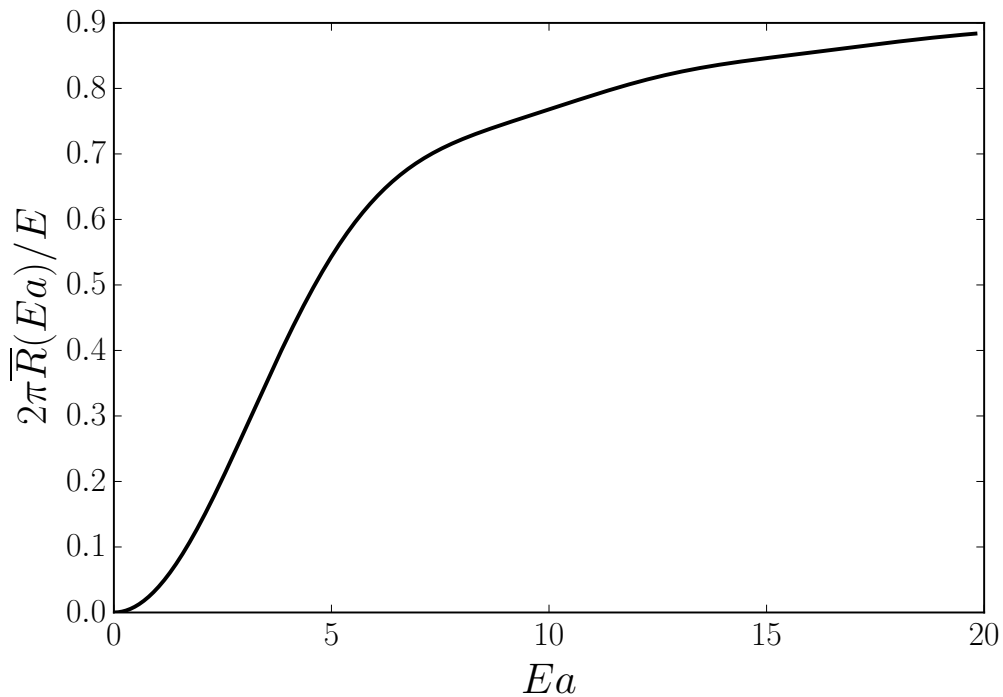

Figure 3.6: Relative decay rate averaged over the sphere's volume (interior problem) as a function of Ea. It vanishes as $(Ea)^2$, converging monotonically to the free space value as $Ea \to \infty$.

The results of this chapter were published in 2017 [69]. In the next chapter we are concerned with the decay rate of the system trapped in spherical shell cavities.

4

Spontaneous decay rate in spherical shell cavities

Using the same theoretical model applied so far, we investigate the influence of two concentric spherical surfaces on the spontaneous decay process of an excited system trapped between the radii, as ilustraded in Fig. 4.1.

It is important to emphasize that $G^+(x(\tau), x(\tau'))$, as the cases previously studied, is completely dependent on the geometry of the problem, and is also used here to obtain the transition probability. At the surface of the concentric spheres Wightman's function satisfies Dirichlet boundary conditions and is null by construction. It has been previously demonstrated that, when the atom is positioned near infinite plates satisfying Dirichlet boundary conditions, the decay rate is substantially suppressed. For the case treated here, Wightman's function can also be obtained through the method of images, where the atom induces infinite images inside and outside the shell (see Fig. 4.1). Therefore, the function incorporates contributions
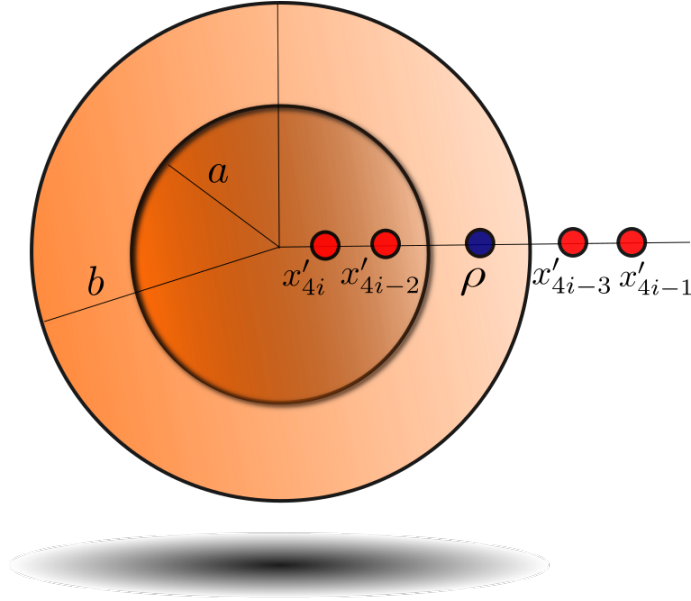
Figure 4.1: Schematic view of the two-level system (bullet at ρ) and four representative images at x'_{4i}, x'_{4i-1}, x'_{4i-2}, x'_{4i-3}.

from an infinite set of variable image charges and can be written as

$$
G^+(x(\tau), x'(\tau')) = \frac{1}{4\pi^2}\Bigg\{ \frac{-1}{(\zeta - i\epsilon)^2 - |x - x'|^2}
$$

$$
+ \lim_{N\to\infty} \sum_{i=1}^{N} \Bigg[\frac{q_{4i-3}}{(\zeta - i\epsilon)^2 - |x - x'_{4i-3}|^2}
$$

$$
+ \frac{q_{4i-2}}{(\zeta - i\epsilon)^2 - |x - x'_{4i-2}|^2}
$$

$$
- \frac{q_{4i-1}}{(\zeta - i\epsilon)^2 - |x - x'_{4i-1}|^2}
$$

$$
- \frac{q_{4i}}{(\zeta - i\epsilon)^2 - |x - x'_{4i}|^2} \Bigg] \Bigg\},
$$

(4.1)

where $\zeta = \tau - \tau'$, x is an arbitrary position, x' is the atom's position; x'_{4i-3}, x'_{4i-2}, x'_{4i-1} and x'_{4i} denotes any of the possible positions of the successive image charges,

obtained from repeated applications of the method of images, i. e.,

$$x_1^{'} = \frac{b^2}{\rho}, \; x_5^{'} = \frac{b^2}{\rho}\frac{b^2}{a^2}, \; ... \; ,x_{4i-3}^{'} = \frac{b^2}{\rho}\left(\frac{b^2}{a^2}\right)^{i-1}$$

$$x_2^{'} = \frac{a^2}{\rho}, \; x_6^{'} = \frac{a^2}{\rho}\frac{a^2}{b^2}, \; ... \; ,x_{4i-2}^{'} = \frac{a^2}{\rho}\left(\frac{a^2}{b^2}\right)^{i-1}$$

$$x_3^{'} = \frac{b^2\rho}{a^2}, \; x_7^{'} = \frac{b^2\rho}{a^2}\frac{b^2}{a^2}, \; ... \; ,x_{4i-1}^{'} = \frac{b^2\rho}{a^2}\left(\frac{b^2}{a^2}\right)^{i-1}$$

$$x_4^{'} = \frac{a^2\rho}{b^2}, \; x_8^{'} = \frac{a^2\rho}{b^2}\frac{a^2}{b^2}, \; ... \; ,x_{4i}^{'} = \frac{a^2\rho}{b^2}\left(\frac{a^2}{b^2}\right)^{i-1},$$

with ρ being some position of the two-level monopole between the radii of the inner and outer spheres ($a \leq \rho \leq b$) and a and b are their radii, respectively. In Eq. 4.1, $q_{4i-3}^{'}$, $q_{4i-2}^{'}$, $q_{4i-1}^{'}$ and $q_{4i}^{'}$ represents all the possible moduli of the image's effective charges calculated using the method of images and given by

$$q_{4i-3} = \left[\frac{b}{\rho}\left(\frac{b}{a}\right)^{i-1}\right]^2$$

$$q_{4i-2} = \left[\frac{a}{\rho}\left(\frac{a}{b}\right)^{i-1}\right]^2$$

$$q_{4i-1} = \left[\frac{b}{a}\left(\frac{b}{a}\right)^{i-1}\right]^2$$

$$q_{4i} = \left[\frac{a}{b}\left(\frac{a}{b}\right)^{i-1}\right]^2,$$

representing any of the infinite image charges. It was possible to write the four representative image charges of any of the infinite images through the successive application of the method of images to obtain the first 12 image charges of the infinite set that appears in the Eq. 4.1. This allowed us to generalize and infer "the

face" of all others, as can be seen below:

$$q_1 = \left(\frac{b}{\rho}\right)^2, \; q_5 = \left(\frac{b}{\rho}\left(\frac{b}{a}\right)\right)^2, \; q_9 = \left(\frac{b}{\rho}\left(\frac{b}{a}\right)^2\right)^2 ...$$

$$q_2 = \left(\frac{a}{\rho}\right)^2, \; q_6 = \left(\frac{a}{\rho}\left(\frac{a}{b}\right)\right)^2, \; q_{10} = \left(\frac{a}{\rho}\left(\frac{a}{b}\right)^2\right)^2 ...$$

$$q_3 = \left(\frac{b}{a}\right)^2, \; q_7 = \left(\frac{b}{a}\left(\frac{b}{a}\right)\right)^2, \; q_{11} = \left(\frac{b}{a}\left(\frac{b}{a}\right)^2\right)^2 ...$$

$$q_4 = \left(\frac{a}{b}\right)^2, \; q_8 = \left(\frac{a}{b}\left(\frac{a}{b}\right)\right)^2, \; q_{12} = \left(\frac{a}{b}\left(\frac{a}{b}\right)^2\right)^2 ...$$

where each line of the equation was generalized to obtain the set mentioned above. Notice that in Eq. 4.1, the set of terms containing q_{4i-3} and q_{4i-2} denotes contributions of image charges whose signals are opposite to the source charge, while the set of terms q_{4i-1} and q_{4i} represents image contributions with the same signal of the source charge. In Fig. 4.2 we plot the magnitude of the image charges as a function of their respective positions, both in the internal and external regions of the spherical shell.

Note that in order to obtain Wightman's function given by Eq. 4.1, we consider all the terms of the series that incorporate the contributions of the atom trapped between the concentric spheres shown in Fig. 4.1 as well as its infinite images. As we illustrate in Fig. 4.3, Wightman's function given by Eq. 4.1 satisfies the Dirichlet boundary conditions and diverges over the source. For more details on the treatment of Green's function for concentric spheres see Ref. [70].

The asymptotic decay rate associated with spontaneous emission processes is usually defined as $R = \frac{\partial F(E,\tau_f)}{\partial \tau_f}$, after renormalizing logarithmic singularities in the transition probability [55]. Following the prescription developed in [19, 55, 69], the
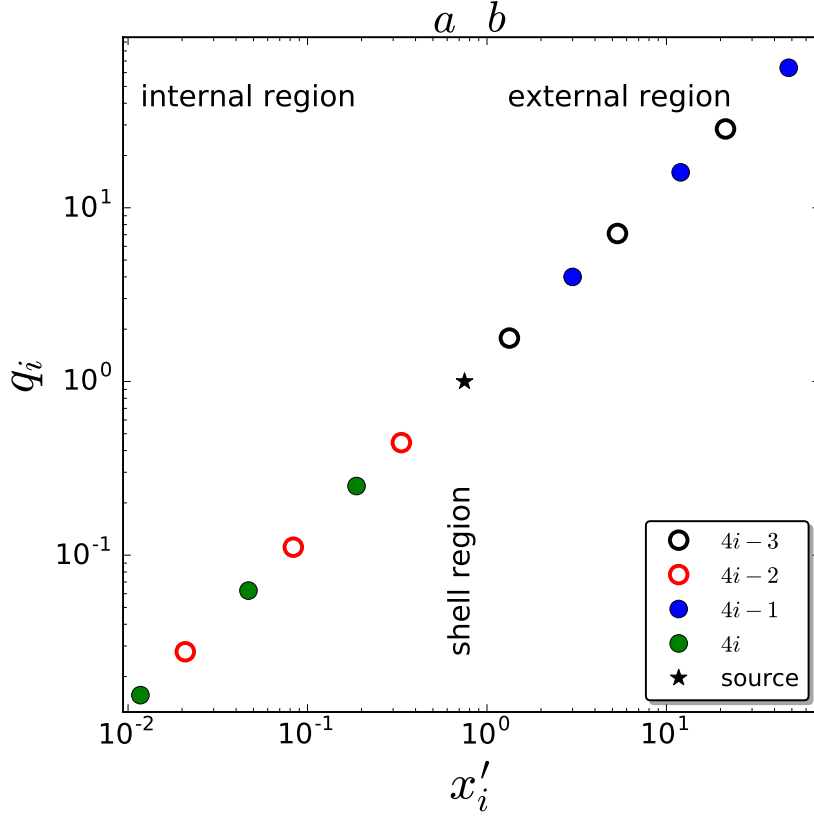
Figure 4.2: Magnitude of the image charges as a function of their respective positions in both internal and external regions of a spherical shell of radii $a = 0.5$ and $b = 1$. Filled (open) circles represent image charges with the same (opposite) sign of the source charge (star symbol).

asymptotic decay rate can be written as

$$R(E, \rho, a, b) = \frac{E}{2\pi} \left[1 + \sum_i sinc(E\eta_{4i-3}) + sinc(E\eta_{4i-2}) - sinc(E\eta_{4i-1}) \right. $$

$$\left. - sinc(E\eta_{4i}) \right].$$

where $\eta_j = \frac{\rho - x'_j}{\sqrt{q_j}}$. The averaged decay rate over the volume of the spherical shell is given by

$$\overline{R} = \frac{3}{b^3 - a^3} \int_a^b \rho^2 d\rho R(E, \rho, a, b).$$

Figure 4.3: Density plot of the Wightman function given by Eq. 4.1 with $\zeta = 0$ for two representative values of radii (a) $a = 10$ and $b = 20$; (b) $a = 10$ and $b = 100$. The represented plane crosses the source charge and the center of the spheres.The Wightman function is null at the surfaces, satisfying the Dirichlet boundary conditions and diverges over the source charge.

This quantity accounts for the average decay rate of randomly quenched emitters uniformly distributed between the two concentric spheres.

It is important to consider three factors for the analysis, and understand the decay rate behavior of the two-level detector positioned between two concentric spheres of radii a and b (always the atomic system at position ρ so that $a \le \rho \le b$):

i) The relation between the radii of spheres; ii) The distance ρ from the detector to the center of the concentric spheres; iii) The wavelength $\lambda \propto 1/E$ of the emitted radiation. In this section, we provide a detailed analysis of the spontaneous decay rate dependence considering those factors.

In Fig. 4.4, we plot the relative decay rate (the spontaneous decay rate for the atomic system trapped in the concentric spheres in units of the decay rate in the free space $R(E\rho, \rho) = E/2\pi$) as a function of the parameter $E\rho$ associated with the energy of the two-level monopole. We fixed the atom's positions as $\rho = (a + b)/2$.

We consider in Fig. 4.4 four different shell's geometries: (a) two cases $a << 1$ with b finite and $a = b/2$. In the latter case the spacement between the spherical surfaces belong to the same order of their radii; (b) $a/b \to 1$ or equivalently $a \to b$ for which both surfaces radii are larger than the spacement between them; (c) $a = 1$ and much smaller than b. For the cases described in (a), the solid line (blue) represents the relative decay rate when the $a << 1$. In this case, the relative decay rate has a considerable peak in the low energy range (high wavelength of emitted radiation) and converges slowly to the free space in the high energy limit, as occurred when the two-level system was placed inside a single perfectly reflecting sphere [69]. Still in (a), the dashed line (red) represents the two-level monopole trapped between two concentric spheres with $a = b/2$. It is interesting to stress that, in this case, we observe a low energies range for which the decay rate oscillates around zero as well as irregular peaks in the decay rate. See that it is possible to suppress the spontaneous emission in the aforementioned low energy regime. The negative values in the decay rate have been previously attributed to the large interaction time and associated with the limit of validity of the perturbation theory or to non-Markovian re-absorption processes [55, 71–74].

As seen in (b) (Fig. 4.4), when the spheres have similar radii ($a/b \to 1$ or equivalent $a \to b$), the relative decay rate has a low-energy range for which the decay is suppressed, having an enhancement in the relative rate thereafter. These results converge to the ones obtained for the two-level monopole placed between

two parallel reflecting plates [19], as expected because the physical situation in the referential of the atomic system is very similar, i. e., the radii of the spheres are much larger than the distance of the two-level monopole to their surfaces.

Notice that in the case shown in (c), there is an improvement of the relative decay rate in the low energy regime, with the relative spontaneous decay oscillating and converging smoothly to the free space in the high energy regime. For this case, the results are equivalent to those obtained for the two-level monopole placed in the exterior region of a perfectly reflecting spherical surface (see Ref. [69]). In addition, the aspect of the relative decay rate is identical to that shown in the solid line (blue) in (a) [69].

We also investigated the dependence of the spontaneous decay rate on the position of the detector within the spherical shell. Typical dependences on the detector's position are reported in Fig.4.5 for the case of a spherical shell with inner radius $a = 0.5$ and outer radius $b = 1$. The decay rate is quite suppressed for low energies (large wavelengths of the emitted radiation). As the quantum of emitted radiation energy increases, the decay rate of a detector placed at the center of the shell approaches the one expected for a detector placed in the free vaccum because the wavelength of the emitted radiation becomes much smaller than the distance to both shell's surfaces. Oscillations in the decay rate are developed when the atom approaches the vicinity of the boundaring surfaces, ultimately vanishing when the radiation's wavelength becomes much larger than the atom-surface distance.

In Fig. 4.6, we plot the average decay rate calculated over the volume of the spherical shell as a function of the parameter $E\rho$ associated with the energy of the two-level monopole. Here we also considered a fixed value position ($\rho = (a + b)/2$) from the center of the spheres for the same shell's geometries commented above.

In (a) (Fig. 4.6), the solid line (blue) represents the average relative decay rate when the $a << 1$ and the decay rate vanishes as $(E\rho)^2$, converging monotonically to the free space value as $E\rho \rightarrow \infty$, as expected for the case of the atomic system inside a single sphere [69]. Still in (a), the dashed line (red) represents the two-level

monopole trapped between the two concentric spheres for $a = b/2$. In this case, we observe a low energy range in which the average relative decay rate oscillates around zero as well as the development of irregular peaks. In (b), when $a > 1$ and much smaller then b, the average relative decay rate (solid line in blue) converges to those obtained for the exterior problem of a two-level system placed outside a single sphere [69]. In this case, the average relative decay rate converges to the free atomic system in the limit of high energies having an aspect similar to the rate of the two-level system inside a single sphere (interior problem). Still in (b), the dashed line in red represents the case where the radii of the spheres $a/b \to 1$ (or equivalently $a \to b$). The average relative decay rate converges the one for the two-level system positioned between parallel plates, i.e., there is a low energies regime for which the rate is completely suppressed with regular oscillations associated with the emergence of new field modes (see more details in Ref. [19]). Furthermore, for any of the analyzed cases in Fig. 4.6, the average relative decay rate is substantially suppressed when the wavelength λ of the emitted radiation becomes larger than the size of the spherical shell cavity. In the opposite regime, the average decay rate converges slowly to the free space value.

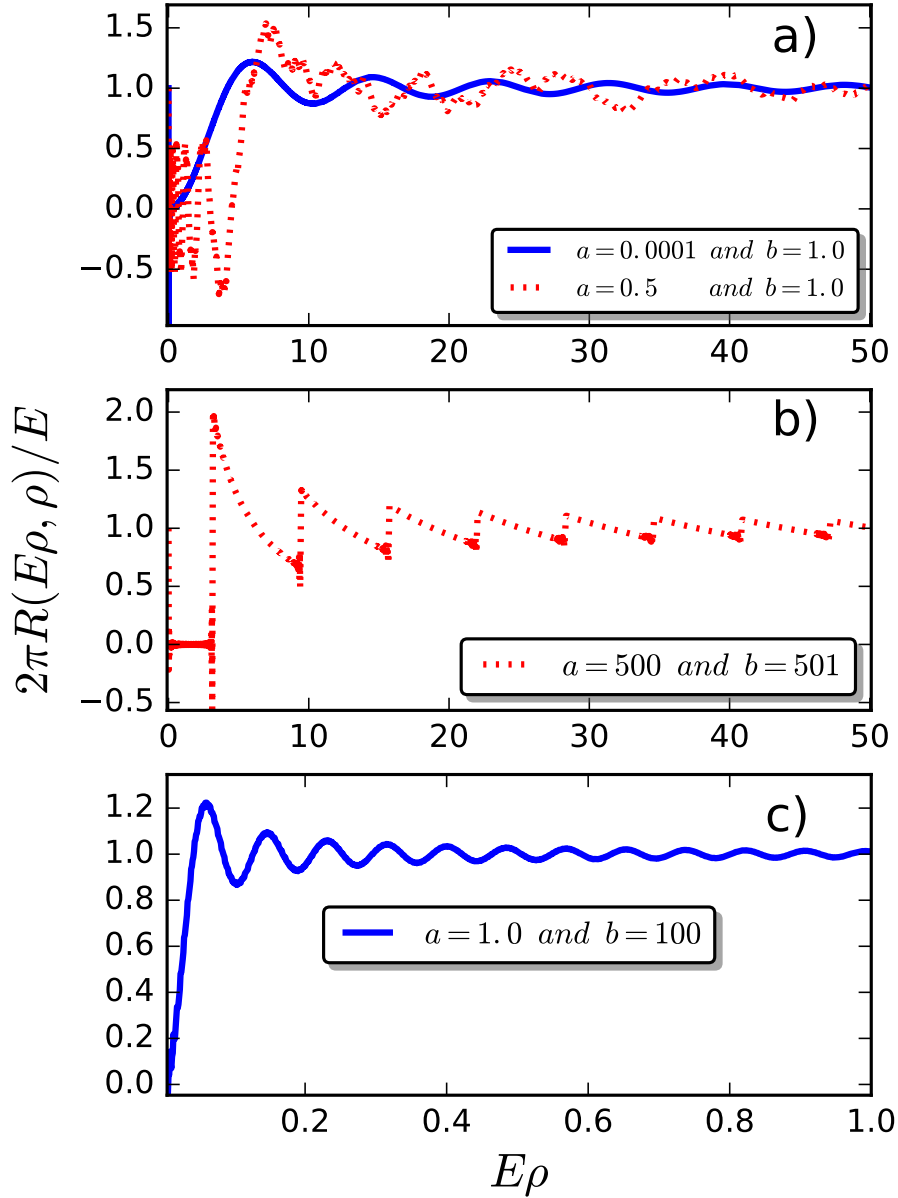The results of this chapter were published in 2019 [75].

Figure 4.4: Relative decay rate (measured in units of the free space decay rate) as a function of $E\rho$ for different relations between the radii of the spheres. In (a), we have $a << 1$ and $a = b/2$. For the first case ($a << 1$), represented by the solid line (blue), the results converge to those obtained for the case of the two-level monopole placed inside a perfectly reflecting sphere. For $a = b/2$ (dashed red line), exist a low energy range for which the decay rate oscillates around zero. In (b), for $a/b \to 1$, the relative decay rate converges to that obtained in the case of parallel plates. In (c), we recover the case of an atomic system positioned in the exterior of a single sphere.
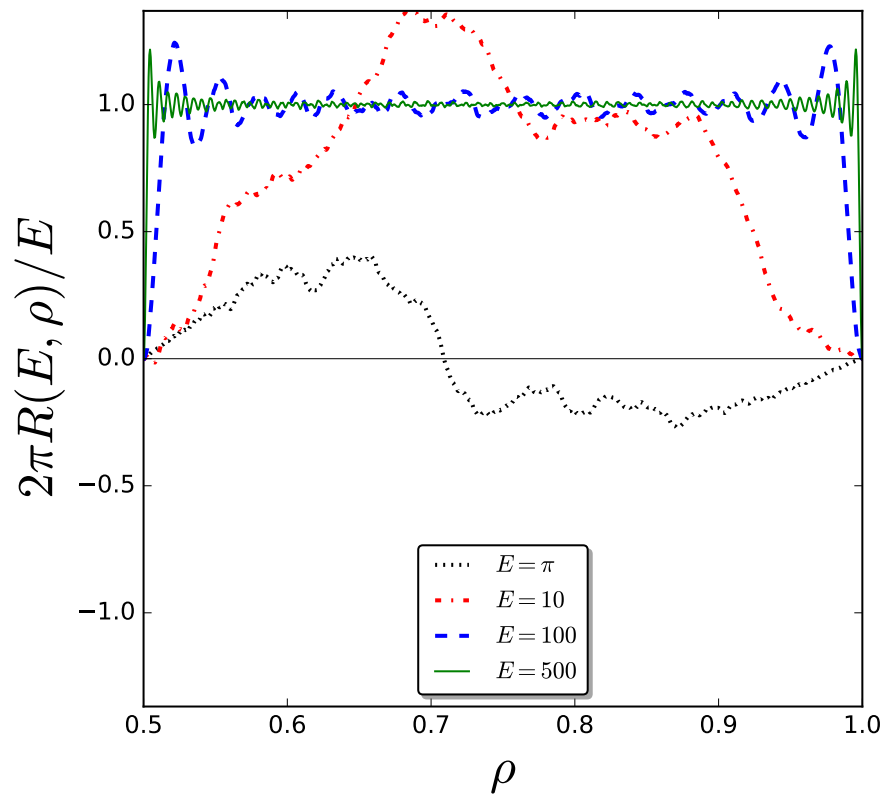
Figure 4.5: Spontaneous decay rate as a function of the detector position within a spherical shell with radii $a = 0.5$ and $b = 1$. Distinct cases of emitted radiation energies are illustrated. Spontaneous decay is strongly suppressed for low energies. At high energies, it vanishes near the surfaces and exhibits an oscillatory convergence to the rate at the free vacuum when the detector is moved far from the surfaces.
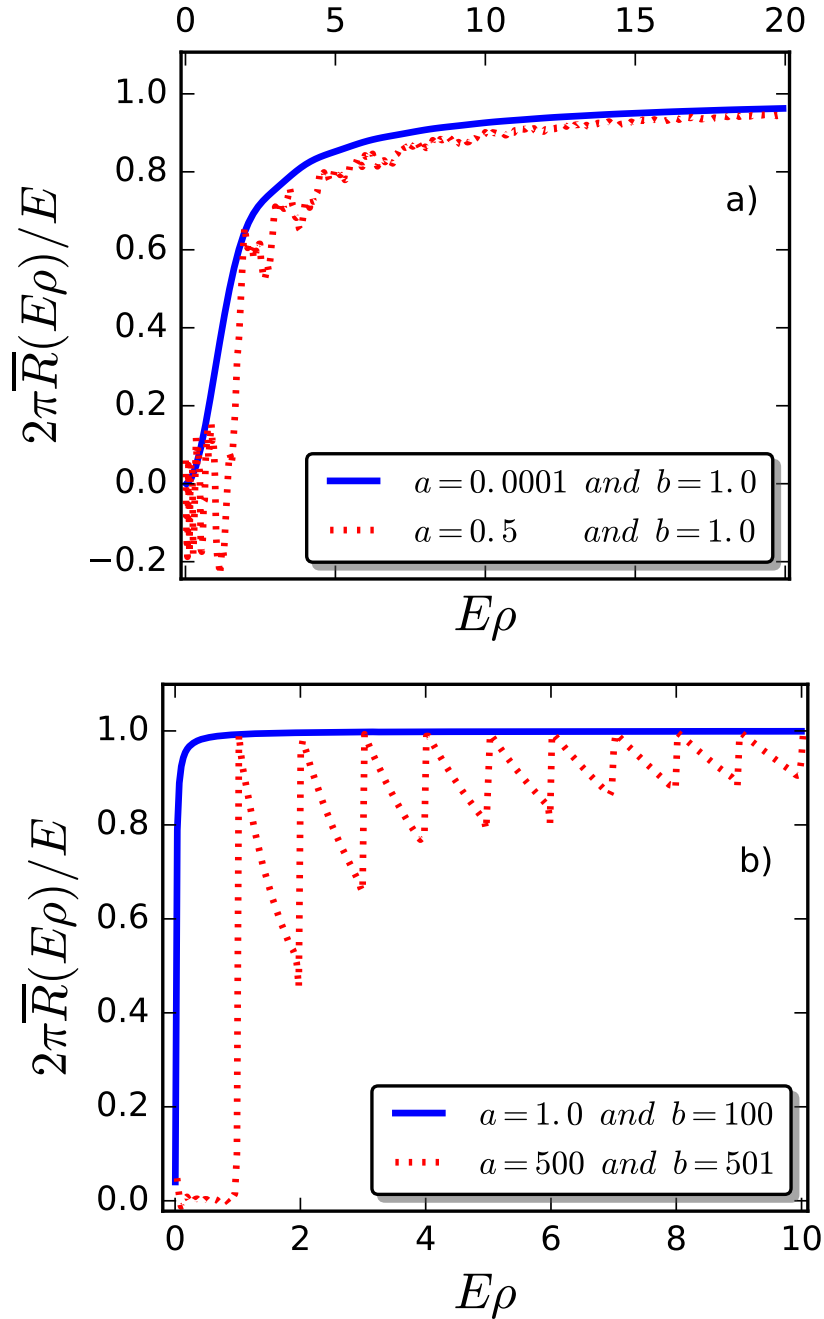
Figure 4.6: Average relative decay rate over the spherical shell volume as a function of $E\rho$. In (a) (solid line in blue), when $a << 1$, the average relative decay rate vanishes as $(E\rho)^2$, converging monotonically to the free space value as $E\rho \to \infty$. Still in (a), the average relative decay rate for $a = b/2$ (dashed line in red) oscillates around zero in the range of low energies, having irregular peaks thereafter, converging to the free space for high energies. In (b), the solid line in blue accounts for the average rate for the system positioned outside a single sphere. Still in (b), for $a/b \to 1$ (dashed line in red) the decay rate vanishes at low energies, converging to free space in the high energy regime depicting regular oscillations.

5

Summary and Conclusions

In short, we have used a simple theoretical model to investigate the influence of a spherical surface on the spontaneous decay rate process of an excited system. Within a first-order perturbation theory, we provided an analytical expression for the spontaneous decay rate of a two-level monopole coupled to an Hermitian massless scalar field. We demonstrated that both cases of the two-level system placed in the exterior and in the interior of the sphere with a perfectly reflecting surface can be similarly described.

We provided a detailed analysis of the dependence of the spontaneous decay rate on the energy of the emitted radiation (or equivalently on its wavelength), the sphere's radius and the emitter's position. In particular, we showed that the spontaneous decay rate measured in units of the free space decay rate depicts damped oscillations as a function of either the radiation energy or the emitter's position with simple asymptotic scaling laws. Besides, we found that the decay rate in the interior of the sphere is always suppressed in relation to the free space decay in the low energy regime, irrespective of the emitter's position. At higher energies it also develops damped oscillations. The volume averaged relative decay rate showed two distinct regimes: a quadratic vanishing for small energies and a slow convergence to the free space behavior at high energies.

We use the same method to investigate the influence of two concentric perfectly

reflecting spheres on the spontaneous decay rate of a trapped excited system. We showed that the results already obtained in the literature for the two-level system between parallel plates and in the vicinity of a single sphere can be recovered as asymptotic cases of the problem treated here. Furthermore, for the two concentric spheres, we provide the same detailed analysis of the dependence of the spontaneous decay rate on the energy of the emitted radiation (or equivalently on its wavelength) as well as on the different relation between the radii of the concentric spheres. We observed a low energy range for which the decay rate oscillates around zero as well as irregular peaks in the decay rate. We have verified that it is possible to suppress the spontaneous emission in the mentioned low energy range. In the opposite regime, the decay rate converges slowly to the free space value. The same characteristics were observed for the average relative decay rate. It is important to stress that the decay rate develops irregular oscillations as a function of the quantum of energy radiated within the spherical shell, in contrast with the regular oscillations observed for the similar process occurring in a cavity composed by parallel plates. These irregular oscillations reflect the non-uniform spacement and variability of the infinite set of image charges.

It is interesting to stress that the present approach provides a clear picture of the influence of curved bounding surfaces in the spontaneous emission processes, caused by the modification of the vacuum field modes in the vicinity of the spherical surfaces. The detailed understanding of these important effects finds great relevance in the control and adjustment of spontaneous emission processes, which can be fundamental in the definition of the performance of optoelectronic devices that are usually based on photosensible particles trapped in spherical coats [49]. The present approach can be extended to account for polarization effects due to the coupling between the electrical dipole of the emitter, and the electromagnetic field in the vacuum state [40, 76]. We hope that the present work can stimulate further contributions aiming to uncover the influence of other shell geometries in the decay process of trapped emitters.

Bibliography

[1] A. Einstein. The Quantum Theory of Radiation. *Physikalische Zeitschrift*, 18:128, march 1917.

[2] Theodore A. Pelion. Some observable effects of the quantum-mechanical fluctuations of the electromagnetic field. *Physical Review*, 74(9):1157, november 1948.

[3] E. T. Jaynes and F. W. Cummings. Comparison of quantum and semiclassical radiation theories with application to the beam maser. *Proceedings of the IEEE*, 51(1), january 1962.

[4] E. M. Purcell. Spontaneous Emission Probabilities at Radio Frequencies. *Physical Review*, 69(11-12):681, jun 1946.

[5] P.W. Milonni and P.L. Knight. Spontaneous emission between mirrors. *Optics Communications*, 9(2):119–122, oct 1973.

[6] Jeong-Ki Hwang, Han-Youl Ryu, and Yong-Hee Lee. Spontaneous emission rate of an electric dipole in a general microcavity. *Physical Review B*, 60(7):4688–4695, nov 1999.

[7] E Betzig and R J Chichester. Single Molecules Observed by Near-Field Scanning Optical Microscopy. *Science*, 262(5138):1422–1425, nov 1993.

[8] T. H. Taminiau, F. D. Stefani, F. B. Segerink, and N. F. van Hulst. Optical antennas direct single-molecule emission. *Nature Photonics*, 2(4):234–237, mar 2008.

[9] Sergei Kühn, Ulf Håkanson, Lavinia Rogobete, and Vahid Sandoghdar. Enhancement of Single-Molecule Fluorescence Using a Gold Nanoparticle as an Optical Nanoantenna. *Physical Review Letters*, 97(1):017402, jul 2006.

[10] M. Khajavikhan, A. Simic, M. Katz, J. H. Lee, B. Slutsky, A. Mizrahi, V. Lomakin, and Y. Fainman. Thresholdless nanoscale coaxial lasers. *Nature*, 482(7384):204–207, feb 2012.

[11] Martin Frimmer and A. Femius Koenderink. Spontaneous emission control in a tunable hybrid photonic system. *Physical Review Letters*, 110(21):217405, may 2013.

[12] P. Stehle. Atomic Radiation in a Cavity. *Physical Review A*, 2(1):102–106, jul 1970.

[13] G. Barton. Quantum Electrodynamics of Spinless Particles between Conducting Plates. *Proceedings of the Royal Society A: Mathematical, Physical and Engineering Sciences*, 320(1541):251–275, dec 1970.

[14] Michael R. Philpott. Fluorescence from molecules between mirrors. *Chemical Physics Letters*, 19(3):435–439, apr 1973.

[15] P. Goy, J. M. Raimond, M. Gross, and S. Haroche. Observation of cavity-enhanced single-atom spontaneous emission. *Physical Review Letters*, 50(24):1903–1906, jun 1983.

[16] Randall G. Hulet, Eric S. Hilfer, and Daniel Kleppner. Inhibited Spontaneous Emission by a Rydberg Atom. *Physical Review Letters*, 55(20):2137–2140, nov 1985.

[17] W. Jhe, A. Anderson, E. A. Hinds, D. Meschede, L. Moi, and S. Haroche. Suppression of Spontaneous Decay at Optical Frequencies: Test of Vacuum-Field Anisotropy in Confined Space. *Physical Review Letters*, 58(14):1497–1497, apr 1987.

[18] H. M. França, T. W. Marshall, and E. Santos. Spontaneous emission in confined space according to stochastic electrodynamics. *Physical Review A*, 45(9):6436–6442, may 1992.

[19] L. H. Ford, N. F. Svaiter, and Marcelo L. Lyra. Radiative properties of a two-level system in the presence of mirrors. *Physical Review A*, 49(2):1378–1386, 1994.

[20] P S Davids and P B Lerner. Suppression of atomic radiation in a cylindrical nanocavity. *Zeitschrift fr Physik D Atoms, Molecules and Clusters*, 33(3):203–210, sep 1995.

[21] Martti Kauranen, Yves Van Rompaey, Jeffery J. Maki, and André Persoons. Nonvanishing Field between a Dipole Oscillator and a Reflecting Boundary during Suppression of Dipole Radiation. *Physical Review Letters*, 80(5):952–955, feb 1998.

[22] M. J. A. de Dood, L. H. Slooff, A. Polman, A. Moroz, and A. van Blaaderen. Modified spontaneous emission in erbium-doped SiO[sub 2] spherical colloids. *Applied Physics Letters*, 79(22):3585, 2001.

[23] Ho Trung Dung, Ludwig Knöll, and Dirk-Gunnar Welsch. Decay of an excited atom near an absorbing microsphere. *Physical Review A*, 64(1):013804, may 2001.

[24] Kerry J. Vahala. Optical microcavities. *Nature*, 424(6950):839–846, aug 2003.

[25] V. V. Klimov, M. Ducloy, and V. S. Letokhov. Spontaneous emission rate and level shift of an atom inside a dielectric microsphere. *Journal of Modern Optics*, 43(3):549–563, mar 1996.

[26] Alexander Moroz. Spectroscopic properties of a two-level atom interacting with a complex spherical nanoshell. *Chemical Physics*, 317(1):1–15, oct 2005.

[27] R. Carminati, J.-J. Greffet, C. Henkel, and J.M. Vigoureux. Radiative and non-radiative decay of a single molecule close to a metallic nanoparticle. *Optics Communications*, 261(2):368–375, may 2006.

[28] Herbert Walther, Benjamin T H Varcoe, Berthold-Georg Englert, and Thomas Becker. Cavity quantum electrodynamics. *Reports on Progress in Physics*, 69(5):1325–1382, may 2006.

[29] V Yannopapas and N V Vitanov. Spontaneous emission of a two-level atom placed within clusters of metallic nanoparticles. *Journal of Physics: Condensed Matter*, 19(9):096210, mar 2007.

[30] K. K. Pukhov, T. T. Basiev, and Yu. V. Orlovskii. Spontaneous emission in dielectric nanoparticles. *JETP Letters*, 88(1):12–18, sep 2008.

[31] L.H. Ford and Thomas A. Roman. Effects of vacuum fluctuation suppression on atomic decay rates. *Annals of Physics*, 326(8):2294–2306, aug 2011.

[32] F. A. Inam, T. Gaebel, C. Bradac, L. Stewart, M. J. Withford, J. M. Dawes, J. R. Rabeau, and M. J. Steel. Modification of spontaneous emission from nanodiamond colour centres on a structured surface. *New Journal of Physics*, 13(7):073012, jul 2011.

[33] C. Sauvan, J. P. Hugonin, I. S. Maksymov, and P. Lalanne. Theory of the Spontaneous Optical Emission of Nanosize Photonic and Plasmon Resonators. *Physical Review Letters*, 110(23):237401, jun 2013.

[34] Serge Haroche. Controlling photons in a box and exploring the quantum to classical boundary. *Annalen der Physik*, 525(10-11):753–776, nov 2013.

[35] Zahra Mohammadi and Fardin Kheirandish. Energy-level shifts and the decay rate of an atom in the presence of a conducting wedge. *Physical Review A*, 92(6):062118, dec 2015.

[36] A. Bienfait, J. J. Pla, Y. Kubo, X. Zhou, M. Stern, C. C. Lo, C. D. Weis, T. Schenkel, D. Vion, D. Esteve, J. J. L. Morton, and P. Bertet. Controlling spin relaxation with a cavity. *Nature*, 531(7592):74–77, feb 2016.

[37] Han Xiong, Marlan Scully, and M. Zubairy. Correlated Spontaneous Emission Laser as an Entanglement Amplifier. *Physical Review Letters*, 94(2):023601, jan 2005.

[38] E. Arias, J. G. Dueñas, G. Menezes, and N. F. Svaiter. Boundary effects on radiative processes of two entangled atoms. *Journal of High Energy Physics*, 2016(7):147, jul 2016.

[39] Yiquan Yang, Jiawei Hu, and Hongwei Yu. Entanglement dynamics for uniformly accelerated two-level atoms coupled with electromagnetic vacuum fluctuations. *Physical Review A*, 94(3):032337, sep 2016.

[40] G. Menezes and N. F. Svaiter. Radiative processes of uniformly accelerated entangled atoms. *Physical Review A*, 93(5):052117, may 2016.

[41] K. H. Drexhage. Progress in Optics. *Amsterdam: North Holland*, 12(7):165–229, 1974.

[42] F. De Martini, G. Innocenti, G. R. Jacobovitz, and P. Mataloni. Anomalous Spontaneous Emission Time in a Microscopic Optical Cavity. *Physical Review Letter*, 59(26):2955–2958, december 1987.

[43] Gerald Gabrielse and Hans Dehmelt. Observation of inhibited spontaneous emission. *Physical Review Letters*, 55(1):67–70, july 1985.

[44] W. Jhe, A. Anderson, E. A. Hinds, D. Meschede, L. Moi, and S. Haroche. Suppression of spontaneous decay at optical frequencies: Test of vacuum-field anisotropy in confined space. *Physical Review Letters*, 58(7):666–669, feb 1987.

[45] Herbert Walther, Benjamin T H Varcoe, Berthold-Georg Englert, and Thomas Becker. Experiments on cavity quantum electrodynamics. *Physics Letters*, 219(3–6):63–281, 1992.

[46] Piers Andrew. *Molecular fluorescence near metallic interfaces*. Doctoral thesis, University of Exeter, England, 1998.

[47] Piers Andrew and William L. Barnes. Molecular fluorescence above metallic gratings. *Phys. Rev. B*, 64:125405, Sep 2001.

[48] J. Zhang, M. Wubs, P. Ginzburg, G. Wurtz, and A. V. Zayats. Transformation quantum optics: designing spontaneous emission using coordinate transformations. *Journal of Optics*, 18:044029–044040, 2016.

[49] L. Dong, A. Sugunan, J. Hu, S. Zhou, S. Li, S. Popov, M. S. Toprak, A. T. Friberg, and M. Muhammed. Photoluminescence from quasi-type-II spherical CdSe-CdS core-shell quantum dots. *Applied Optics*, 52(1):105–109, 2013.

[50] C. Liao, K. Fan, R. Xu, H. Zhang, C. Lu, Y. Cui, and J. Zhang. Laser-annealing-made amplified spontaneous emission of "giant" CdSe/CdS core/shell nanocrystals transferred from bulk-like shell to quantum-confined core. *Photon. Res.*, 3(5):200–205, 2015.

[51] M. S. R. Miltão. Casimir energy for a double spherical shell: A global mode sum approach. *Physical Review D*, 78(6):065023, sep 2008.

[52] W. G. Unruh. Notes on black-hole evaporation. *Physical Review D*, 14(4):870–892, aug 1976.

[53] B.S. DeWitt. Quantum gravity : the new synthesis. In Stephen Hawking and Werner Israel, editors, *General Relativity: an Einstein Centenary Survey*, chapter Quantum gr, page 944. Cambridge University Press, 1979.

[54] P C W Davies, Z X Liu, and A C Ottewill. Particle detectors in the presence of boundaries. *Classical and Quantum Gravity*, 6(7):1041–1051, jul 1989.

[55] B. F. Svaiter and N. F. Svaiter. Inertial and noninertial particle detectors and vacuum fluctuations. *Physical Review D*, 46(12):5267–5277, dec 1992.

[56] B F Svaiter and N F Svaiter. Quantum processes: stimulated and spontaneous emission near cosmic strings. *Classical and Quantum Gravity*, 11(2):347, feb 1994.

[57] F. Benatti and R. Floreanini. Entanglement generation in uniformly accelerating atoms: Reexamination of the Unruh effect. *Physical Review A*, 70(1):012112, jul 2004.

[58] Jialin Zhang and Hongwei Yu. Unruh effect and entanglement generation for accelerated atoms near a reflecting boundary. *Physical Review D*, 75(10):104014, may 2007.

[59] André G. S. Landulfo and George E. A. Matsas. Sudden death of entanglement and teleportation fidelity loss via the Unruh effect. *Physical Review A*, 80(3):032315, sep 2009.

[60] Jason Doukas and Benedict Carson. Entanglement of two qubits in a relativistic orbit. *Physical Review A*, 81(6):062320, jun 2010.

[61] David C. M. Ostapchuk, Shih-Yuin Lin, Robert B. Mann, and B. L. Hu. Entanglement dynamics between inertial and non-uniformly accelerated detectors. *Journal of High Energy Physics*, 2012(7):72, jul 2012.

[62] Xiaobao Liu, Zehua Tian, Jieci Wang, and Jiliang Jing. Radiative process of two entanglement atoms in de Sitter spacetime. *Physical Review D*, 97(10):105030, may 2018.

[63] Claude Cohen-Tannoudji; Bernard Diu; Franck Laloe. *Quantum Mechanics*. John Wiley & Sons. Inc, 1977.

[64] Jun John Sakurai. *Modern quantum mechanics; rev. ed.* Addison-Wesley, Reading, MA, 1994.

[65] Roy J. Glauber. The quantum theory of optical coherence. *Phys. Rev.*, 130:2529–2539, Jun 1963.

[66] F. De Martini, M. Marrocco, P. Mataloni, L. Crescentini, and R. Loudon. Spontaneous emission in the optical microscopic cavity. *Physical Review A*, 43(5):2480–2497, mar 1991.

[67] S. Dutra and P. Knight. Spontaneous emission in a planar Fabry-Pérot microcavity. *Physical Review A*, 53(5):3587–3605, may 1996.

[68] D. T. Alves, C. Farina, and A. C. Tort. Spontaneous emission between two parallel plates, one or both infinitely permeable. *Physical Review A*, 61(3):034102, feb 2000.

[69] R. P. A. Lima, F. N. Lima, and Marcelo L. Lyra. Spontaneous decay of a two-level system close to a perfectly reflecting sphere. *Annals of Physics*, 372:162–170, 2017.

[70] J. T. Chen, H. C. Shieh, J. J. Tsai, and J. W. Lee. Equivalence between Trefftz method and method of fundamental solutions for the Green's function

of concentric spheres using the addition theorem and image concept. *WIT Transactions on Modelling and Simulation*, 49:23–34, 2009.

[71] P. Langlois. Causal particle detectors and topology. *Annals of Physics*, 321:2027–2070, april 2006.

[72] P. C. W. Davies and A. C. Ottewill. Detection of negative energy: 4-dimensional examples. *Physical Review D*, 65(1):104014, may 2002.

[73] Nina Megier, Dariusz Chruściński, Jyrki Piilo, and Walter T. Strunz. Eternal non-Markovianity: from random unitary to Markov chain realisations. *Sci. Rep.*, 7(1):6379, dec 2017.

[74] Dimitris Moustos and Charis Anastopoulos. Non-Markovian time evolution of an accelerated qubit. *Physical Review D*, 95:025020–13, jan 2017.

[75] F. N. Lima, R. P. A. Lima, and Marcelo L. Lyra. Spontaneous Radiation of a Two-Level System Confined in a Reflective Spherical Shell Quantum Dot. *Brazilian Journal of Physics (Springer Nature)*, 43(4):1–9, 2019.

[76] G. Menezes and N. F. Svaiter. Vacuum fluctuations and radiation reaction in radiative processes of entangled states. *Physical Review A*, 92(6):062131, dec 2015.

Appendix (Participation in conferences)

IX Workshop da Pós-Graduação

Controle da taxa de emissão espontânea de átomos aprisionados em microcavidades esféricas.

Francisco Nogueira Lima[1,2*], Marcelo Leite Lyra[2]

1 Instituto Federal do Piauí, Campus São Raimundo Nonato, São Raimundo Nonato-PI, Brasil

2 Instituto de Física, Universidade Federal de Alagoas, Maceió-AL, Brasil

IF-UFAL, Maceió-AL (2016)

XL Encontro Nacional de Física da Matéria Condensada

Spontaneous decay of a two-level system close to a perfectly reflecting sphere.

LIMA, F. N.[1,2], LIMA, R.P.A.[2], LYRA, M.L.[2]

1 Instituto Federal do Piauí, Campus São Raimundo Nonato, São Raimundo Nonato-PI, Brasil

2 Instituto de Física, Universidade Federal de Alagoas, Maceió-AL, Brasil

Hotel Atlântico Búzios, Búzios-RJ (2017)

24th Central European Workshop on Quantum Optics

Spontaneous decay of a two-level system close to a perfectly reflecting sphere.

LIMA, F. N.[1,2], LYRA, M.L.[2], LIMA, R.P.A.[2]

1 Instituto Federal do Piauí, Campus São Raimundo Nonato, São Raimundo Nonato-PI, Brasil

2 Instituto de Física, Universidade Federal de Alagoas, Maceió-AL, Brasil

Denmark Technical University (DTU), Lyngby, Denmark (2017)

X Workshop da Pós-Graduação

Spontaneous decay of a two-level system close to a perfectly reflecting sphere.

LIMA, F. N.[1,2], LIMA, R.P.A.[2], LYRA, M.L.[2]

1 Instituto Federal do Piauí, Campus São Raimundo Nonato, São Raimundo Nonato-PI, Brasil

2 Instituto de Física, Universidade Federal de Alagoas, Maceió-AL, Brasil

IF-UFAL, Maceió-AL (2017)

XI Workshop da Pós-Graduação

Spontaneous decay of a two-level detector trapped in a reflective spherical shell.

LIMA, F. N.[1,2], LIMA, R.P.A.[2], LYRA, M.L.[2]

1 Instituto Federal do Piauí, Campus São Raimundo Nonato, São Raimundo Nonato-PI, Brasil

2 Instituto de Física, Universidade Federal de Alagoas, Maceió-AL, Brasil

IF-UFAL, Maceió-AL (2018)

Publications

CrossMark
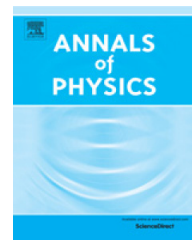
Spontaneous decay of a two-level system close to a perfectly reflecting sphere

R.P.A. Lima [a], F.N. Lima [b], M.L. Lyra [a,*]

[a] *GFTC and GISC, Instituto de Física, Universidade Federal de Alagoas, 57072-970, Maceió-AL, Brazil*
[b] *Instituto Federal do Piauí, 64770-000, São Raimundo Nonato-PI, Brazil*

ARTICLE INFO

ABSTRACT

Within a first-order time-dependent perturbation approach, we compute the spontaneous decay rate of a two-level system placed in the vicinity of a perfectly reflecting spherical surface. We consider a model system on which the emitter is represented by a two-level monopole coupled to a Hermitian massless scalar field. Using the method of images, we determine the appropriate Green's function evaluated in the world line of the atom. The change in the spontaneous decay rate results from the interaction of the atom with its image. We provide a detailed analysis of the dependence of the decay rate on the sphere's radius, the atom's location, and the emitted radiation frequency. Both exterior and interior problems are discussed.

1. Introduction

Tuning the rate of spontaneous emission of radiation by excited single atoms, molecules and quantum dots has been considered as a fundamental step towards the development of a new class of quantum optical devices. These include nanospectrometers and nanolasers, as well as electroluminescent and photonic band-gap structures [1–5].

Since the seminal work of Purcell [6], it has been known that the environment has a profound influence on the decay rate of excited systems. In particular, when the excited system is close to

interfaces, the imposed boundary conditions modify the density of possible electromagnetic modes. As result, the decay rate changes due to the system's coupling with the modified vacuum quantum fluctuations.

Over the last decades, several works have explored the possibility of enhancement or suppression of the decay rate of emitters placed near conducting walls, wedges, spheres and cylinders, or trapped in microcavities such as parallel walls, spheres and ellipsoids [7–32]. In particular, when a two-level system is trapped between parallel walls, the spontaneous decay process can be substantially suppressed when the distance between the walls is much smaller than the wavelength of the emitted radiation. On the other hand, the decay rate can be strongly enhanced due to the emergence of resonant modes. Recently, the spontaneous decay rate of quantum entangled atoms near interfaces has been a subject of increasing interest due to the possibility of generating and controlling quantum entangled radiation fields [33–36].

In the present work, we study the spontaneous decay rate of a two-level system close to a sphere with a perfectly reflecting surface, within a first-order time-dependent perturbation approach. Experiments performed with spherical SiO_2 colloids with two different diameters doped with Erbium at different concentrations showed a large difference in the spontaneous emission rate for both colloid sizes [18]. However, two factors that influence the spontaneous decay process are usually superposed: the modification of the field quantum fluctuations and polarization effects [20,26,28]. In order to focus on the specific contribution of the modified field fluctuations, we will consider a simple model on which the atom is represented by a two-level monopole coupled to a massless scalar field. Although not including polarization features, such model captures the essential ingredients needed to understand the influence of the field's mode changes induced by the presence of bounding surfaces on the atom's spontaneous emission. This approach has been successfully used in the literature to describe the process of photodetection [37–40], the influence of parallel mirrors and strings on the radiation process [15,41] and, more recently, on the entanglement generation by accelerated atoms [34,42–46].

This work is organized as follows. In the next section, we will present the main lines related to the first-order perturbation theory for the spontaneous decay rate of an excited monopole coupled to a scalar massless field. We also compute the decay rate for the case on which the two-level system is placed in the vicinity of a sphere with a perfectly reflecting surface. In Section 4, we provide a detailed analysis of the dependence of the decay rate on the atom's position, the radius of the sphere, as well as on the frequency of the emitted radiation. In Section 5, we summarize our main findings and draw some perspectives. Throughout this work, we will use units of $\hbar = c = 1$.

2. The spontaneous emission process

2.1. First-order perturbation theory

We start by briefly reviewing the main lines of the standard theoretical description of the radioactive processes of atoms. The system's Hilbert space is taken as the direct product of the Hilbert space of the atom and the quantized field. The total Hamiltonian can be generally written as $H = H_A + H_F + H_{int}$, where H_A is the noninteracting atom's Hamiltonian, H_F is the Hamiltonian of the free field and H_{int} represents the coupling between the atom and the background field. In order to investigate the spontaneous decay process, we consider the initial state of the system to be in the form $|\tau_i\rangle = |e\rangle \otimes |\phi_i\rangle$, where $|e\rangle$ is the excited state of the atom and $|\phi_i\rangle$ is the initial vacuum state of the field. In the interaction picture, the time evolution of the combined atom–field state is governed by the evolution operator

$$U(\tau_f, \tau_i) = 1 - i \int_{\tau_i}^{\tau_f} H_{int}(\tau')U(\tau', \tau_i)d\tau'. \tag{1}$$

From the above equation, the state of the system at time τ_f can be formally written as $|\tau_f\rangle = U(\tau_f, \tau_i)|\tau_i\rangle$. In the regime of weak atom–field coupling, the interaction Hamiltonian can be taken as a small perturbation. Up to first-order in the perturbation expansion, the evolution operator assumes

the simpler form

$$U(\tau_f, \tau_i) = 1 - i \int_{\tau_i}^{\tau_f} H_{int}(\tau) d\tau. \tag{2}$$

The probability amplitude for the transition from the initial state at τ_i into the final state $|g\rangle \otimes |\phi_f\rangle$ is given by

$$\langle g\phi_f | U(\tau_f, \tau_i) | e\phi_i \rangle = -i \int_{\tau_i}^{\tau_f} \langle g\phi_f | H_{int}(\tau) | e\phi_i \rangle d\tau, \tag{3}$$

where $|\phi_f\rangle$ is an arbitrary state of the field and $|g\rangle$ is the atom's ground state.

2.2. A two-level monopole coupled to a scalar massless field

Here, we will consider the simplest model for the coupling between the atom and the field that captures the essential features associated with the spontaneous emission process. The atom is represented by a two-level monopole system which is coupled to a Hermitian massless scalar field. The interaction Hamiltonian at time τ can be written as

$$H_{int}(\tau) = c_1 m(\tau) \phi(x(\tau)), \tag{4}$$

where c_1 is a small coupling constant, $m(\tau)$ is the monopole operator of the atom, and $\phi(x)$ is the scalar field operator at the atom's position. This model has been previously used to describe a detector of scalar fields [37,38,40], as well as to study the spontaneous decay of quantum entangled atoms [42–46,34]. Within this approach, the transition probability from the atom's excited state at $\tau_i = 0$ into the ground state at τ_f is given by

$$P(E, \tau_f) = c_1^2 |\langle e|m(0)|g\rangle|^2 F(E, \tau_f), \tag{5}$$

where the term $c_1^2 |\langle e|m(0)|g\rangle|^2$ is known as the atom's selectivity and $F(E, \tau_f)$ is the field's response function

$$F(E, \tau_f) = \int_0^{\tau_f} d\tau \int_0^{\tau_f} d\tau' e^{iE(\tau-\tau')} G^+(x(\tau), x(\tau')). \tag{6}$$

Here $E = E_e - E_g > 0$ represents the frequency $\omega = E$ in units of $\hbar = 1$ of the emitted radiation. $G^+(x(\tau), x(\tau')) = \langle 0|\phi(x(\tau))\phi(x(\tau'))|0\rangle$ is the positive scalar field Wightman function in the vacuum field state $|0\rangle$.

3. Spontaneous decay rate in the vicinity of a reflecting sphere

Let us start by reviewing the main result concerning the process of spontaneous emission by an excited two-level system interacting with the vacuum of a scalar quantum field in the free space. In the particular case on which the atom is at rest in the empty Minkowski space, the Wightman function is given by

$$G_M^+(x(\tau), x(\tau')) = -\frac{1}{4\pi^2} \frac{1}{(\zeta - i\epsilon)^2}, \tag{7}$$

where $\zeta = \tau - \tau'$. The spontaneous emission process is usually characterized by the asymptotic decay rate defined as $R = \frac{\partial F(E, \Delta\tau)}{\partial \Delta\tau}\big|_{\Delta\tau \to \infty}$, with $\Delta\tau = \tau_f - \tau_i$. It is straightforward to show that, in the case of an atom at rest in the empty space, it can be put in the form

$$R_M(E) = -\frac{1}{4\pi^2} \int_{-\infty}^{+\infty} d\zeta \frac{e^{iE\zeta}}{(\zeta - i\epsilon)^2}. \tag{8}$$
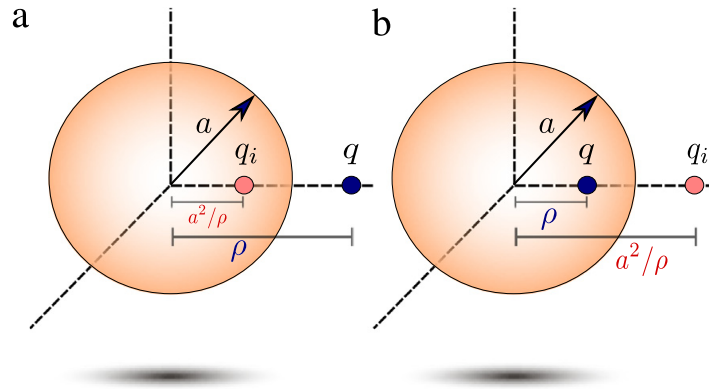
Fig. 1. Schematic view of the two-level system (dark blue bullet) and its respective image (clear red bullet) in the vicinity of a perfectly reflecting sphere of radius a. The two-level system is placed at a distance ρ from the center of the sphere. (a) Exterior problem; (b) Interior problem. (For interpretation of the references to color in this figure legend, the reader is referred to the web version of this article.)

The above integral can be performed by exploring the residue theorem and taking the limit $\epsilon \to 0$ to give $R_M(E) = \frac{E}{2\pi}$. Therefore, the spontaneous decay rate in the empty space is proportional to the frequency of the emitted radiation.

In the presence of perfectly reflecting surfaces, the Wightman function has to satisfy appropriate boundary conditions at the surfaces. The problem of a two-level monopole coupled to a scalar massless field in the vicinity of reflecting plates has been previously addressed [15]. It has been shown that the decay rate is substantially suppressed when the atom is placed close to the walls due to the imposed Dirichlet boundary conditions. Further, it has been explicitly demonstrated that the decay rate can be fully suppressed when the atom is placed between parallel walls when the distance between them is smaller than half of the radiation wavelength. Enhancement of the decay rate, as compared to the corresponding rate in the free space, has also been achieved when new field modes are supported by the cavity. The decay rate presents periodic modulations as a function of the cavity dimension or the atom's distance to the plates. All these features are in agreement with experiments, as well as with theoretical models of dipole atoms coupled with the vector quantized electromagnetic field [47–49,31]. These findings support the conjecture that the simplified description based in a monopole two-level system coupled to a scalar field can indeed capture the essential mechanism behind the process of spontaneous emission near surface boundaries.

Motivated by experiments showing a pronounced change in the decay rate of atoms trapped in spherical cavities [18], we will extend the above approach to the case of an atom placed in the vicinity of a perfectly reflecting spherical surface (see Fig. 1). Let us start placing the atom in the exterior region of a sphere of radius a. The Wightman function can be obtained using the method of images. The atom induces the emergence of an image monopole in the interior region. The image's position and monopole charge are such that the field vanishes in the surface of the sphere, as imposed by the Dirichlet boundary conditions. The Wightman function can then be written as

$$G^+(x(\tau), x'(\tau')) = -\frac{1}{4\pi^2} \frac{1}{(\zeta - i\epsilon)^2 + |x - x'|^2} + \frac{1}{4\pi^2} \frac{1}{(\zeta - i\epsilon)^2 + |x - x_i'|^2/q_i}, \qquad (9)$$

where x is an arbitrary position in the exterior region, x' is the atom's position, x_i' is the image's position and q_i is the modulus of the image's effective charge (its sign is opposite to the atom's monopole). When the atom is placed at a distance ρ from the center of the sphere $x' = (\rho, 0, 0)$, G^+ vanishes in all points x at the surface of the sphere, for any value of ζ, provided that $x_i' = (a^2/\rho, 0, 0)$ and $q_i = (a/\rho)^2$. In order to compute the spontaneous decay rate, the Wightman function at the world line of the atom at rest ($x = x'$) is needed. In this case, it assumes the simpler form

$$G^+(x(\tau), x(\tau')) = -\frac{1}{4\pi^2} \frac{1}{(\zeta - i\epsilon)^2} + \frac{1}{4\pi^2} \frac{1}{(\zeta - i\epsilon)^2 + |\rho - a^2/\rho|^2/(a/\rho)^2}. \qquad (10)$$

Notice that it reduces to the Wightman function in the empty space for $a \to 0$ and for $\rho \to \infty$, as expected. It vanishes at $\rho = a$ according to the imposed Dirichlet boundary condition.
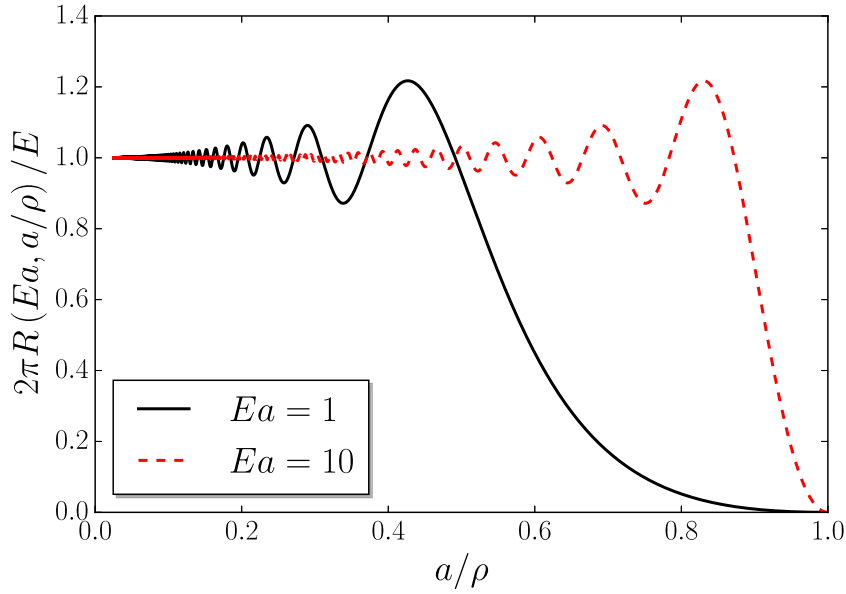
Fig. 2. Relative decay rate $2\pi R/E$ as a function of a/ρ (exterior problem) for two representative values of Ea. It vanishes at the surface of the sphere by construction, converging to the free space value at large distances. In the regime of small energies, the distance of maximum overshooting scales as $E^{-1/2}$.

The asymptotic decay rate can be directly calculated by replacing the Wightman function on the empty Minkowski space in Eq. (8), by the above function that incorporates both contributions of the monopole and its image. The algebraic procedure is similar to the one used to compute the decay rate near infinite plates [15]. The resulting asymptotic decay rate assumes the form

$$R(E, \rho, a) = \frac{E}{2\pi} \left(1 - \frac{\sin[(\rho^2/a - a)E]}{(\rho^2/a - a)E} \right). \tag{11}$$

Notice that when the distance of the atom to the sphere ρ is much larger than the radius a, the decay rate becomes the same as the one in the free space. The same limit is also achieved when the wavelength of the emitted radiation $\lambda \propto 1/E$ is much smaller than the distance of the atom to the sphere.

The case of the atom placed in the interior region of the sphere can also be solved using the method of images. The resulting expression for the Wightman function in the world line of the atom and the subsequent spontaneous decay rate are exactly the same ones obtained for the exterior problem with the restriction of $0 < \rho/a < 1$. It is interesting to stress that when the atom is placed at the center of the sphere, the decay rate becomes identical to that of a two-level system placed at a distance $a/2$ of a perfectly reflecting infinite plate [15].

4. Dependence of the decay rate on the distinct length scales

There are three distinct length scales that influence the decay rate of the present two-level model system near a spherical surface, namely, the radius a of the sphere, the distance ρ of the atom to the center of the sphere, and the wavelength $\lambda \propto 1/E$ of the emitted radiation. In what follows, we provide a detailed analysis of the dependence of the spontaneous decay rate on these length scales for both exterior and interior problems.

In Fig. 2 we plot the relative decay rate (the spontaneous decay rate in the vicinity of the sphere $R(Ea, a/\rho)$ in units of the decay rate in the free space $R(E) = E/2\pi$) as a function of the inverse of the distance ρ of the two-level system to the center of the sphere normalized by the sphere's radius. Two representative values of Ea are shown. The spontaneous decay vanishes at the surface of the sphere by construction, as imposed by the Dirichlet boundary condition. As ρ increases (decreasing values of a/ρ), the decay rate converges to its free space value presenting oscillations with decaying amplitudes. At its maximum overshooting, the spontaneous decay rate becomes approximately 21% larger than
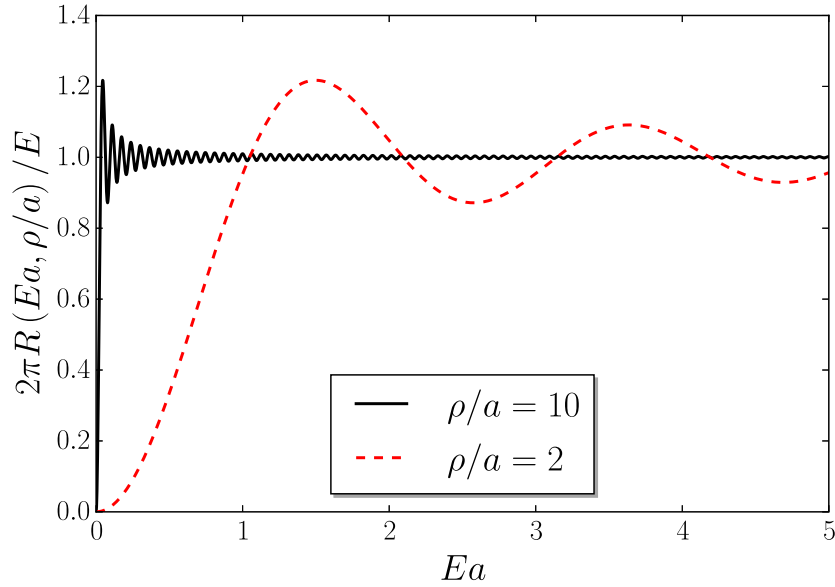
Fig. 3. Relative decay rate (measured in units of the free space decay rate) as a function of Ea for two representative values of a/ρ (exterior problem). The crossover from the small to the high energy regime occurs through damped oscillations with the maximum overshooting energy scaling as $1/\rho^2$ at large distances.

that in the free space. This maximum relative decay rate is achieved at larger distances of the atom to the surface when the wavelength of the emitted radiation becomes larger (smaller energy), with the atom's position of maximum overshooting scaling as $E^{-1/2}$.

To clearly illustrate the dependence of the decay rate on the energy of the emitted radiation, we plot in Fig. 3 the relative decay rate as a function of Ea for two fixed distances of the atom to the sphere's center. The decay rate converges to the free space value for very large energies, irrespective to the atom's distance to the sphere. In this regime, the wavelength of the emitted radiation becomes much smaller than the other length scales. The relative decay rate vanishes in the opposite regime of $Ea \to 0$. The crossover from the low to the high energy regime also occurs via damped oscillations, with the energy corresponding to the maximum relative decay rate scaling as $1/\rho^2$ when $\rho/a \gg 1$.

Let us now discuss the spontaneous decay process for the case of a two-level system trapped in the interior of the sphere. We start by plotting the relative decay rate as a function of Ea for distinct positions of the atom (see Fig. 4). When the atom is placed at the center of the sphere, we have already commented that the decay rate becomes exactly the same as that for a two-level monopole placed at a distance $a/2$ of an infinite reflecting place [15]. When the atom is displaced towards the sphere surface, the wavelength of the decay rate oscillations increases, with the energy of the first peak scaling with the distance of the atom to the surface $d = a - \rho$ proportionally to $1/d$ in the limit of $d \to 0$.

A series of interesting features can be extracted from the dependence of the decay rate on the atom's position for the interior problem (see Fig. 5). We depict typical curves by considering some relevant energy values. For $Ea < \pi$ the decay rate is always smaller than that in the free space, irrespective of the atom's position. For smaller energies, the relative decay rate is further suppressed. The maximum overshooting of the relative decay rate at the sphere's center occurs at $Ea \simeq 4.49$. For this energy, the relative decay rate decays monotonically to zero as the atom is displaced towards the sphere's surface. For larger energies, the relative decay rate develops damped oscillations.

We finish our analysis by reporting the decay rate averaged over the sphere's volume

$$\overline{R} = \frac{1}{4\pi a^3/3} \int_0^a 4\pi \rho^2 d\rho R(Ea, \rho/a). \tag{12}$$

This quantity accounts for the average decay rate of randomly quenched emitters uniformly distributed inside the sphere. The volume averaged spontaneous decay rate normalized by the free space decay is shown in Fig. 6 as a function of Ea. It vanishes quadratically as $Ea \to 0$. Therefore,
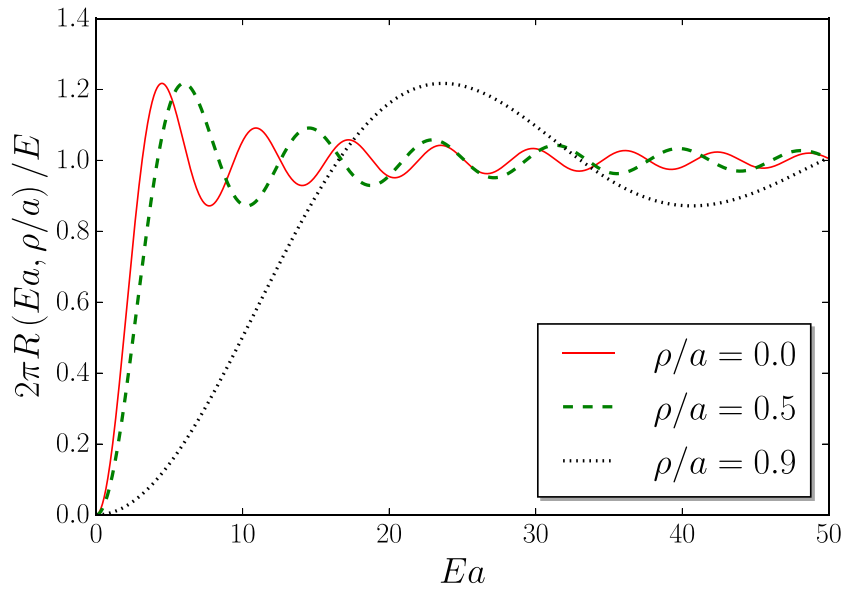
Fig. 4. Relative decay rate as a function of *Ea* for three representative values of ρ/a (interior problem). The maximum overshooting scales as the inverse of the atom's distance to the surface $d = \rho - a$ when $\rho/a \to 1$.
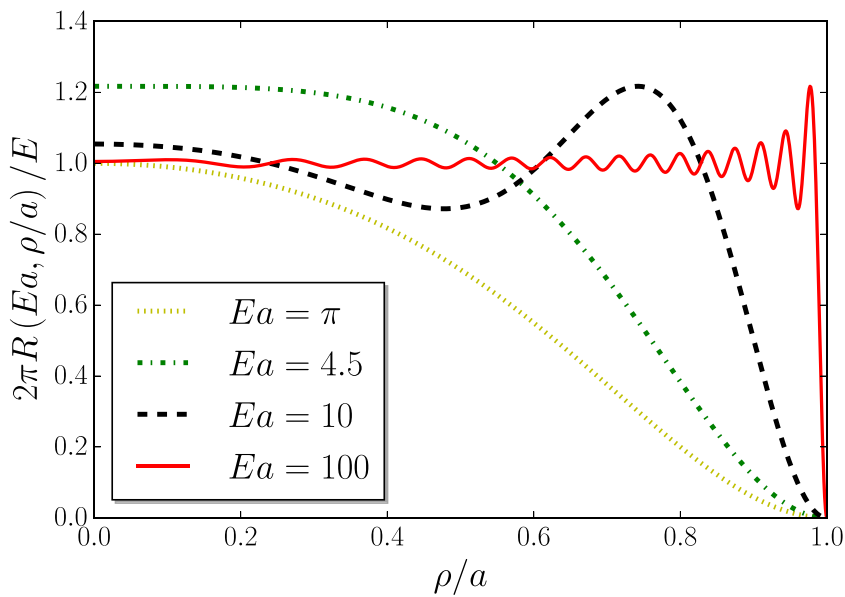

Fig. 5. Relative decay rate $2\pi R/E$ as a function of ρ/a (interior problem) for some representative values of *Ea*. For $Ea < \pi$ the decay rate is smaller than the one in the free space, irrespective of the atom's position. The maximum overshooting occurs at the sphere's center for $Ea \simeq 4.49$. Oscillations are developed for larger energies.

the average decay rate is substantially suppressed when the wavelength λ of the emitted radiation becomes larger than the size of the sphere. In the opposite regime of $a \gg \lambda$, the average decay rate slowly converges to the free space value. The crossover between these two regimes takes place at $a/\lambda \sim 1$.

5. Summary and conclusions

In summary, we have used a simple theoretical model to investigate the influence of a spherical surface on the spontaneous decay rate process of an excited system. Within a first-order perturbation theory, we provided an analytical expression for the spontaneous decay rate of a two-level monopole coupled to a Hermitian massless scalar field. We demonstrated that both cases of the two-level system
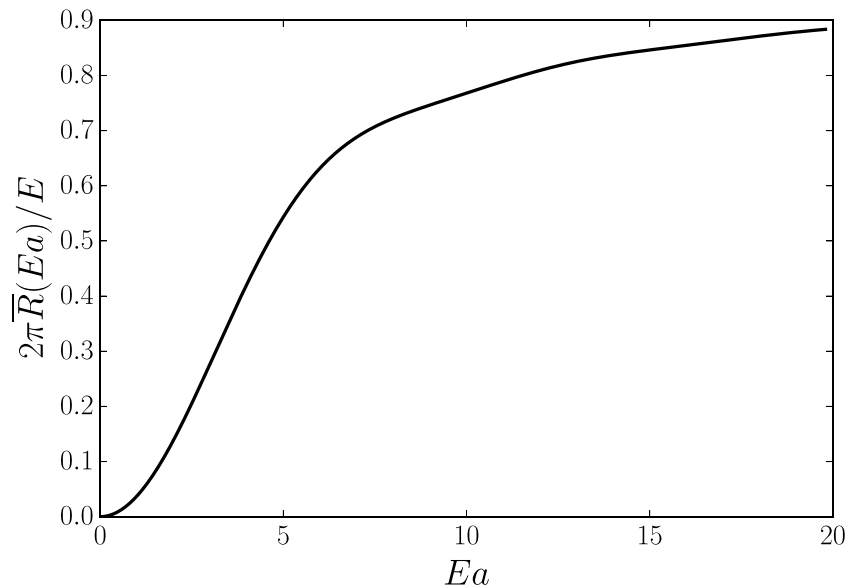
Fig. 6. Relative decay rate averaged over the sphere's volume (interior problem) as a function of Ea. It vanishes as $(Ea)^2$, converging monotonically to the free space value as $Ea \to \infty$.

placed in the exterior and in the interior of the sphere with a perfectly reflecting surface can be similarly described.

We provided a detailed analysis of the dependence of the spontaneous decay rate on the energy of the emitted radiation (or equivalently on its wavelength), the sphere's radius and the emitter's position. In particular, we showed that the spontaneous decay rate measured in units of the free space decay rate depicts damped oscillations as a function of either the radiation energy or the emitter's position with simple asymptotic scaling laws. Further, we found that the decay rate in the interior of the sphere is always suppressed in relation to the free space decay in the low energy regime, irrespective of the emitter's position. At higher energies it also develops damped oscillations. The volume averaged relative decay rate showed two distinct regimes: a quadratic vanishing for small energies and a slow convergence to the free space behavior at high energies.

It is worthy to emphasize that the present approach does not capture polarization effects. However, it provides a clear picture of the bare influence of bounding surfaces on the spontaneous emission process caused by the consequent modification of the vacuum field modes near the surface. A deeper understanding of such basic physical mechanism is fundamental in the search of techniques to control and tune the radiation process of trapped emitters. It would be interesting to extend the here reported study for the case of emitters trapped in other structures such as cylinders and shells. We hope the present work will stimulate future contributions along these lines.

Acknowledgments

References

[1] E. Betzig, R.J. Chichester, Science 262 (1993) 1422–1425.
[2] T.H. Taminiau, F.D. Stefani, F.B. Segerink, N.F. van Hulst, Nat. Photonics 2 (2008) 234–237.
[3] S. Kühn, U. Håkanson, L. Rogobete, V. Sandoghdar, Phys. Rev. Lett. 97 (2006) 017402.
[4] M. Khajavikhan, A. Simic, M. Katz, J.H. Lee, B. Slutsky, A. Mizrahi, V. Lomakin, Y. Fainman, Nature 482 (2012) 204–207.
[5] M. Frimmer, A.F. Koenderink, Phys. Rev. Lett. 110 (2013) 217405.
[6] E.M. Purcell, Phys. Rev. 69 (1946) 681.
[7] P. Stehle, Phys. Rev. A 2 (1970) 102–106.

 [8] G. Barton, Proc. R. Soc. Ser. A Math. Phys. Eng. Sci. 320 (1970) 251–275.
 [9] M.R. Philpott, Chem. Phys. Lett. 19 (1973) 435–439.
[10] P. Milonni, P. Knight, Opt. Commun. 9 (1973) 119–122.
[11] P. Goy, J.M. Raimond, M. Gross, S. Haroche, Phys. Rev. Lett. 50 (1983) 1903–1906.
[12] R.G. Hulet, E.S. Hilfer, D. Kleppner, Phys. Rev. Lett. 55 (1985) 2137–2140.
[13] W. Jhe, A. Anderson, E.A. Hinds, D. Meschede, L. Moi, S. Haroche, Phys. Rev. Lett. 58 (1987) 666–669; Erratum Phys. Rev. Lett. 58 (1987) 1497.
[14] H.M. França, T.W. Marshall, E. Santos, Phys. Rev. A 45 (1992) 6436–6442.
[15] L.H. Ford, N.F. Svaiter, M.L. Lyra, Phys. Rev. A 49 (1994) 1378–1386.
[16] P.S. Davids, P.B. Lerner, Z. Phys. D 33 (1995) 203–210.
[17] M. Kauranen, Y. Van Rompaey, J.J. Maki, A. Persoons, Phys. Rev. Lett. 80 (1998) 952–955.
[18] M.J.A. de Dood, L.H. Slooff, A. Polman, A. Moroz, A. van Blaaderen, Appl. Phys. Lett. 79 (2001) 3585.
[19] H.T. Dung, L. Knöll, D.-G. Welsch, Phys. Rev. A 64 (2001) 013804.
[20] K.J. Vahala, Nature 424 (2003) 839–846.
[21] V.V. Klimov, M. Ducloy, V.S. Letokhov, J. Modern Opt. 43 (1996) 549–563.
[22] A. Moroz, Chem. Phys. 317 (2005) 1–15.
[23] R. Carminati, J.-J. Greffet, C. Henkel, J. Vigoureux, Opt. Commun. 261 (2006) 368–375.
[24] H. Walther, B.T.H. Varcoe, B.-G. Englert, T. Becker, Rep. Progr. Phys. 69 (2006) 1325–1382.
[25] V. Yannopapas, N.V. Vitanov, J. Phys.: Condens. Matter 19 (2007) 096210.
[26] K.K. Pukhov, T.T. Basiev, Y.V. Orlovskii, JETP Lett. 88 (2008) 12–18.
[27] L. Ford, T.A. Roman, Ann. Physics 326 (2011) 2294–2306.
[28] F.A. Inam, T. Gaebel, C. Bradac, L. Stewart, M.J. Withford, J.M. Dawes, J.R. Rabeau, M.J. Steel, New J. Phys. 13 (2011) 073012.
[29] C. Sauvan, J.P. Hugonin, I.S. Maksymov, P. Lalanne, Phys. Rev. Lett. 110 (2013) 237401.
[30] S. Haroche, Ann. Phys. 525 (2013) 753–776.
[31] Z. Mohammadi, F. Kheirandish, Phys. Rev. A 92 (2015) 062118.
[32] A. Bienfait, J.J. Pla, Y. Kubo, X. Zhou, M. Stern, C.C. Lo, C.D. Weis, T. Schenkel, D. Vion, D. Esteve, J.J.L. Morton, P. Bertet, Nature 531 (2016) 74–77.
[33] H. Xiong, M. Scully, M. Zubairy, Phys. Rev. Lett. 94 (2005) 023601.
[34] E. Arias, J.G. Dueñas, G. Menezes, N.F. Svaiter, J. High Energy Phys. 2016 (2016) 147.
[35] Y. Yang, J. Hu, H. Yu, Phys. Rev. A 94 (2016) 032337.
[36] G. Menezes, N.F. Svaiter, Phys. Rev. A 93 (2016) 052117.
[37] W.G. Unruh, Phys. Rev. D 14 (1976) 870–892.
[38] B. DeWitt, in: S. Hawking, W. Israel (Eds.), General Relativity: An Einstein Centenary Survey, Cambridge University Press, 1979, p. 944.
[39] P.C.W. Davies, Z.X. Liu, A.C. Ottewill, Classical Quantum Gravity 6 (1989) 1041–1051.
[40] B.F. Svaiter, N.F. Svaiter, Phys. Rev. D 46 (1992) 5267–5277.
[41] B.F. Svaiter, N.F. Svaiter, Classical Quantum Gravity 11 (1994) 347.
[42] F. Benatti, R. Floreanini, Phys. Rev. A 70 (2004) 012112.
[43] J. Zhang, H. Yu, Phys. Rev. D 75 (2007) 104014.
[44] A.G.S. Landulfo, G.E.A. Matsas, Phys. Rev. A 80 (2009) 032315.
[45] J. Doukas, B. Carson, Phys. Rev. A 81 (2010) 062320.
[46] D.C.M. Ostapchuk, S.-Y. Lin, R.B. Mann, B.L. Hu, J. High Energy Phys. 2012 (2012) 72.
[47] F. De Martini, M. Marrocco, P. Mataloni, L. Crescentini, R. Loudon, Phys. Rev. A 43 (1991) 2480–2497.
[48] S. Dutra, P. Knight, Phys. Rev. A 53 (1996) 3587–3605.
[49] D.T. Alves, C. Farina, A.C. Tort, Phys. Rev. A 61 (2000) 034102.

Spontaneous Radiation of a Two-Level System Confined in a Reflective Spherical Shell Quantum Dot

F. N. Lima, R. P. A. Lima & M. L. Lyra

Springer

Springer

ATOMIC PHYSICS

Spontaneous Radiation of a Two-Level System Confined in a Reflective Spherical Shell Quantum Dot

Spontaneous Radiation of a Two-Level System in a Spherical Shell

F. N. Lima[1] · R. P. A. Lima[2] · M. L. Lyra[3] (ID)

Abstract

Using a first-order time-dependent perturbation theory, we calculate the spontaneous emission rate of a two-level system trapped between perfectly reflecting concentric spheres. The emitter is represented by a two-level monopole coupled to a Hermitian massless scalar field satisfying Dirichlet boundary conditions in such quantum-confined low-dimensional structure. We obtained the appropriate Green's function evaluated in worldline of the atom which incorporates contributions from an infinite set of variable image charges. We provide an analytical expression for the decay rate to investigate the radiation process of the trapped atomic system. We perform a broad analysis of the dependence of the decay rate for different relations between the radii of spheres and the emitted radiation energy. We unveil regimes of strong suppression of the spontaneous emission rate as well as the development of irregular oscillations as a function of the quantum of emitted energy.

Keywords Spontaneous radiation · Cavity quantum electrodynamics · Perturbation theory · Scalar field theory

1 Introduction

The control of spontaneous emission processes is fundamental for the appropriate performance of optoelectronic devices, such as lighting screens, lasers, optical amplifiers, and solar cells. The possibility of adjusting or controlling the spontaneous emission of radiation by excited systems

has been interpreted as an important advance for the development of a new class of quantum optical devices, such as nanospectrometers and nanolasers [1–5].

Field-theoretical approaches have provided important insights on the influence of boundary walls on the radiative process of detectors estimulated by the fluctuations of the quantum vaccum. It has been known for a long time that the environment has a strong influence on spontaneous decay processes [6]. Recently, it has been shown that the spontaneous emission can be either enhanced or suppressed using invisibility cloaks or gradient index lenses, with modification of the local density of optical states [7]. When the excited system is close to the interfaces, the boundary conditions modify the density of possible electromagnetic modes. The possibility of enhancement or suppression of the radiative emission rate of emitters positioned near conducting walls, wedges, spheres, and cylinders, or trapped in microcavities such as parallel walls, spheres, and ellipsoids, has been extensively explored in recent years [8–33]. Currently, the spontaneous decay rate of quantum entangled atoms close to interfaces has been a subject of growing interest of the scientific community [34–37]. For a two-level system trapped between parallel walls, the decay process can be substantially suppressed when

✉ F. N. Lima
nogueira@ifpi.edu.br

R. P. A. Lima
rodrigo@fis.ufal.br

M. L. Lyra
marcelo@fis.ufal.br

1 Instituto Federal do Piauí, São Raimundo Nonato-PI, 64770-000 Brazil

2 GFTC and GISC, Instituto de Física, Universidade Federal de Alagoas, Maceió-AL, 57072-970 Brazil

3 GFTC, Instituto de Física, Universidade Federal de Alagoas, Maceió-AL, 57072-970, Brazil

Ⓢ Springer

the distance between the walls is much smaller than the wavelength of the emitted radiation and strongly enhanced due to the emergence of resonant modes (see, Ref. [16]). When a two-level monopole is close to a perfectly reflecting single sphere, it was recently demonstrated that the decay rate is always suppressed in relation to the free-space decay in the low-energy regime (atom in the interior of the single sphere), irrespective of the emitter's position [38].

In the present work, motivated by experiments performed with CdSe-CdS core-shell quantum dots that showed that the involved dimensions for different samples has significant relevance in the decay process [39], as well as studies on the amplification of the spontaneous emission of such synthesized quantum-confined nanocrystals [40], we investigate the spontaneous decay rate of a two-level system trapped between perfectly reflecting concentric spheres (as shown in Fig. 1). Recently, the Casimir effect between two spherical shells has been investigated [41]. Here, we will use the time-dependent perturbation theory within a first-order approach to obtain an analytical expression for the asymptotic decay rate, together with the method of images to obtain the appropriate Green's function that incorporates contributions of the trapped atomic system and its infinite set of images, satisfying Dirichlet boundary conditions. This approach does not include polarization features but captures the essential ingredients needed to understand the influence of the field's mode changes induced by the presence of

spherical shell cavities on the atom's spontaneous emission and the main specific contribution of the modified field fluctuations [21, 27, 29]. This approach has been previously used with success in the description of photodetection processes [42–45], in the investigation of the influence of parallel mirrors and strings on the radiation process [16, 46], and in recent studies of entanglement effects on radiative processes [35, 47–52].

This paper is organized as follows. In the next section, we will briefly present the main aspects of the first-order perturbation theory and of the method of images applied to an excited monopole coupled to Hermitian massless scalar field. Further, we compute the decay rate of the atomic system placed between two concentric spheres with radii a and b. In Section 3, we provide a broad analysis and discussion of the dependence of the decay rate for different relations between the radii of two concentric spheres, and the emitted radiation energy. In Section 4, we summarize our most important findings and present some perspectives for future works. Throughout this text, we will use units of $\hbar = c = 1$.

2 Model and Formalism

We use a simple theoretical model to investigate the influence of spherical surfaces on the spontaneous decay

Fig. 1 Schematic view of the two-level system (bullet at ρ) and four representative images at $x'_{4i}, x'_{4i-1}, x'_{4i-2}, x'_{4i-3}$
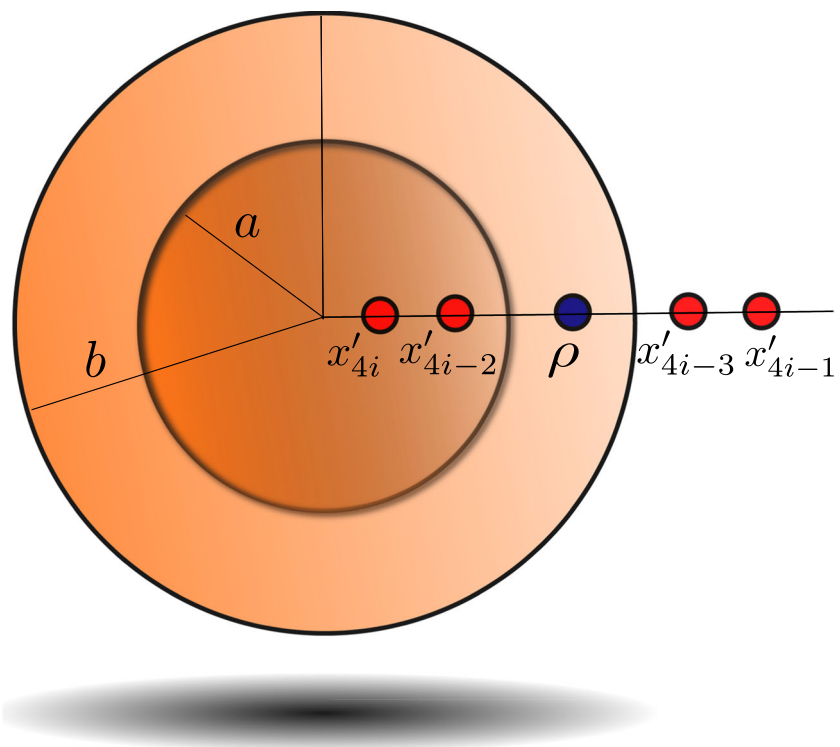
process of an excited system. The model contains the essential features of the spontaneous emission process. The atom is represented by a two-level monopole coupled to a Hermitian massless scalar field.

For completeness, let us begin by briefly reviewing the main points of the standard field-theoretical description. The total Hamiltonian of the system is given by $H = H_A + H_F + H_{int}$, where H_A is the noninteracting atom's Hamiltonian, H_F is the Hamiltonian of the free field and H_{int} is the coupling between the atom and the field.

If we consider that the initial state of the system to be in the form $|\tau_i\rangle = |e\rangle \otimes |\phi_i\rangle$, where $|e\rangle$ is the excited state of the atom and $|\phi_i\rangle$ is the initial vacuum state of the field, the time evolution in the interaction picture is governed by the evolution operator and the probability amplitude for the transition from the initial state at τ_i into the final state $|g\rangle \otimes |\phi_f\rangle$ is given by the following:

$$\langle g\phi_f|U(\tau_f, \tau_i)|e\phi_i\rangle = -i \int_{\tau_i}^{\tau_f} \langle g\phi_f|H_{int}(\tau)|e\phi_i\rangle d\tau, \quad (1)$$

where $|\phi_f\rangle$ is an arbitrary state of the field and $|g\rangle$ is the atom's ground state.

Details of the full formalism can be found in [16, 38, 45]. The interaction Hamiltonian at time τ is written as $H_{int}(\tau) = c_1 m(\tau)\phi(x(\tau))$, where c_1 is a small coupling constant, $m(\tau)$ is the monopole operator of the atom, $\phi(x)$ is the scalar field operator at the atom's position, and the transition probability from the atom's excited state at $\tau_i = 0$ into the ground state at τ_f is proportional on the field's response function $F(E, \tau_f)$ given by the following:

$$F(E, \tau_f) = \int_0^{\tau_f} d\tau \int_0^{\tau_f} d\tau' e^{iE(\tau - \tau')} G^+(x(\tau), x(\tau')), \quad (2)$$

where $E = E_e - E_g > 0$ represents the frequency $\omega = E$ in units of $\hbar = 1$ of the emitted radiation.

It is important to emphasize that $G^+(x(\tau), x(\tau')) = \langle 0|\phi(x(\tau))\phi(x(\tau'))|0\rangle$, known as the positive scalar field Wigthman function in the vacuum field state $|0\rangle$, is completely dependent on the geometry of the problem and will be used to obtain the transition probability, as described below.

At the surface of the concentric spheres, the Wightman function satisfies Dirichlet boundary conditions and is null by construction. It has been previously demonstrated that, when the atom is positioned near to infinite plates satisfying Dirichlet boundary conditions, the decay rate is substantially suppressed.

For the case treated here, the Wightman function can be obtained through the method of images, where the atom induces infinite images inside and outside the shell region (see, Fig. 1). Therefore, the function incorporates

contributions from an infinite set of variable image charges and can be written as follows:

$$G^+(x(\tau), x'(\tau')) = \frac{1}{4\pi^2} \left\{ \frac{-1}{(\zeta - i\epsilon)^2 - |x - x'|^2} + \lim_{N \to \infty} \sum_{i=1}^{N} \left[\frac{q_{4i-3}}{(\zeta - i\epsilon)^2 - |x - x'_{4i-3}|^2} + \frac{q_{4i-2}}{(\zeta - i\epsilon)^2 - |x - x'_{4i-2}|^2} - \frac{q_{4i-1}}{(\zeta - i\epsilon)^2 - |x - x'_{4i-1}|^2} - \frac{q_{4i}}{(\zeta - i\epsilon)^2 - |x - x'_{4i}|^2} \right] \right\}, \quad (3)$$

where $\zeta = \tau - \tau'$, x is an arbitrary position, x' is the atom's position; x'_{4i-3}, x'_{4i-2}, x'_{4i-1}, and x'_{4i} denotes any of the possible positions of the successive image charges, obtained from repeated applications of the method of images, i. e.,

$$x'_1 = \frac{b^2}{\rho}, \quad x'_5 = \frac{b^2}{\rho}\frac{b^2}{a^2}, \quad ..., x'_{4i-3} = \frac{b^2}{\rho}\left(\frac{b^2}{a^2}\right)^{i-1}$$

$$x'_2 = \frac{a^2}{\rho}, \quad x'_6 = \frac{a^2}{\rho}\frac{a^2}{b^2}, \quad ..., x'_{4i-2} = \frac{a^2}{\rho}\left(\frac{a^2}{b^2}\right)^{i-1}$$

$$x'_3 = \frac{b^2\rho}{a^2}, \quad x'_7 = \frac{b^2\rho}{a^2}\frac{b^2}{a^2}, \quad ..., x'_{4i-1} = \frac{b^2\rho}{a^2}\left(\frac{b^2}{a^2}\right)^{i-1}$$

$$x'_4 = \frac{a^2\rho}{b^2}, \quad x'_8 = \frac{a^2\rho}{b^2}\frac{a^2}{b^2}, \quad ..., x'_{4i} = \frac{a^2\rho}{b^2}\left(\frac{a^2}{b^2}\right)^{i-1}, \quad (4)$$
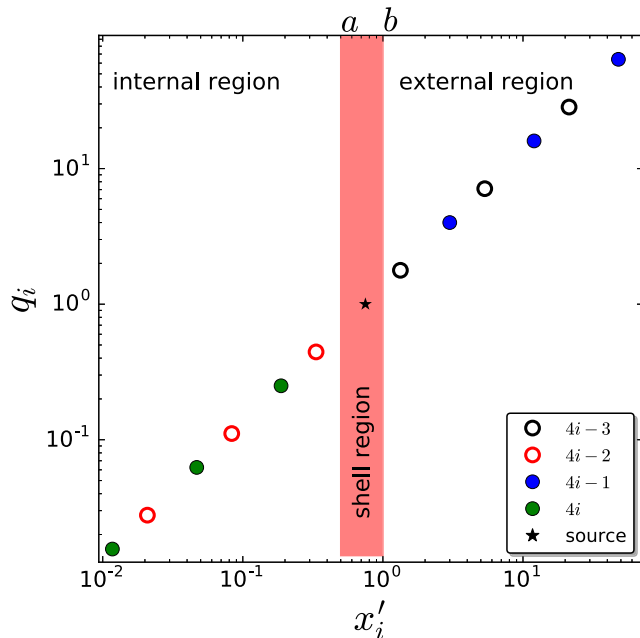

Fig. 2 Magnitude of the image charges as a function of their respective positions on both internal and external regions of a spherical shell of radii $a = 0.5$ and $b = 1$. Filled (open) circles represent image charges with the same (opposite) sign of the source charge (star symbol)

with ρ being some position of the two-level monopole between the radii of the inner and outer spheres ($a \leq \rho \leq b$) and a and b are their radii, respectively. In Eq. 3, q_{4i-3}, q_{4i-2}, q_{4i-1}, and q_{4i} represent all the possible modulus of the image's effective charges calculated using the method of images and are given by $q_j = x'_j/\rho$, representing any of the infinite image charges. Notice that the set of terms containing q_{4i-3} and q_{4i-2} denotes contributions of image charges whose signals are opposite to the source charge, while the set of terms q_{4i-1} and q_{4i} represent image contributions with the same signal of the source charge. In

Fig. 2, we plot the magnitude of the image charges as a function of their respective positions, both in the internal and external regions of the spherical shell.

Note that to obtain the Wightman function given by (3), we consider all the terms of the series that incorporates the contributions of the atom trapped between the concentric spheres shown in Fig. 1, as well as its infinite images. As we illustrate in Fig. 3, the Wightman function given by (3) satisfies the Dirichlet boundary condition and diverges over the source. For more details on the treatment of the Green's function for concentric spheres, see Ref. [53].

The asymptotic decay rate associated with spontaneous emission processes is usually defined as $R = \frac{\partial F(E, \tau_f)}{\partial \tau_f}$, after renormalizing logarithmic singularities in the transition proba-
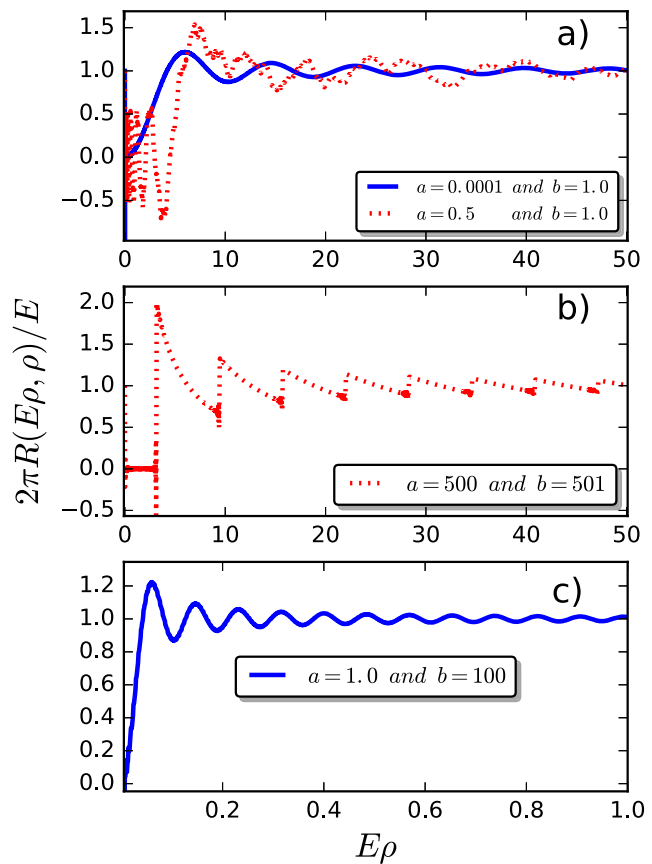

Fig. 3 Density plot of the Wightman function given by Eq. 3 with $\zeta = 0$ for two representative values of radii **a** $a = 10$ and $b = 20$; **b** $a = 10$ and $b = 100$. The represented plane crosses the source charge and the center of the spheres. The Wightman function is null at the surfaces, satisfying the Dirichlet boundary conditions and diverges over the source charge

Fig. 4 Relative decay rate (measured in units of the free-space decay rate) as a function of $E\rho$ for different relations between the radii of the spheres. In **a**, we have $a \ll 1$ and $a = b/2$. For the first case ($a \ll 1$), represented by the solid line (blue), the results converge to those obtained for the case of the two-level monopole placed inside a perfectly reflecting sphere. For $a = b/2$ (dashed red line), exist a low-energy range for which the decay rate oscillates around zero. In **b**, for $a/b \to 1$, the relative decay rate converges to that obtained in the case of parallel plates. In **c**, we recover the case of an atomic system positioned in the exterior of a single sphere

bility [45]. Following the prescription developed in [16, 38, 45], the asymptotic decay rate can be written as follows:

$$R(E, \rho, a, b) = \frac{E}{2\pi} \left[1 + \sum_i \text{sinc}(E\eta_{4i-3}) \right.$$
$$\left. + \text{sinc}(E\eta_{4i-2}) - \text{sinc}(E\eta_{4i-1}) - \text{sinc}(E\eta_{4i}) \right]. \quad (5)$$

where $\eta_j = \frac{\rho - x'_j}{\sqrt{q_j}}$. The averaged decay rate over the volume of the spherical shell is given by the following:

$$\overline{R} = \frac{3}{b^3 - a^3} \int_a^b \rho^2 d\rho R(E, \rho, a, b). \quad (6)$$

This quantity accounts for the average decay rate of randomly quenched emitters uniformly distributed between the two concentric spheres.

## 3 Spontaneous Decay Rate in Spherical Shell Cavities

It is important to consider three factors for the analysis and understanding of the decay rate behavior of the two-level detector positioned between two concentric reflecting spheres of radii a and b (always the atomic system at position ρ such that $a \leq \rho \leq b$): (i) the relation between the radii of spheres; (ii) the distance ρ from the detector to the center of the concentric spheres; (iii) the wavelength $\lambda \propto 1/E$ of the emitted radiation. In this section, we provide a detailed analysis of the spontaneous decay rate dependence considering these factors.

In Fig. 4, we plot the relative decay rate (the spontaneous decay rate for the atomic system trapped between the concentric spheres in units of the decay rate in the free-space $R(E\rho, \rho) = E/2\pi$) as a function of the parameter $E\rho$ associated with the energy of the two-level monopole. We fixed the atom's positions as $\rho = (a + b)/2$.

We consider in Fig. 4 four different shell geometries: (a) two cases $a \ll 1$ with b finite and $a = b/2$. In the later case, the spacement between the spherical surfaces is of the same order of their radii; (b) $a/b \to 1$ or equivalently $a \to b$ for which both surfaces radii are much larger the spacement between them; (c) $a = 1$ and much smaller then b. For the cases described in (a), the solid line (blue) represents the relative decay rate when the $a \ll 1$. In this case, the relative decay rate has a considerable peak in the low-energy range (high wavelength of emitted radiation) and converges slowly to the free space in the high energy limit, as occurred when the two-level system was placed inside of a single perfectly reflecting sphere [38]. Still in (a), the dashed line (red) represents the two-level monopole trapped between two concentric spheres with $a = b/2$. It is interesting to stress that, in this case, we observe a

Fig. 5 Spontaneous decay rate as a function of the detector position within a spherical shell with radii $a = 0.5$ and $b = 1$. Distinct cases of emitted radiation energies are illustrated. Spontaneous decay is strongly suppressed for low energies. At high energies, it vanishes near the surfaces and exhibits an oscillatory convergence to the rate at the free vacuum when the detector is moved far from the surfaces
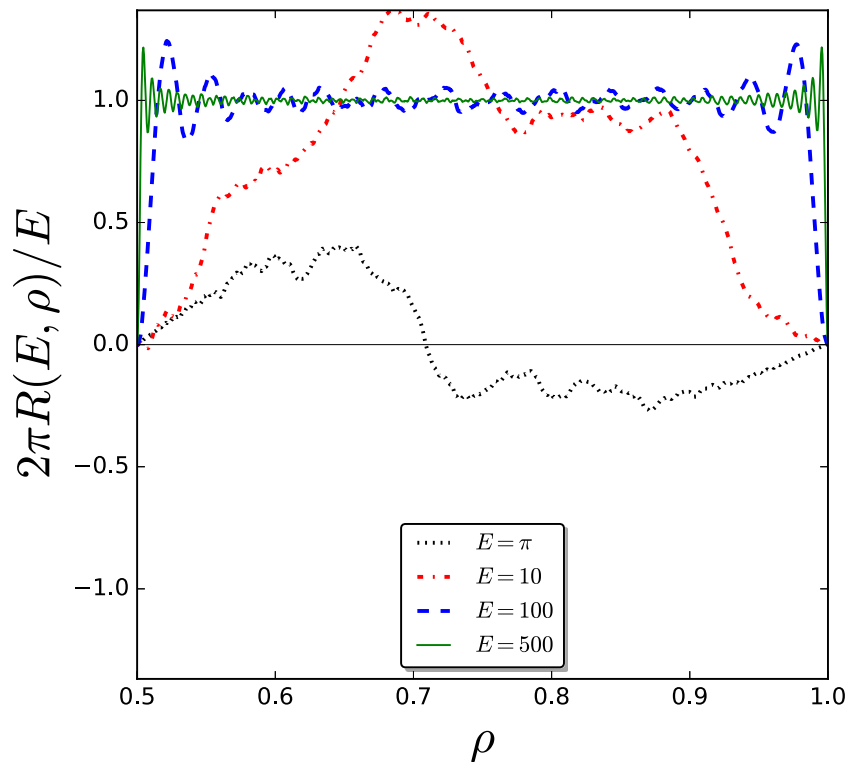
range of low energies for which the decay rate oscillates around zero, as well as irregular peaks in the decay rate. See that it is possible to suppress the spontaneous emission in the mentioned low-energy regime. Negative values in the decay rate have been previously attributed to the large interaction time and associated with the limit of validity of the perturbation theory or to non-Markovian reabsorption processes [45, 54–57].

As it can be seen in Fig. 4b, when the spheres have similar radii ($a/b \rightarrow 1$ or equivalently $a \rightarrow b$), the relative decay rate has a low-energy range for which the decay is fully suppressed, having an enhancement in the relative rate thereafter. This results converges to that obtained for the two-level monopole placed between two parallel reflecting plates [16], as expected because the physical situation in the referential of the atomic system is very similar, i. e., the radii of the spheres is much larger than the distance of the two-level monopole to their surfaces.

Notice that in the case shown in (c), there is an improvement of the relative decay rate in the low-energy regime, with the relative spontaneous decay oscillating and converging smoothly to the free space rate in the high-energy regime. For this case, the results are equivalent to those obtained for the two-level monopole placed in the exterior region of a perfectly reflecting spherical surface (see, Ref. [38]). In addition, the aspect of the relative decay rate is identical to that shown in the solid line (blue) in Fig. 4a [38].

We also investigated the dependence of the spontaneous decay rate on the position of the detector within the spherical shell. Typical dependences on the detector's position are reported in Fig. 5 for the case of a spherical shell with inner radius $a = 0.5$ and outer radius $b = 1$. The decay rate is quite suppressed for low energies (large wavelengths of the emitted radiation). As the quantum of emitted radiation energy increases, the decay rate of a detector placed at the center of the shell approaches that expected for a detector placed in the free vacuum because the wavelength of the emitted radiation becomes much smaller than the distance to both shell surfaces. Oscillations in the decay rate are developed when the atom approaches the vicinity of the bounding surfaces, ultimately vanishing when the radiation's wavelength becomes much larger than the atom-surface distance.

In Fig. 6, we plot the average decay rate calculated over the volume of the spherical shell as a function of the parameter $E\rho$ associated with the energy of the two-level monopole. Here, we also considered a fixed value position ($\rho = (a + b)/2$) from the center of the spheres for the same shell geometries commented above.

In Fig. 6a, the solid line (blue) represents the average relative decay rate when $a \ll 1$ with the decay rate vanishing as $(E\rho)^2$ and converging monotonically to the free-space value as $E\rho \rightarrow \infty$, as expected for the case

of a detector placed inside a single reflecting sphere [38]. Still in Fig. 6a, the dashed line (red) represents the two-level monopole trapped between two concentric spheres with $a = b/2$. In this case, we observe a low-energy range in which the average relative decay rate oscillates around zero, as well as the development of irregular peaks. In Fig. 6b, when $a > 1$ and much smaller then b, the average relative decay rate (solid line in blue) converges to those obtained for the exterior problem of a two-level system placed outside a single sphere [38]. In this case, the average relative decay rate converges to that of a free atomic system in the limit of
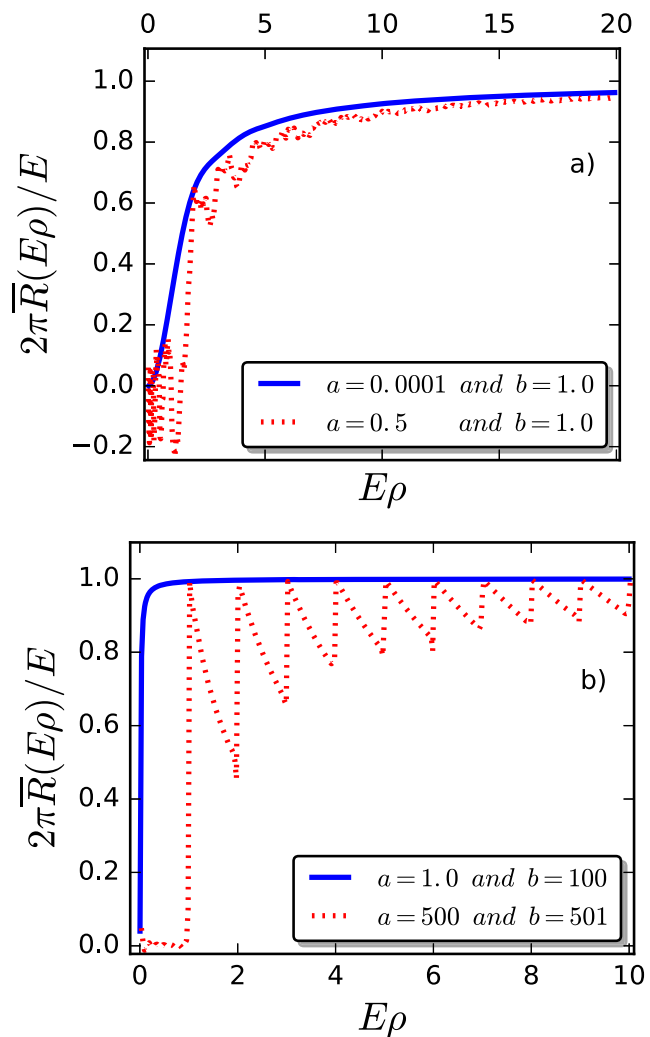

Fig. 6 Average relative decay rate over the spherical shell volume as a function of $E\rho$. In **a** (solid line in blue), when $a \ll 1$, the average relative decay rate vanishes as $(E\rho)^2$, converging monotonically to the free-space value as $E\rho \rightarrow \infty$. Still in **a**, the average relative decay rate for $a = b/2$ (dashed line in red) oscillates around zero in the range of low energies, having irregular peaks thereafter, converging to the free space for high energies. In **b**, the solid line in blue accounts for the average rate for the system positioned outside a single sphere. Still in **b**, for $a/b \rightarrow 1$ (dashed line in red), the decay rate vanishes at low energies, converging to free space in the high-energy regime depicting regular oscillations

high energies, having an aspect similar to the rate of the two-level system inside a single sphere (interior problem). Still in Fig. 6b, the dashed line in red represents the case where the radii of the spheres $a/b \to 1$ (or equivalently $a \to b$). The average relative decay rate converges to that for the two-level system positioned between parallel plates, i.e., there is a low-energies regime for which the rate is completely suppressed with regular oscillations associated with the emergence of new field modes (see more details in Ref. [16]). Furthermore, for any of the analyzed cases in Fig. 6, the average relative decay rate is substantially suppressed when the wavelength λ of the emitted radiation becomes much larger than the size of the spherical shell cavity. In the opposite regime, the average decay rate converges slowly to the free-space value.

4 Summary and Conclusions

In summary, we used a simple field-theoretical model containing the essential characteristics needed to describe spontaneous decay processes to investigate the influence of two concentric perfectly reflecting spheres on the decay rate of a trapped excited system. Using time-dependent perturbation theory within a first-order approximation, we calculated an analytical expression for the spontaneous decay rate of a two-level monopole coupled to a Hermitian massless scalar field.

We showed that the results already obtained in the literature for the two-level system between parallel plates and in the vicinity of a single sphere can be recovered as asymptotic cases of the problem treated here. Furthermore, we provide a detailed analysis of the dependence of the spontaneous decay rate on the energy of the emitted radiation (or equivalently on its wavelength), as well as on the different relation between the radii of the concentric spheres and the detector's position. We observed a low-energy range for which the decay rate oscillates around zero, as well as irregular peaks in the decay rate. We have verified that it is possible to suppress the spontaneous emission in the mentioned low-energy range. In the opposite regime, the decay rate converges slowly to the free-space value. The same characteristics were observed for the average relative decay rate. It is important to stress that the decay rate develops irregular oscillations as a function of the quantum of energy radiated within the spherical shell, in contrast with the regular oscillations observed for the similar process occurring in a cavity composed by parallel plates. These irregular oscillations reflect the non-uniform spacement and variability of the infinite set of image charges.

It is interesting to stress that the present approach provides a clear picture of the influence of curved bounding surfaces on the spontaneous emission processes. The changes in the decay rate are a direct consequence of the modification of the vacuum field modes in the vicinity of the spherical surfaces. The detailed understanding of these important effects finds great relevance in the control and adjustment of spontaneous emission processes. These are fundamental in the definition of the performance of optoelectronic devices which are usually based on photosensible particles trapped in spherical coats [39]. The present approach can be extended to account for polarization effects due to the coupling between the electrical dipole of the emitter and the electromagnetic field in the vacuum state [37, 58]. We hope that the present work can stimulate further contributions aiming to uncover the influence of other shell geometries in the decay process of trapped emitters.

References

1. E. Betzig, R.J. Chichester, Single molecules observed by near-field scanning optical microscopy, Science (5138). https://doi.org/10.1126/science.262.5138.1422 (1422)
2. T.H. Taminiau, F.D. Stefani, F.B. Segerink, N.F. van Hulst, Optical antennas direct single-molecule emission, Nat. Photonics (4), 234. https://doi.org/10.1038/nphoton.2008.32
3. S. Kühn, U. Håkanson, L. Rogobete, V. Sandoghdar, Enhancement of single-molecule fluorescence using a gold nanoparticle as an optical nanoantenna, Phys. Rev. Lett. (1), 017402. https://doi.org/10.1103/PhysRevLett.97.017402
4. M. Khajavikhan, A. Simic, M. Katz, J.H. Lee, B. Slutsky, A. Mizrahi, V. Lomakin, Y. Fainman, Thresholdless nanoscale coaxial lasers, Nature (7384), 204. https://doi.org/10.1038/nature10840
5. M. Frimmer, A.F. Koenderink, Spontaneous emission control in a tunable hybrid photonic system, Phys. Rev. Lett. (21), 217405. https://doi.org/10.1103/PhysRevLett.110.217405
6. E.M. Purcell, Spontaneous emission probabilities at radio frequencies, Phys. Rev. (11-12), 681. https://doi.org/10.1103/PhysRev.69.674
7. J. Zhang, M. Wubs, P. Ginzburg, G. Wurtz, A.V. Zayats, Transformation quantum optics: designing spontaneous emission using coordinate transformations. J. Opt. **18**, 044029 (2016). https://doi.org/10.1088/2040-8978/18/4/044029
8. P. Stehle, Atomic radiation in a cavity, Phys. Rev. A (1), 102. https://doi.org/10.1103/PhysRevA.2.102
9. G. Barton, Quantum electrodynamics of spinless particles between conducting plates, Proceedings of the Royal Society A: Mathematical, Phys. Eng. Sci. (1541), 251. https://doi.org/10.1098/rspa.1970.0208
10. M.R. Philpott, Fluorescence from molecules between mirrors, Chem. Phys. Lett. (3), 435. https://doi.org/10.1016/0009-2614(73)80399-9
11. P. Milonni, P. Knight, Spontaneous emission between mirrors, Opt. Commun. (2), 119. https://doi.org/10.1016/0030-4018(73)90239-3
12. P. Goy, J.M. Raimond, M. Gross, S. Haroche, Observation of cavity-enhanced single-atom spontaneous emission, Phys. Rev. Lett. (24), 1903. https://doi.org/10.1103/PhysRevLett.50.1903
13. R.G. Hulet, E.S. Hilfer, D. Kleppner, Inhibited spontaneous emission by a Rydberg atom, Phys. Rev. Lett. (20), 2137. https://doi.org/10.1103/PhysRevLett.55.2137